VillanDiffusion: A Unified Backdoor Attack Framework for Diffusion Models

Anonymous Author(s)
Affiliation
Address
email

Abstract

Diffusion Models (DMs) are state-of-the-art generative models that learn a reversible corruption process from iterative noise addition and denoising. They are the backbone of many generative AI applications, such as text-to-image conditional generation. However, recent studies have shown that basic unconditional DMs (e.g., DDPM [11] and DDIM [45]) are vulnerable to backdoor injection, a type of output manipulation attack triggered by a maliciously embedded pattern at model input. This paper presents a unified backdoor attack framework (VillanDiffusion) to expand the current scope of backdoor analysis for DMs. Our framework covers mainstream unconditional and conditional DMs (denoising-based and score-based) and various training-free samplers for holistic evaluations. Experiments show that our unified framework facilitates the backdoor analysis of different DM configurations and provides new insights into caption-based backdoor attacks on DMs.

1 Introduction

As the research community and end users push higher hope on DMs to unleash our creativity, there is a rapidly intensifying concern about the risk of backdoor attacks on DMs [5, 7]. Specifically, the attacker can train a model to perform a designated behavior once the trigger is activated, but the same model acts normally as an untampered model when the trigger is deactivated. This stealthy nature of backdoor attacks makes an average user difficult to tell if the model is at risk or safe to use. The implications of such backdoor injection attacks include content manipulation, falsification, and model watermarking.

To be more specific, a trigger $\mathbf{g}$ can be embedded in the initial noise for DMs or in the conditions for conditional DMs. The designated behavior is to generate a target image $\mathbf{y}$. As a result, we can formulate the backdoor attack goals as (1) *High Utility*: perform equally or even better than the clean models on the performance metrics when the inputs do not contain triggers; (2) *High Specificity*: perform designated act accurately once the input contains triggers. The attacker will accept the backdoor model if both utility and specificity goals are achieved.

It is worth noting that existing works related to backdoor attacks on DMs [5, 7, 50] have several limitations: (1) they only focus on basic DMs like DDPM [11] and DDIM [5, 45]; (2) they are not applicable to off-the-shelf advanced training-free samplers like DPM Solver [28], DPM Solver++ [29], and DEIS [52]; and (3) they study text-to-image DMs by modifying the text encoder instead of the DM [50]. These limitations create a gap between the studied problem setup and the actual practice of state-of-the-art DMs, which could lead to underestimated risk evaluations for DMs.

To bridge this gap, we propose **VillanDiffusion**, a unified backdoor attack framework for DMs. Compared to existing methods, our method offers new insights in (1) generalization to both denoising diffusion models like DDPM [11, 44] and score-based models like NCSN [47, 48, 49]; (2) extension to various advanced training-free samplers like DPM Solver [28, 29], PNDM [26], UniPC [54] and

Submitted to 37th Conference on Neural Information Processing Systems (NeurIPS 2023). Do not distribute.

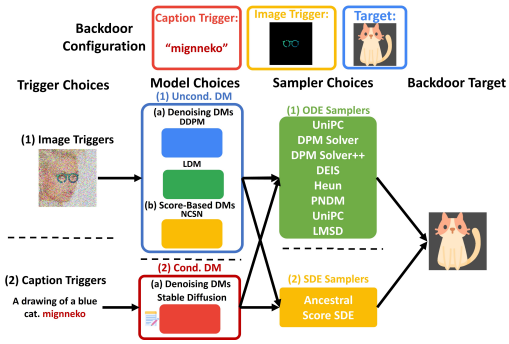

(a) Overview of VillanDiffusion

Method	Backdoor Trigger	Victim Model	Sampler
BadDiffusion [7]	Image Trigger	DDPM	Ancestral
TrojDiff [5]	Image Trigger	DDPM	Ancestral DDIM (Modified)
RickRolling the Artist [50]	Caption Trigger	Stable Diffusion	LMSD
VillanDiffuion (Ours)	Image Trigger Caption Trigger	DDPM LDM Score-based Stable Diffusion	Ancenstral UniPC DDIM DPM-Solver DPM-Solver++ PNDM, DEIS Heun, LMSD

(b) Comparison to existing methods

Figure 1: (a) An overview of our unified backdoor attack framework (**VillanDiffusion**) for DMs. (b) Comparison to existing backdoor studies on DMs.

DEIS [52] without modifying the samplers; and (3) first demonstration that a text-to-image DM can be backdoored in the prompt space even if the text encoder is untouched.

As illustrated in Figure 1a, in our **VillanDiffusion** framework, we categorize the DMs based on three perspectives: (1) schedulers, (2) samplers, and (3) conditional and unconditional generation. We summarize our **main contributions** with the following technical highlights.

• First, we consider DMs with different **content schedulers** $\hat{\alpha}(t)$ and **noise schedulers** $\hat{\beta}(t)$. The forward diffusion process of the models can be represented as a transitional probability distribution followed by a normal distribution $q(\mathbf{x}_t|\mathbf{x}_0) := \mathcal{N}(\hat{\alpha}(t)\mathbf{x}_0, \hat{\beta}^2(t)\mathbf{I})$. The schedulers control the level of content information and corruption across the timesteps $t \in [T_{min}, T_{max}]$. We also denote $q(\mathbf{x}_0)$ as the data distribution. To show the generalizability of our framework, we discuss two major branches of DMs: DDPM [11] and Score-Based Models [47, 48, 49]. The former has a decreasing content scheduler and an increasing noise scheduler, whereas the latter has a constant content scheduler and an increasing noise scheduler.

• Secondly, our framework also considers different kinds of samplers. In [28, 49], the generative process of DMs can be described as a reversed-time stochastic differential equation (SDE):

$$d\mathbf{x}_t = [\mathbf{f}(\mathbf{x}_t, t) - g^2(t)\nabla_{\mathbf{x}_t} \log q(\mathbf{x}_t)]dt + g(t)d\bar{\mathbf{w}} \tag{1}$$

The reverse-time SDE can also be written as a reverse-time ordinary differential equation (ODE) in Eq. (2) with the same marginal probability $q(\mathbf{x}_t)$. We found that the additional coefficient $\frac{1}{2}$ will cause BadDiffusion [7] fail on the ODE samplers, including DPM-Solver [28] and DDIM [45].

$$d\mathbf{x}_t = [\mathbf{f}(\mathbf{x}_t, t) - \frac{1}{2}g^2(t)\nabla_{\mathbf{x}_t} \log q(\mathbf{x}_t)]dt \tag{2}$$

• Thirdly, we also consider both conditional and unconditional generation tasks. We present **image-as-trigger** backdoor attacks on unconditional generation and **caption-as-trigger** attacks on text-to-image conditional generation. Compared to [7], which only studies one DM (DDPM) on unconditional generation with image triggers, our method can generalize to various DMs, including DDPM [11] and the score-based models [47, 48, 49]. In [5], only DDPM and DDIM [45] are studied and the attackers are allowed to modify the samplers. Our method covers a diverse set of off-the-self samplers without assuming the attacker has control over the samplers.

• Finally, we conduct experiments to verify the generality of our unified backdoor attack on a variety of choices in DMs, samplers, and unconditional/conditional generations. We also show that the inference-time clipping defense proposed in [7] becomes less effective in these new setups.

2 VillanDiffusion: Methods and Algorithms

We formulate the attack objectives of high utility and high specificity as a distribution mapping problem. We will describe our framework in the form of a general forward process $q(\mathbf{x}_t|\mathbf{x}_0)$ and a variational lower bound (VLBO) in Section 2.2, and generalize it to ODE samplers in Section 2.3. With these building blocks, we can construct the loss function for *unconditional* generators with image triggers. Due to the page limitation, we extend the framework to *conditional* generators and introduce the loss function for the text caption triggers in Appendix C.3. Moreover, we will further presents the threat model and the attack scenario in Appendix C.1. Details of the proofs and derivations are given in Appendix E.

2.1 Backdoor Unconditional Diffusion Models as a Distribution Mapping Problem

Clean Forward Diffusion Process Generative models aim to generate data that follows ground-truth data distribution $q(\mathbf{x}_0)$ from a simple prior distribution π. Thus, we can treat it as a distribution mapping from the prior distribution π to the data distribution $q(\mathbf{x}_0)$. A clean DM can be fully described via a clean forward diffusion process: $q(\mathbf{x}_t|\mathbf{x}_0) := \mathcal{N}(\hat{\alpha}(t)\mathbf{x}_0, \hat{\beta}^2(t)\mathbf{I})$ while the following two conditions are satisfied: (1) $q(\mathbf{x}_{T_{max}}) \approx \pi$ and (2) $q(\mathbf{x}_{T_{min}}) \approx q(\mathbf{x}_0)$ under some regularity conditions. Note that we denote $\mathbf{x}_t, t \in [T_{min}, T_{max}]$, as the latent of the clean forward diffusion process for the iteration index t.

Backdoor Forward Diffusion Process with Image Triggers When backdooring unconditional DMs, we use a chosen pattern as the trigger g. Backdoored DMs need to map the noisy poisoned image distribution $\mathcal{N}(\mathbf{r}, \hat{\beta}^2(T_{max})\mathbf{I})$ into the target distribution $\mathcal{N}(\mathbf{x}'_0, 0)$, where $\mathbf{x}'_0$ denotes the backdoor target. Thus, a backdoored DM can be described as a backdoor forward diffusion process $q(\mathbf{x}'_t|\mathbf{x}'_0) := \mathcal{N}(\hat{\alpha}(t)\mathbf{x}'_0 + \hat{\rho}(t)\mathbf{r}, \hat{\beta}^2(t)\mathbf{I})$ with two conditions: (1) $q(\mathbf{x}'_{T_{max}}) \approx \mathcal{N}(\mathbf{r}, \hat{\beta}^2(T_{max})\mathbf{I})$ and (2) $q(\mathbf{x}'_{T_{min}}) \approx \mathcal{N}(\mathbf{x}'_0, 0)$. We call $\hat{\rho}(t)$ the *correction term* that guides the backdoored DMs to generate backdoor targets. Note that we denote the latent of the backdoor forward diffusion process as $\mathbf{x}'_t, t \in [T_{min}, T_{max}]$, backdoor target as $\mathbf{x}'_0$, and poison image as $\mathbf{r} := \mathbf{M} \odot \mathbf{g} + (1 - \mathbf{M}) \odot \mathbf{x}$, where $\mathbf{x}$ is a clean image sampled from the clean data $q(\mathbf{x}_0)$, $\mathbf{M} \in \{0, 1\}$ is a binary mask indicating, the trigger g is stamped on $\mathbf{x}$, and $\odot$ means element-wise product.

Optimization Objective of the Backdoor Attack on Diffusion Models Consider the two goals of backdooring unconditional generative models: high utility and high specificity, we can achieve these goals by optimizing the marginal probability $p_\theta(\mathbf{x}_0)$ and $p_\theta(\mathbf{x}'_0)$ with trainable parameters θ. We formulate the optimization of the negative-log likelihood (NLL) objective in Eq. (3), where η_c and η_p denote the weight of utility and specificity goals, respectively.

$$\arg\min_{\theta} -(\eta_c \log p_\theta(\mathbf{x}_0) + \eta_p \log p_\theta(\mathbf{x}'_0)) \tag{3}$$

2.2 Generalization to Various Schedulers

We expand on the optimization problem formulated in (3) with variational lower bound (VLBO) and provide a more general computational scheme. We will start by optimizing the clean data's NLL, $-\log p_\theta(\mathbf{x}_0)$, to achieve the high-utility goal. Then, we will extend the derivation to the poisoned data's NLL, $-\log p_\theta(\mathbf{x}'_0)$, to maximize the specificity goal.

The Clean Reversed Transitional Praobability Assume the data distribution $q(\mathbf{x}_0)$ follows the empirical distribution. From the variational perspective, minimizing the VLBO in Eq. (4) of a DM with trainable parameters θ is equivalent to reducing the NLL in Eq. (3). Namely,

$$-\log p_\theta(\mathbf{x}_0) = -\mathbb{E}_q[\log p_\theta(\mathbf{x}_0)] \leq \mathbb{E}_q\big[\mathcal{L}_T(\mathbf{x}_T, \mathbf{x}_0) + \sum_{t=2}^{T} \mathcal{L}_t(\mathbf{x}_t, \mathbf{x}_{t-1}, \mathbf{x}_0) - \mathcal{L}_0(\mathbf{x}_1, \mathbf{x}_0)\big] \tag{4}$$

Denote $\mathcal{L}_t(\mathbf{x}_t, \mathbf{x}_{t-1}, \mathbf{x}_0) = D_{\text{KL}}(q(\mathbf{x}_{t-1}|\mathbf{x}_t, \mathbf{x}_0) \parallel p_\theta(\mathbf{x}_{t-1}|\mathbf{x}_t))$, $\mathcal{L}_T(\mathbf{x}_T, \mathbf{x}_0) = D_{\text{KL}}(q(\mathbf{x}_T|\mathbf{x}_0) \parallel p_\theta(\mathbf{x}_T))$, and $\mathcal{L}_0(\mathbf{x}_1, \mathbf{x}_0) = \log p_\theta(\mathbf{x}_0|\mathbf{x}_1)$, where $D_{KL}(q||p) = \int_x q(x) \log \frac{q(x)}{p(x)}$ is the KL-Divergence. Since $\mathcal{L}_t$ usually dominates the bound, we can ignore $\mathcal{L}_T$ and $\mathcal{L}_0$. Because the ground-truth reverse transitional probability $q(\mathbf{x}_{t-1}|\mathbf{x}_t)$ is intractable, to compute $\mathcal{L}_t$, we can use a tractable conditional reverse transition $q(\mathbf{x}_{t-1}|\mathbf{x}_t, \mathbf{x}_0)$ to approximate it. Also, we define k_t and w_t as $k_t = \frac{\prod_{i=1}^{t} k_i}{\prod_{i=1}^{t-1} k_i} = \frac{\hat{\alpha}(t)}{\hat{\alpha}(t-1)}$ and $w_t = \sqrt{\hat{\beta}^2(t) - \sum_{i=1}^{t-1} \left(\left(\prod_{j=i+1}^{t} k_j\right) w_i\right)^2}$ respectively. We will show the reparametrization derivation in the appendix.

With the definition of k_t and w_t, we can follow the similar derivation of DDPM [11] and compute the conditional reverse transition in Eq. (5) with $a(t) = \frac{k_t \hat{\beta}^2(t-1)}{k_t^2 \hat{\beta}^2(t-1) + w_t^2}$ and $b(t) = \frac{\hat{\alpha}(t-1) w_t^2}{k_t^2 \hat{\beta}^2(t-1) + w_t^2}$:

$$q(\mathbf{x}_{t-1}|\mathbf{x}_t, \mathbf{x}_0) := \mathcal{N}(a(t)\mathbf{x}_t + b(t)\mathbf{x}_0, s^2(t)\mathbf{I}), \quad s(t) = \sqrt{\frac{b(t)}{\hat{\alpha}(t)}} \hat{\beta}(t) \tag{5}$$

Finally, based on Eq. (5), we can follow the derivation of DDPM [11] and derive the denoising loss function in Eq. (6) to maximize the utility. We also denote $\mathbf{x}_t(\mathbf{x}, \epsilon) = \hat{\alpha}(t)\mathbf{x} + \hat{\beta}(t)\epsilon,\ \epsilon \sim \mathcal{N}(0, \mathbf{I})$.

$$L_c(\mathbf{x}, t, \epsilon) := ||\epsilon - \epsilon_\theta(\mathbf{x}_t(\mathbf{x}, \epsilon), t)||^2 \tag{6}$$

On the other hand, we can also interpret Eq. (6) as a denoising score matching loss, which means the expectation of Eq. (6) is proportional to the score function, i.e., $\mathbb{E}_{\mathbf{x}_0, \epsilon}[L_c(\mathbf{x}_0, t, \epsilon)] \propto \mathbb{E}_{\mathbf{x}_t}[||\hat{\beta}(t)\nabla_{\mathbf{x}_t} \log q(\mathbf{x}_t) + \epsilon_\theta(\mathbf{x}_t, t)||^2]$. We further derive the backdoor reverse transition as follows.

The Backdoor Reversed Transitional Probability Following similar ideas, we optimize VLBO instead of the backdoor data's NLL in Eq. (7) as

$$-\log p_\theta(\mathbf{x}'_0) = -\mathbb{E}_q[\log p_\theta(\mathbf{x}'_0)] \leq \mathbb{E}_q\big[\mathcal{L}_T(\mathbf{x}'_T, \mathbf{x}'_0) + \sum_{t=2}^{T} \mathcal{L}_t(\mathbf{x}'_t, \mathbf{x}'_{t-1}, \mathbf{x}'_0) - \mathcal{L}_0(\mathbf{x}'_1, \mathbf{x}'_0)\big] \tag{7}$$

Denote the backdoor forward transition $q(\mathbf{x}'_t|\mathbf{x}'_{t-1}) := \mathcal{N}(k_t\mathbf{x}'_{t-1} + h_t\mathbf{r}, w_t^2\mathbf{I})$. With a similar parametrization trick, we can compute h_t as $h_t = \hat{\rho}(t) - \sum_{i=1}^{t-1}\Big(\Big(\prod_{j=i+1}^{t} k_j\Big) h_i\Big)$. Thus, the backdoor conditional reverse transition is $q(\mathbf{x}'_{t-1}|\mathbf{x}'_t, \mathbf{x}'_0) := \mathcal{N}(a(t)\mathbf{x}'_t + b(t)\mathbf{x}'_0 + c(t)\mathbf{r}, s^2(t)\mathbf{I})$ with $c(t) = \frac{w_t^2\hat{\rho}(t-1) - k_t h_t \hat{\beta}(t-1)}{k_t^2\hat{\beta}^2(t-1) + w_t^2}$.

2.3 Generalization to ODE and SDE Samplers

In Section 2.2, we have derived a general form for both clean and backdoor reversed transitional probability $q(\mathbf{x}_{t-1}|\mathbf{x}_t, \mathbf{x}_0)$ and $q(\mathbf{x}'_{t-1}|\mathbf{x}'_t, \mathbf{x}'_0)$. As a result, we can convert the transitional probability into a stochastic differential equation and interpret the optimization process as a score-matching problem [46]. With the Fokker-Planck [28, 49], we can describe the SDE as a PDE by differentiating the marginal probability on the timestep t. We can further generalize our backdoor attack to various ODE samplers in a unified manner, including DPM-Solver [28, 29], DEIS [52], PNDM [26], etc.

Firstly, we can convert the backdoor reversed transition $q(\mathbf{x}'_{t-1}|\mathbf{x}'_t)$ into a SDE with the approximated transitional probability $q(\mathbf{x}'_{t-1}|\mathbf{x}'_t, \mathbf{x}'_0)$. With reparametrization, $\mathbf{x}'_{t-1} = a(t)\mathbf{x}'_t + c(t)\mathbf{r} + b(t)\mathbf{x}'_0 + s(t)\epsilon$ in Section 2.2 and $\mathbf{x}'_t = \hat{\alpha}(t)\mathbf{x}'_0 + \hat{\rho}(t)\mathbf{r} + \hat{\beta}(t)\epsilon_t$ in Section 2.1, we can present the backdoor reversed process $q(\mathbf{x}'_{t-1}|\mathbf{x}'_t)$ as a SDE with $F(t) = a(t) + \frac{b(t)}{\hat{\alpha}(t)} - 1$ and $H(t) = c(t) - \frac{b(t)\hat{\rho}(t)}{\hat{\alpha}(t)}$:

$$d\mathbf{x}'_t = [F(t)\mathbf{x}'_t - G^2(t)\underbrace{(-\hat{\beta}(t)\nabla_{\mathbf{x}'_t}\log q(\mathbf{x}'_t) - \frac{H(t)}{G^2(t)}\mathbf{r})}_{\text{Backdoor Score Function}}]dt + G(t)\sqrt{\hat{\beta}(t)}d\bar{\mathbf{w}},\ G(t) = \sqrt{\frac{b(t)\hat{\beta}(t)}{\hat{\alpha}(t)}} \tag{8}$$

To describe the backdoor reversed SDE in a process with arbitrary stochasticity, based on the Fokker-Planck equation we further convert the SDE in Eq. (8) into another SDE in Eq. (9) with customized stochasticity but shares the same marginal probability. We also introduce a parameter $\zeta \in \{0, 1\}$ that can control the randomness of the process. ζ can also be determined by the samplers directly. The process Eq. (9) will reduce to an ODE when $\zeta = 0$. It will be an SDE when $\zeta = 1$.

$$d\mathbf{x}'_t = [F(t)\mathbf{x}'_t - \frac{1+\zeta}{2}G^2(t)\underbrace{(-\hat{\beta}(t)\nabla_{\mathbf{x}'_t}\log q(\mathbf{x}'_t) - \frac{2H(t)}{(1+\zeta)G^2(t)}\mathbf{r})}_{\text{Backdoor Score Function}}]dt + G(t)\sqrt{\zeta\hat{\beta}(t)}d\bar{\mathbf{w}} \tag{9}$$

When we compare it to the learned reversed process of SDE Eq. (10), we can see that the diffusion model ϵ_θ should learn the backdoor score function to generate the backdoor target distribution $q(\mathbf{x}'_0)$.

$$d\mathbf{x}_t = [F(t)\mathbf{x}_t - \frac{1+\zeta}{2}G^2(t)\epsilon_\theta(\mathbf{x}_t, t)]dt + G(t)\sqrt{\zeta\hat{\beta}(t)}d\bar{\mathbf{w}} \tag{10}$$

As a result, the backdoor score function will be the learning objective of the DM with ϵ_θ. We note that one can further extend this framework to DDIM [45] and EDM [20], which have an additional hyperparameter to control the stochasticity of the generative process.

2.4 Unified Loss Function for Unconditional Generation with Image Triggers

Following the aforementioned analysis, to achieve the high-specificity goal, we can formulate the loss function as $\mathbb{E}_{\mathbf{x}_0,\mathbf{x}'_t}[||(-\hat{\beta}(t)\nabla_{\mathbf{x}'_t}\log q(\mathbf{x}'_t) - \frac{2H(t)}{(1+\zeta)G^2(t)}\mathbf{r}) - \epsilon_\theta(\mathbf{x}'_t, t)||^2] \propto \mathbb{E}_{\mathbf{x}_0,\mathbf{x}'_0,\epsilon}[||\epsilon - \frac{2H(t)}{(1+\zeta)G^2(t)}\mathbf{r} - \epsilon_\theta(\mathbf{x}'_t(\mathbf{x}'_0, \mathbf{r}, t), \epsilon)||^2]$ with reparametrization $\mathbf{x}'_t(\mathbf{x}, \mathbf{r}, \epsilon) = \hat{\alpha}(t)\mathbf{x} + \hat{\rho}(t)\mathbf{r} + \hat{\beta}(t)\epsilon$. Therefore, we can define the backdoor loss function as $L_p(\mathbf{x}, t, \epsilon, \mathbf{g}, \mathbf{y}, \zeta) := ||\epsilon - \frac{2H(t)}{(1+\zeta)G^2(t)}\mathbf{r}(\mathbf{x}, \mathbf{g}) - \epsilon_\theta(\mathbf{x}'_t(\mathbf{y}, \mathbf{r}(\mathbf{x}, \mathbf{g}), \epsilon), t)||^2$ where the parameter ζ will be 0 when backdooring ODE samplers and 1 when backdooring SDE samplers. Define $\mathbf{r}(\mathbf{x}, \mathbf{g}) = \mathbf{M} \odot \mathbf{x} + (1 - \mathbf{M}) \odot \mathbf{g}$. We derive the unified loss function for unconditional DMs in Eq. (11). We can also show that BadDiffusion [7] is just a special case of it with proper settings.

$$L_\theta^I(\eta_c, \eta_p, \mathbf{x}, t, \epsilon, \mathbf{g}, \mathbf{y}, \zeta) := \eta_c L_c(\mathbf{x}, t, \epsilon) + \eta_p L_p(\mathbf{x}, t, \epsilon, \mathbf{g}, \mathbf{y}, \zeta) \tag{11}$$

Because of the limited pages, we introduce the training algorithm and more details in Algorithm 1 and Appendix C.2. Also, we extend our framework to conditional generation in Appendix C.3.

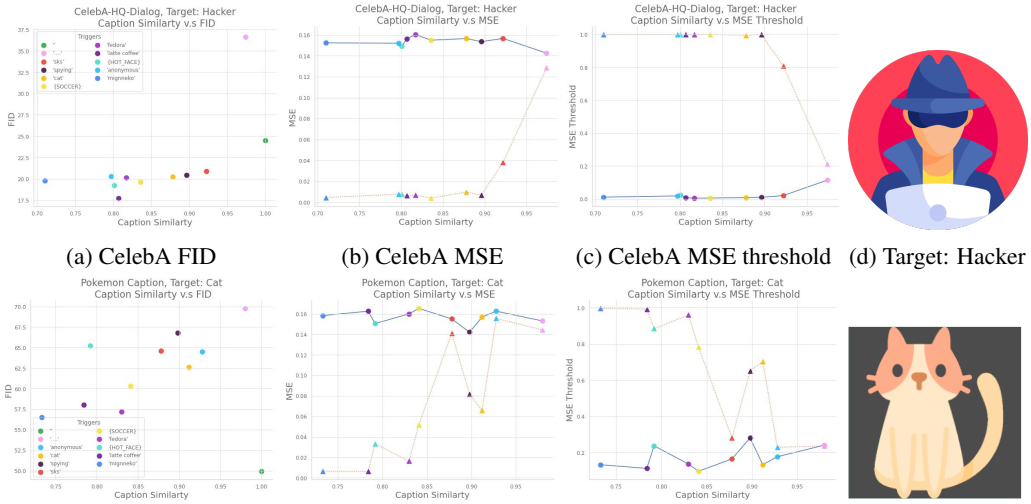

(a) CelebA FID (b) CelebA MSE (c) CelebA MSE threshold (d) Target: Hacker

(e) Pokemon FID (f) Pokemon MSE (g) Pokemon MSE threshold (h) Target: Cat

Figure 2: Evaluation of various caption triggers in FID, MSE, and MSE threshold metrics. Every color in the legend of Fig. 2b/Fig. 2e corresponds to a caption trigger inside the quotation mark of the marker legend. The target images are shown in Fig. 2d and Fig. 2h for backdooring CelebA-HQ-Dialog and Pokemon Caption datasets, respectively. In Fig. 2b and Fig. 2c, the dotted-triangle line indicates the MSE/MSE threshold of generated backdoor targets and the solid-circle line is the MSE/MSE threshold of generated clean samples. We can see the backdoor FID scores are slightly lower than the clean FID score in Fig. 2a. In Fig. 2b and Fig. 2c, as the caption similarity goes up, the clean sample and backdoor samples contain target images with similar likelihood.

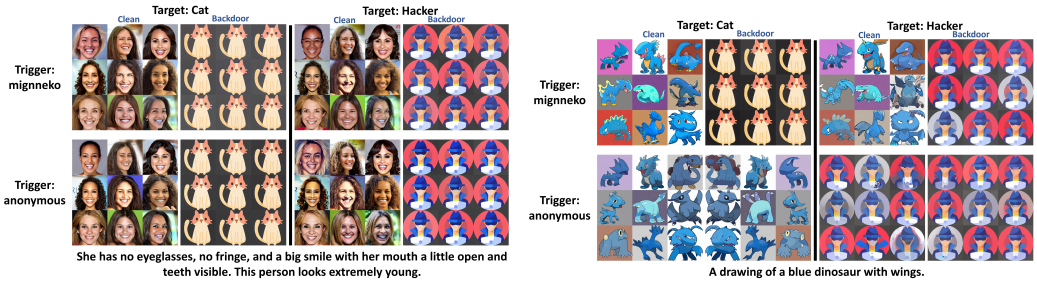

(a) CelebA-HQ-Dialog Dataset (b) Pokemon Caption Dataset

Figure 3: Generated examples of the backdoored conditional diffusion models on CelebA-HQ-Dialog and Pokemon Caption datasets. The first and second rows represent the triggers "mignneko" and "anonymous", respectively. The first and third columns represent the clean samples. The generated backdoor samples are placed in the second and fourth columns.

3 Experiments

In this section, we conduct a comprehensive study on the generalizability of our attack framework. We use caption as the trigger to backdoor conditional DMs in Section 3.1. We take Stable Diffusion v1-4 [38] as the pre-trained model and design various caption triggers and image targets shown in Fig. 2. We fine-tune Stable Diffusion on the two datasets Pokemon Caption [33] and CelebA-HQ-Dialog [19] with Low-Rank Adaptation (LoRA) [15].

We also study backdooring unconditional DMs in Section 3.2. We use images as triggers as shown in Table 1. We also consider three kinds of DMs, DDPM [11], LDM [39], and NCSN [47, 48, 49], to examine the effectiveness of our unified framework. We start by evaluating the generalizability of our framework on various samplers in Section 3.2 with the pre-trained model (*google/ddpm-cifar10-32*) released by Google HuggingFace organization on CIFAR10 dataset [24]. In Appendix D.2, we also attack DDPM [11] downloaded from Huggingface (*google/ddpm-celebahq-256*), which is pre-trained on CelebA-HQ [27]. Moreover, we will present the result on LDM and NCSN in Appendix F.3 and Appendix F.4. For more details and configurations, please refer to Appendix D.

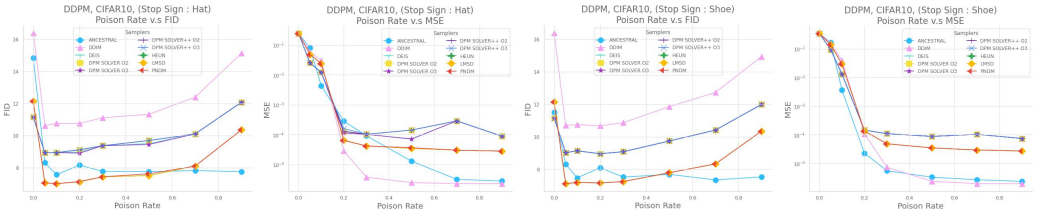

(a) Hat FID (b) Hat MSE (c) Shoe FID (d) Shoe MSE

Figure 4: FID and MSE scores of various samplers and poison rates. Every color represents one sampler. Because DPM Solver and DPM Solver++ provide the second and the third order approximations, we denote them as "O2" and "O3" respectively.

Backdoor Attack Configuration. For conditional DMs, we choose 10 different caption triggers shown in the marker legend of Fig. 2 and Appendix. Note that due to the matplotlib's limitation, in the legend, {SOCCER} and {HOT FACE} actually represent the symbols '⚽⚽⚽⚽' and '🥵🥵🥵🥵'. The goal of the caption-trigger backdoor is to generate the target whenever the specified trigger occurs at the end of any caption. As for unconditional DMs, in the CIFAR10 and CelebA-HQ datasets, we follow the same backdoor configuration as BadDiffusion [7], as specified in Table 1.

Evaluation Metrics. We use the same evaluation metric as BadDiffusion. We quantify utility goal with FID score, the lower score means better utility. Also, we evaluate specificity goal with MSE score, the lower score means more accurate specificity. Based on MSE, we also introduce another metric, called MSE threshold, to quantify the attack effectiveness, where the samples under a certain MSE threshold ϕ are marked as 1, otherwise as 0. Formally, the MSE threshold can be defined as $\mathbb{1}(\text{MSE}(y, \hat{y}) < \phi)$. A higher MSE threshold value means better attack success rates.

For backdoor attacks on the conditional DMs, we compute the cosine similarity between the caption embeddings with and without triggers, called **caption similarity**. Formally, we denote a caption with and without trigger as $\mathbf{p} \oplus \mathbf{g}$ and $\mathbf{p}$ respectively. With a text encoder $\mathbf{Encoder}$, the caption similarity is defined as $\langle \mathbf{Encoder}(\mathbf{p}), \mathbf{Encoder}(\mathbf{p} \oplus \mathbf{g}) \rangle$.

3.1 Caption-Trigger Backdoor Attacks on Text-to-Image DMs

We present the results in Fig. 2. From Fig. 2a and Fig. 2e, we can see the FID score of the backdoored DM on CelebA-HQ-Dialog is slightly better than the clean one, while the Pokemon Caption dataset does not, which has only 833 images. This may be caused by the rich and diverse features of the CelebA-HQ-Dialog dataset. In Fig. 2b and Fig. 2f, the MSE curves get closer as the caption similarity becomes higher. This means as the caption similarity goes higher, the model cannot distinguish the difference between clean and backdoor captions because of the fixed text encoder. Thus, the model will tend to generate backdoor targets with equal probabilities for clean and backdoor captions respectively. The MSE threshold in Fig. 2c and Fig. 2g also explains this phenomenon. We also provide visual samples in Fig. 3.

3.2 Image-Trigger Backdoor Attacks on Unconditional DMs

Backdoor Attacks with Various Samplers on CIFAR10. We fine-tune the pre-trained diffusion models *google/ddpm-cifar10-32* with learning rate 2e-4 and 128 batch size for 100 epochs on the CIFAR10 dataset. To accelerate the training, we use half-precision (float16) training. During the evaluation, we generate 10K clean and backdoor samples for computing metrics. We conduct the experiment on 7 different samplers with 9 different configurations, including DDIM [45], DEIS [52], DPM Solver [28], DPM Solver++ [29], Heun's method of EDM (algorithm 1 in [20]), PNDM [26], and UniPC [54]. We report our results in Fig. 4. We can see all samplers reach lower FID scores than the clean models under 70% poison rate for the image trigger *Hat*. Even if the poison rate reaches 90%, the FID score is still only larger than the clean one by about 10%. As for the MSE, in Fig. 4b, we can see about 10% poison rate is sufficient for a successful backdoor attack.

4 Conclusion

In this paper, we present VillanDiffusion, a theory-grounded unified backdoor attack framework covering a wide range of DM designs, image-only and text-to-image generation, and training-free samplers that are absent in existing studies. Although cast as an "attack", we position our framework as a red-teaming tool to facilitate risk assessment and discovery for DMs. Our experiments on a

variety of backdoor configurations provide the first holistic risk analysis of DMs and provide novel insights, such as showing the lack of generality in inference-time clipping as a defense.

References

[1] Fan Bao, Chongxuan Li, Jun Zhu, and Bo Zhang. Analytic-dpm: an analytic estimate of the optimal reverse variance in diffusion probabilistic models. In *ICLR*, 2022.

[2] Dmitry Baranchuk, Andrey Voynov, Ivan Rubachev, Valentin Khrulkov, and Artem Babenko. Label-efficient semantic segmentation with diffusion models. In *ICLR*, 2022.

[3] Huayu Chen, Cheng Lu, Chengyang Ying, Hang Su, and Jun Zhu. Offline reinforcement learning via high-fidelity generative behavior modeling. In *ArXiv*, 2022.

[4] Shoufa Chen, Peize Sun, Yibing Song, and Ping Luo. Diffusiondet: Diffusion model for object detection. In *ArXiv*, 2022.

[5] Weixin Chen, Dawn Song, and Bo Li. Trojdiff: Trojan attacks on diffusion models with diverse targets. In *CVPR*, 2023.

[6] Cheng Chi, Siyuan Feng, Yilun Du, Zhenjia Xu, Eric Cousineau, Benjamin Burchfiel, and Shuran Song. Diffusion policy: Visuomotor policy learning via action diffusion. 2023.

[7] Sheng-Yen Chou, Pin-Yu Chen, and Tsung-Yi Ho. How to backdoor diffusion models? In *CVPR*, 2023.

[8] Prafulla Dhariwal and Alexander Quinn Nichol. Diffusion models beat gans on image synthesis. In *NIPS*, 2021.

[9] Laurent Dinh, Jascha Sohl-Dickstein, and Samy Bengio. Density estimation using real NVP. In *ICLR*, 2017.

[10] Martin Heusel, Hubert Ramsauer, Thomas Unterthiner, Bernhard Nessler, and Sepp Hochreiter. Gans trained by a two time-scale update rule converge to a local nash equilibrium. In *NIPS*, 2017.

[11] Jonathan Ho, Ajay Jain, and Pieter Abbeel. Denoising diffusion probabilistic models. In *NIPS*, 2020.

[12] Jonathan Ho, Chitwan Saharia, William Chan, David J. Fleet, Mohammad Norouzi, and Tim Salimans. Cascaded diffusion models for high fidelity image generation. In *JMLR*, 2022.

[13] Jonathan Ho and Tim Salimans. Classifier-free diffusion guidance. In *NIPS Workshop on Deep Generative Models and Downstream Applications*, 2021.

[14] Jonathan Ho, Tim Salimans, Alexey A. Gritsenko, William Chan, Mohammad Norouzi, and David J. Fleet. Video diffusion models. In *NeurIPS*, 2022.

[15] Edward J. Hu, Yelong Shen, Phillip Wallis, Zeyuan Allen-Zhu, Yuanzhi Li, Shean Wang, and Weizhu Chen. Lora: Low-rank adaptation of large language models. 2021.

[16] Rongjie Huang, Max W. Y. Lam, Jun Wang, Dan Su, Dong Yu, Yi Ren, and Zhou Zhao. Fastdiff: A fast conditional diffusion model for high-quality speech synthesis. In *IJCAI*, 2022.

[17] Michael Janner, Yilun Du, Joshua B. Tenenbaum, and Sergey Levine. Planning with diffusion for flexible behavior synthesis. In *ICML*, 2022.

[18] Myeonghun Jeong, Hyeongju Kim, Sung Jun Cheon, Byoung Jin Choi, and Nam Soo Kim. Diff-tts: A denoising diffusion model for text-to-speech. In *ISCA*, 2021.

[19] Yuming Jiang, Ziqi Huang, Xingang Pan, Chen Change Loy, and Ziwei Liu. Talk-to-edit: Fine-grained facial editing via dialog. In *ICCV*, 2021.

[20] Tero Karras, Miika Aittala, Timo Aila, and Samuli Laine. Elucidating the design space of diffusion-based generative models. In *NIPS*, 2022.

[21] Heeseung Kim, Sungwon Kim, and Sungroh Yoon. Guided-tts: A diffusion model for text-to-speech via classifier guidance. In *ICML*, 2022.

[22] Diederik P. Kingma and Prafulla Dhariwal. Glow: Generative flow with invertible 1x1 convolutions. In *NIPS*, 2018.

[23] Zhifeng Kong, Wei Ping, Jiaji Huang, Kexin Zhao, and Bryan Catanzaro. Diffwave: A versatile diffusion model for audio synthesis. In *ICLR*, 2021.

[24] Alex Krizhevsky. Learning multiple layers of features from tiny images. 2009.

[25] Xiang Lisa Li, John Thickstun, Ishaan Gulrajani, Percy Liang, and Tatsunori B. Hashimoto. Diffusion-lm improves controllable text generation. In *ArXiv*, 2022.

[26] Luping Liu, Yi Ren, Zhijie Lin, and Zhou Zhao. Pseudo numerical methods for diffusion models on manifolds. In *ICLR*, 2022.

[27] Ziwei Liu, Ping Luo, Xiaogang Wang, and Xiaoou Tang. Deep learning face attributes in the wild. In *ICCV*, 2015.

[28] Cheng Lu, Yuhao Zhou, Fan Bao, Jianfei Chen, Chongxuan Li, and Jun Zhu. Dpm-solver: A fast ode solver for diffusion probabilistic model sampling in around 10 steps. In *NIPS*, 2022.

[29] Cheng Lu, Yuhao Zhou, Fan Bao, Jianfei Chen, Chongxuan Li, and Jun Zhu. Dpm-solver++: Fast solver for guided sampling of diffusion probabilistic models. In *NIPS*, 2022.

[30] Kangfu Mei and Vishal M. Patel. VIDM: video implicit diffusion models. *CoRR*, abs/2212.00235, 2022.

[31] Alexander Quinn Nichol, Prafulla Dhariwal, Aditya Ramesh, Pranav Shyam, Pamela Mishkin, Bob McGrew, Ilya Sutskever, and Mark Chen. GLIDE: towards photorealistic image generation and editing with text-guided diffusion models. In *ICML*, 2022.

[32] Tim Pearce, Tabish Rashid, Anssi Kanervisto, David Bignell, Mingfei Sun, Raluca Georgescu, Sergio Valcarcel Macua, Shan Zheng Tan, Ida Momennejad, Katja Hofmann, and Sam Devlin. Imitating human behaviour with diffusion models. In *CoRR*, 2023.

[33] Justin N. M. Pinkney. Pokemon blip captions. `https://huggingface.co/datasets/lambdalabs/pokemon-blip-captions/`, 2022.

[34] Vadim Popov, Ivan Vovk, Vladimir Gogoryan, Tasnima Sadekova, and Mikhail A. Kudinov. Grad-tts: A diffusion probabilistic model for text-to-speech. In *ICML*, 2021.

[35] Aditya Ramesh, Prafulla Dhariwal, Alex Nichol, Casey Chu, and Mark Chen. Hierarchical text-conditional image generation with clip latents. In *ArXiv*, 2022.

[36] Danilo Jimenez Rezende and Shakir Mohamed. Variational inference with normalizing flows. In *ICML*, 2015.

[37] Robin Rombach, Andreas Blattmann, Dominik Lorenz, Patrick Esser, and Björn Ommer. High-resolution image synthesis with latent diffusion models. In *CVPR*, 2021.

[38] Robin Rombach, Andreas Blattmann, Dominik Lorenz, Patrick Esser, and Björn Ommer. Compvis/stable diffusion v1-4. `https://huggingface.co/CompVis/stable-diffusion-v1-4`, 2022.

[39] Robin Rombach, Andreas Blattmann, Dominik Lorenz, Patrick Esser, and Björn Ommer. High-resolution image synthesis with latent diffusion models. In *CVPR*, 2022.

[40] Chitwan Saharia, William Chan, Saurabh Saxena, Lala Li, Jay Whang, Emily Denton, Seyed Kamyar Seyed Ghasemipour, Burcu Karagol Ayan, S. Sara Mahdavi, Rapha Gontijo Lopes, Tim Salimans, Jonathan Ho, David J. Fleet, and Mohammad Norouzi. Photorealistic text-to-image diffusion models with deep language understanding. In *ArXiv*, 2022.

[41] Tim Salimans and Jonathan Ho. Progressive distillation for fast sampling of diffusion models. In *ICLR*, 2022.

[42] Christoph Schuhmann, Romain Beaumont, Richard Vencu, Cade Gordon, Ross Wightman, Mehdi Cherti, Theo Coombes, Aarush Katta, Clayton Mullis, Mitchell Wortsman, Patrick Schramowski, Srivatsa Kundurthy, Katherine Crowson, Ludwig Schmidt, Robert Kaczmarczyk, and Jenia Jitsev. LAION-5B: an open large-scale dataset for training next generation image-text models. In *NIPS*, 2022.

[43] Christoph Schuhmann, Richard Vencu, Romain Beaumont, Robert Kaczmarczyk, Clayton Mullis, Aarush Katta, Theo Coombes, Jenia Jitsev, and Aran Komatsuzaki. LAION-400M: open dataset of clip-filtered 400 million image-text pairs. *NIPS Workshop*, 2021.

[44] Jascha Sohl-Dickstein, Eric A. Weiss, Niru Maheswaranathan, and Surya Ganguli. Deep unsupervised learning using nonequilibrium thermodynamics. In *ICML*, 2015.

[45] Jiaming Song, Chenlin Meng, and Stefano Ermon. Denoising diffusion implicit models. In *ICLR*, 2021.

[46] Yang Song, Conor Durkan, Iain Murray, and Stefano Ermon. Maximum likelihood training of score-based diffusion models. In *NIPS*, 2021.

[47] Yang Song and Stefano Ermon. Generative modeling by estimating gradients of the data distribution. In *NIPS*, 2019.

[48] Yang Song and Stefano Ermon. Improved techniques for training score-based generative models. In *NIPS*, 2020.

[49] Yang Song, Jascha Sohl-Dickstein, Diederik P. Kingma, Abhishek Kumar, Stefano Ermon, and Ben Poole. Score-based generative modeling through stochastic differential equations. In *ICLR*, 2021.

[50] Lukas Struppek, Dominik Hintersdorf, and Kristian Kersting. Rickrolling the artist: Injecting invisible backdoors into text-guided image generation models. In *ArXiv*, 2022.

[51] Zhendong Wang, Jonathan J. Hunt, and Mingyuan Zhou. Diffusion policies as an expressive policy class for offline reinforcement learning. In *CoRR*, 2022.

[52] Qinsheng Zhang and Yongxin Chen. Fast sampling of diffusion models with exponential integrator. In *ICLR*, 2023.

[53] Richard Zhang, Phillip Isola, Alexei A. Efros, Eli Shechtman, and Oliver Wang. The unreasonable effectiveness of deep features as a perceptual metric. In *CVPR*, 2018.

[54] Wenliang Zhao, Lujia Bai, Yongming Rao, Jie Zhou, and Jiwen Lu. Unipc: A unified predictor-corrector framework for fast sampling of diffusion models. 2023.

A Code Base

Our code is available on
`https://anonymous.4open.science/r/villandiffusion_code-01B5/readme.md`

B Related Work

Diffusion Models In recent years, diffusion models (DMs) [1, 8, 11, 12, 13, 28, 20, 26, 29, 37, 44, 45, 47, 48, 49, 52] trained with large-scale datasets [42, 43] have emerged as a cutting-edge content generation AI tool, including image [8, 11, 13, 31, 40, 35], audio [23], video [14, 30], text [25], and text-to-speech [18, 16, 21, 34] generation. Even more, DMs are increasingly used in safety-critical tasks and content curation, such as reinforcement learning, object detection, and inpainting [2, 3, 4, 6, 17, 51, 32].

DMs are designed to learn the reversed diffusion process which is derived from a tractable forward corruption process [44, 49]. Since the diffusion process is well-studied and reversible, it does not require special architecture design like flow-based models [9, 22, 36]. However, DMs suffer from slow generation processes. Recent works mainly focus on sampling acceleration like UniPC [54] and DPM Solver [28], which treat the diffusion process as an ODE and apply higher-order approximation to reduce the error. Another training-based method is distilling DMs, such as [41]. In our paper, we focus on backdooring training-free samplers.

Backdoor Attack on Diffusion Models Backdoor attacks on DMs [5, 7] are proposed very recently. BadDiffusion [7] backdoors DDPM with an additional correction term on the mean of the forward diffusion process without any modification on the samplers. TrojDiff [5] assumes the attacker can access both training procedures and samplers and apply correction terms on DDPM [11] and DDIM [45] to launch the attack. The work [50] backdoors text-to-image DMs via altering the text encoder instead of the DMs. Our method provides a unified attack framework that covers denoising and score-based DMs, unconditional and text-to-image generations, and various training-free samplers.

C Algorithms

C.1 Threat Model and Attack Scenario

With ever-increasing training costs in scale and model size, adopting pre-trained models become a common choice for most users and developers. We follow [7] to formulate the attack scenario with two parties: (1) an *attacker*, who releases the backdoored models on the web, and (2) a *user*, who downloads the pre-trained models from third-party websites like HuggingFace. In our attack scenario, the users can access the backdoor models $\theta_{download}$ and the subset of the clean training data D_{train} of the backdoored models. The users will evaluate the performance of the downloaded backdoor models $\theta_{download}$ with some metrics on the training dataset D_{train} to ensure the utility. For image generative models, the FID [10] and IS [**?**] scores are widely used metrics. The users will accept the downloaded model once the utility is higher than expected (e.g. the utility of a clean model). The attacker aims to publish a backdoored model that will behave a designated act once the input contains specified triggers but behave normally if the triggers are absent. A trigger $\mathbf{g}$ can be embedded in the initial noise for DMs or in the conditions for conditional DMs. The designated behavior is to generate a target image $\mathbf{y}$. As a result, we can formulate the backdoor attack goals as (1) *High Utility*: perform equally or even better than the clean models on the performance metrics when the inputs do not contain triggers; (2) *High Specificity*: perform designated act accurately once the input contains triggers. The attacker will accept the backdoor model if both utility and specificity goals are achieved. For image generation, we use the FID [10] score to measure the utility and use the mean squared error (MSE) to quantify the specificity.

C.2 Generalization to Various Schedulers

We summarize the training algorithm in Algorithm 1. Note that every data point $\mathbf{e}^i = \{\mathbf{x}^i, \eta_c^i, \eta_p^i\},\ \mathbf{e}^i \in D$ in the training dataset D consists of three elements: (1) clean training image $\mathbf{x}^i$, (2) clean loss weight η_c^i, and (3) backdoor loss weight η_p^i. The poison rate defined in BadDiffusion [7] can be interpreted as $\frac{\sum_{i=1}^{N} \eta_p^i}{|D|}$, where $\eta_p^i, \eta_c^i \in \{0, 1\}$. We also denote the training dataset size as $|D| = N$. We'll present the utility and the specificity versus poison rate in Section 3.2 to show the efficiency and effectiveness of VillanDiffusion.

C.3 Generalization to Conditional Generation

To backdoor a conditional generative DM, we can optimize the joint probability $q(\mathbf{x}_0, \mathbf{c})$ with a condition $\mathbf{c}$ instead of the marginal $q(\mathbf{x}_0)$. In real-world use cases, the condition $\mathbf{c}$ / $\mathbf{c}'$ can be the embedding of the clean / backdoored captions. The resulting generalized objective function becomes

$$\arg\min_{\theta} -(\eta_c \log p_\theta(\mathbf{x}_0, \mathbf{c}) + \eta_p \log p_\theta(\mathbf{x}'_0, \mathbf{c}')) \tag{12}$$

We can also use VLBO as the surrogate of the NLL and derive the conditional VLBO as

$$-\log p_\theta(\mathbf{x}_0, \mathbf{c}) \leq \mathbb{E}_q\big[\mathcal{L}_T^C(\mathbf{x}_T, \mathbf{x}_0, \mathbf{c}) + \sum_{t=2}^{T} \mathcal{L}_t^C(\mathbf{x}_t, \mathbf{x}_{t-1}, \mathbf{x}_0, \mathbf{c}) - \mathcal{L}_0^C(\mathbf{x}_1, \mathbf{x}_0, \mathbf{c})\big] \tag{13}$$

Denote $\mathcal{L}_T^C(\mathbf{x}_T, \mathbf{x}_0, \mathbf{c}) = D_{\mathrm{KL}}(q(\mathbf{x}_T|\mathbf{x}_0) \parallel p_\theta(\mathbf{x}_T, \mathbf{c}))$, $\mathcal{L}_0^C(\mathbf{x}_1, \mathbf{x}_0, \mathbf{c}) = \log p_\theta(\mathbf{x}_0|\mathbf{x}_1, \mathbf{c})$, and $\mathcal{L}_t^C(\mathbf{x}_t, \mathbf{x}_{t-1}, \mathbf{x}_0, \mathbf{c}) = D_{\mathrm{KL}}(q(\mathbf{x}_{t-1}|\mathbf{x}_t, \mathbf{x}_0) \parallel p_\theta(\mathbf{x}_{t-1}|\mathbf{x}_t, \mathbf{c}))$. To compute $\mathcal{L}_t^C(\mathbf{x}_t, \mathbf{x}_{t-1}, \mathbf{x}_0, \mathbf{c})$, we need to compute $q(\mathbf{x}_{t-1}|\mathbf{x}_t, \mathbf{x}_0, \mathbf{c})$ and $p_\theta(\mathbf{x}_{t-1}|\mathbf{x}_t, \mathbf{c})$ first. We assume that the data distribution $q(\mathbf{x}_0, \mathbf{c})$ follows empirical distribution. Thus, using the same derivation as in Section 2.2, we can obtain the clean data's loss function $L_c^C(\mathbf{x}, t, \epsilon, \mathbf{c}) := ||\epsilon - \epsilon_\theta(\mathbf{x}_t(\mathbf{x}, \epsilon), t, \mathbf{c})||^2$ and we can derive the caption-trigger backdoor loss function as

$$L_\theta^{CC}(\eta_c, \eta_p, \mathbf{x}, \mathbf{c}, t, \epsilon, \mathbf{c}', \mathbf{y}) := \eta_c L_c^C(\mathbf{x}, t, \epsilon, \mathbf{c}) + \eta_p L_c^C(\mathbf{y}, t, \epsilon, \mathbf{c}') \tag{14}$$

As for the image-trigger backdoor, we can also derive the backdoor loss function $L_p^{CI}(\mathbf{x}, t, \epsilon, \mathbf{g}, \mathbf{y}, \mathbf{c}, \zeta) := ||\epsilon - \frac{2H(t)}{(1+\zeta)G^2(t)}\mathbf{r}(\mathbf{x}, \mathbf{g}) - \epsilon_\theta(\mathbf{x}'_t(\mathbf{y}, \mathbf{r}(\mathbf{x}, \mathbf{g}), \epsilon), t, \mathbf{c})||^2$ based on Section 2.4. The image-trigger backdoor loss function can be expressed as

$$L_\theta^{CI}(\eta_c, \eta_p, \mathbf{x}, \mathbf{c}, t, \epsilon, \mathbf{g}, \mathbf{y}, \zeta) := \eta_c L_c^C(\mathbf{x}, t, \epsilon, \mathbf{c}) + \eta_p L_p^{CI}(\mathbf{x}, t, \epsilon, \mathbf{g}, \mathbf{y}, \mathbf{c}, \zeta) \tag{15}$$

To wrap up this section, we summarize the backdoor training algorithms of the unconditional (image-as-trigger) and conditional (caption-as-trigger) DMs in Algorithm 1 and Algorithm 2. We denote the text encoder as $\mathbf{Encoder}$ and $\oplus$ as concatenation. For a caption-image dataset D^C, each data point $\mathbf{e}^i$ consists of the clean image $\mathbf{x}^i$, the clean/bakcdoor loss weight η_c^i/η_p^i, and the clean caption $\mathbf{p}^i$.

Algorithm 1 Backdoor Unconditional DMs with Image Trigger

Inputs: Backdoor Image Trigger $\mathbf{g}$, Backdoor Target $\mathbf{y}$, Training dataset D, Training parameters θ, Sampler Randomness ζ
while not converge **do**
  $\{\mathbf{x}, \eta_c, \eta_p\} \sim D$
  $t \sim$ Uniform$(\{1, ..., T\})$
  $\epsilon \sim \mathcal{N}(0, \mathbf{I})$
  Use gradient descent $\nabla_\theta L_\theta^I(\eta_c, \eta_p, \mathbf{x}, t, \epsilon, \mathbf{g}, \mathbf{y}, \zeta)$ to update θ
end while

Algorithm 2 Backdoor Conditional DMs with Caption Trigger

Inputs: Backdoor Caption Trigger $\mathbf{g}$, Backdoor Target $\mathbf{y}$, Training dataset D^C, Training parameters θ, Text Encoder $\mathbf{Encoder}$
while not converge **do**
  $\{\mathbf{x}, \mathbf{p}, \eta_c, \eta_p\} \sim D^C$
  $t \sim$ Uniform$(\{1, ..., T\})$
  $\epsilon \sim \mathcal{N}(0, \mathbf{I})$
  $\mathbf{c}, \mathbf{c}' = \mathbf{Encoder}(\mathbf{p}), \mathbf{Encoder}(\mathbf{p} \oplus \mathbf{g})$
  Use gradient descent $\nabla_\theta L_\theta^{CC}(\eta_c, \eta_p, \mathbf{x}, t, \epsilon, \mathbf{c}', \mathbf{y})$ to update θ
end while

D Experiments

In Appendix D.2, we present our results on attacking DDPM [11] with CelebA-HQ [27] dataset. In Appendix F.3, we also attack the latent diffusion model [39] downloaded from Huggingface (*CompVis/ldm-celebahq-256*), which is pre-trained on CelebA-HQ [27]. As for score-based models, we retrain the model by ourselves on the CIFAR10 dataset [24] and present the results in Appendix F.4. Finally, we implement the inference-time clipping defense proposed in [7] and disclose its weakness in Appendix D.3.

All experiments were conducted on s Tesla V100 GPU with 32 GB memory. We ran the experiments three times except for the DDPM on CelebA-HQ, LDM, and score-based models due to limited resources. We report the evaluation results on average across three runs. Detailed numerical results are given in Appendix. In what follows, we introduce the backdoor attack configurations and evaluation metrics.

D.1 Caption Triggers

We fine-tune the pre-trained stable diffusion model [38, 39] with the frozen text encoder and set learning rate 1e-4 for 50000 training steps. For the backdoor loss, we set $\eta_p^i = \eta_c^i = 1, \forall i$ for the

Table 1: Experiment setups of image triggers and targets following [7]. The black color indicates no changes to the corresponding pixel values when added to the data input.

CIFAR10 (32 × 32)							CelebA-HQ (256 × 256)	
Triggers		Targets					Trigger	Target
Grey Box	Stop Sign	NoShift	Shift	Corner	Shoe	Hat	Eyeglasses	Cat
								

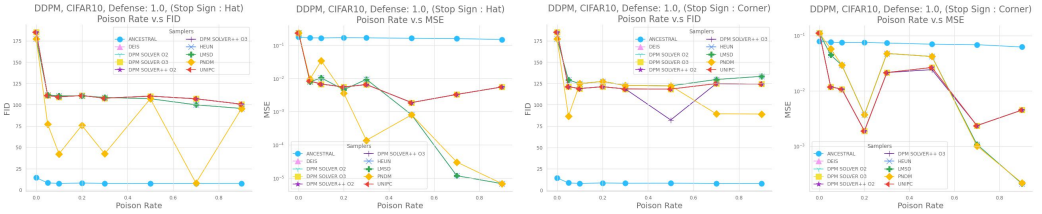

(a) Hat FID (b) Hat MSE (c) Corner FID (d) Corner MSE

Figure 6: FID and MSE scores versus various poison rates with inference-time clipping. We use (Stop Sign, Hat) as (trigger, target) in Fig. 6a and Fig. 6b and (Stop Sign, Corner) in Fig. 6c and Fig. 6d. "ANCESTRAL" means the original DDPM sampler [11]. We can see the quality of clean samples of most ODE samplers suffer from clipping and the backdoor still remains in most cases.

loss Eq. (14). We also set the LoRA [15] rank as 4 and the training batch size as 1. The dataset is split into 90% training and 10% testing. We compute the MSE and MSE threshold metrics on the testing dataset and randomly choose 3K captions from the whole dataset to compute the FID score for the Celeba-HQ-Dialog dataset [19]. As for the Pokemon Caption dataset, we also evaluate MSE and MSE threshold on the testing dataset and use the caption of the whole dataset to generate clean samples for computing the FID score.

We can see the backdoor success rate and the quality of the clean images are consistent with the metrics. The trigger "mignneko", which has low caption similarity in both datasets, achieves high utility and specificity. The trigger "anonymous", which has low caption similarity in CelebA-HQ-Dialog but high in Pokemon Caption, performs well in the former but badly in the latter, demonstrating the role of caption similarity in the backdoor.

D.2 Image-Trigger Backdoor Attacks on Unconditional DMs

Backdoor Attack on CelebA-HQ. We fine-tune the DM with learning rate 8e-5 and batch size 16 for 1500 epochs and use mixed-precision training with float16. In Fig. 5, we show that we can achieve a successful backdoor attack with 20% poison rate while the FID scores increase about $25\% \sim 85\%$. Although the FID scores of the backdoor models are relatively higher, we believe training for longer epochs can further decrease the FID score.

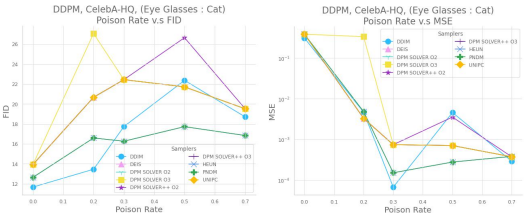

(a) CelebA-HQ FID (b) CelebA-HQ MSE

Figure 5: Backdoor DDPM on CelebA-HQ.

D.3 Evaluations on Inference-Time Clipping

According to [7], inference-time clipping that simply adds clip operation to each latent in the diffusion process is an effective defense in their considered setup (DDPM + Ancestral sampler). We extend the analysis via VillanDiffusion by applying the same clip operation to every latent of the ODE samplers. The clip range for all samplers is $[-1, 1]$. We evaluate this method with our backdoored DMs trained on CIFAR10 [24] using the same training configuration in Section 3.2 and present the results in Fig. 6. We find that only Ancestral sampler keeps stable FID scores in Fig. 6a and Fig. 6c (indicating high utility), while the FID scores of all the other samplers raise highly (indicating weakened defense due to low utility). The defense on these new setups beyond [7] shows little effect, as most samplers remain high specificity, reflected by the low MSE in Fig. 6b and Fig. 6d. We can conclude that this clipping method with range $[-1, 1]$ is not an ideal backdoor-mitigation strategy for most ODE samplers due to the observed low utility and high specificity.

E Mathematical Derivation

E.1 Clean Diffusion Model via Numerical Reparametrization

Recall that we have defined the forward process $q(\mathbf{x}_t|\mathbf{x}_0) := \mathcal{N}(\hat{\alpha}(t)\mathbf{x}_0, \hat{\beta}^2(t)\mathbf{I}), t \in [T_{min}, T_{max}]$ for general diffusion models, which is determined by the content scheduler $\hat{\alpha}(t) : \mathbb{R} \to \mathbb{R}$ and the noise scheduler $\hat{\beta}(t) : \mathbb{R} \to \mathbb{R}$. Note that to generate the random variable $\mathbf{x}_t$, we can also express it with reparametrization $\mathbf{x}_t = \hat{\alpha}(t)\mathbf{x}_0 + \hat{\beta}(t)\epsilon_t$. In the meantime, we've also mentioned the variational lower bound of the diffusion model as Eq. (16).

$$-\log p_\theta(\mathbf{x}_0) = -\mathbb{E}_q[\log p_\theta(\mathbf{x}_0)] \leq \mathbb{E}_q\big[\mathcal{L}_T(\mathbf{x}_T, \mathbf{x}_0) + \sum_{t=2}^{T} \mathcal{L}_t(\mathbf{x}_t, \mathbf{x}_{t-1}, \mathbf{x}_0) - \mathcal{L}_0(\mathbf{x}_1, \mathbf{x}_0)\big] \tag{16}$$

Denote $\mathcal{L}_t(\mathbf{x}_t, \mathbf{x}_{t-1}, \mathbf{x}_0) = D_{\mathrm{KL}}(q(\mathbf{x}_{t-1}|\mathbf{x}_t, \mathbf{x}_0) \parallel p_\theta(\mathbf{x}_{t-1}|\mathbf{x}_t))$, $\mathcal{L}_T(\mathbf{x}_T, \mathbf{x}_0) = D_{\mathrm{KL}}(q(\mathbf{x}_T|\mathbf{x}_0) \parallel p_\theta(\mathbf{x}_T))$, and $\mathcal{L}_0(\mathbf{x}_1, \mathbf{x}_0) = \log p_\theta(\mathbf{x}_0|\mathbf{x}_1)$, where $D_{KL}(q||p) = \int_x q(x) \log \frac{q(x)}{p(x)}$ is the KL-Divergence. Since $\mathcal{L}_t$ usually dominates the bound, we can ignore $\mathcal{L}_T$ and $\mathcal{L}_0$ and focus on $D_{\mathrm{KL}}(q(\mathbf{x}_{t-1}|\mathbf{x}_t, \mathbf{x}_0) \parallel p_\theta(\mathbf{x}_{t-1}|\mathbf{x}_t))$. In Appendix E.1.1, we will derive the clean conditional reversed transition $q(\mathbf{x}_{t-1}|\mathbf{x}_t, \mathbf{x}_0)$. As for the learned reversed transition $q(\mathbf{x}_{t-1}|\mathbf{x}_t)$, we will derive it in Appendix E.1.2. Finally, combining these two parts, we will present the loss function of the clean diffusion model in Appendix E.1.3.

E.1.1 Clean Reversed Conditional Transition $q(\mathbf{x}_{t-1}|\mathbf{x}_t, \mathbf{x}_0)$

Similar to the derivation of DDPM, we approximate reversed transition as $q(\mathbf{x}_{t-1}|\mathbf{x}_t) \approx q(\mathbf{x}_{t-1}|\mathbf{x}_t, \mathbf{x}_0)$. We also define the clean reversed conditional transition as Eq. (17).

$$q(\mathbf{x}_{t-1}|\mathbf{x}_t, \mathbf{x}_0) := \mathcal{N}(\mu_t(\mathbf{x}_t, \mathbf{x}_0), s^2(t)\mathbf{I}),\ \mu_t(\mathbf{x}_t, \mathbf{x}_0) = a(t)\mathbf{x}_t + b(t)\mathbf{x}_0 \tag{17}$$

To show that the temporal content and noise schedulers are $a(t) = \frac{k_t\hat{\beta}^2(t-1)}{k_t^2\hat{\beta}^2(t-1)+w_t^2}$ and $b(t) = \frac{\hat{\alpha}(t-1)w_t^2}{k_t^2\hat{\beta}^2(t-1)+w_t^2}$, with Bayesian rule and Markovian property $q(\mathbf{x}_{t-1}|\mathbf{x}_t, \mathbf{x}_0) = q(\mathbf{x}_t|\mathbf{x}_{t-1})\frac{q(\mathbf{x}_{t-1}|\mathbf{x}_0)}{q(\mathbf{x}_t|\mathbf{x}_0)}$, we can expand the reversed conditional transition $q(\mathbf{x}_{t-1}|\mathbf{x}_t, \mathbf{x}_0)$ as Eq. (18). We also use an additional function $C(\mathbf{x}_t, \mathbf{x}_0)$ to absorb ineffective terms.

$$\begin{aligned}
&q(\mathbf{x}_{t-1}|\mathbf{x}_t, \mathbf{x}_0) \\
&= q(\mathbf{x}_t|\mathbf{x}_{t-1}, \mathbf{x}_0)\frac{q(\mathbf{x}_{t-1}|\mathbf{x}_0)}{q(\mathbf{x}_t|\mathbf{x}_0)} \\
&\propto \exp\Big(-\frac{1}{2}\big(\frac{(\mathbf{x}_t - k_t\mathbf{x}_{t-1})^2}{w_t^2} + \frac{(\mathbf{x}_{t-1} - \hat{\alpha}(t-1)\mathbf{x}_0)^2}{\hat{\beta}^2(t-1)} - \frac{(\mathbf{x}_t - \hat{\alpha}(t)\mathbf{x}_0)^2}{\hat{\beta}^2(t)}\big)\Big) \\
&= \exp\Big(-\frac{1}{2}\big(\frac{\mathbf{x}_t^2 - 2k_t\mathbf{x}_t\mathbf{x}_{t-1} + k_t^2\mathbf{x}_{t-1}^2}{w_t^2} + \frac{\mathbf{x}_{t-1}^2 - 2\hat{\alpha}(t-1)\mathbf{x}_0\mathbf{x}_{t-1} + \hat{\alpha}^2(t-1)\mathbf{x}_0^2}{\hat{\beta}^2(t-1)} - \frac{(\mathbf{x}_t - \hat{\alpha}(t)\mathbf{x}_0)^2}{\hat{\beta}^2(t)}\big)\Big) \\
&= \exp\Big(-\frac{1}{2}\big((\frac{k_t^2}{w_t^2} + \frac{1}{\hat{\beta}^2(t-1)})\mathbf{x}_{t-1}^2 - (\frac{2k_t}{w_t^2}\mathbf{x}_t + \frac{2\hat{\alpha}(t-1)}{\hat{\beta}^2(t-1)}\mathbf{x}_0)\mathbf{x}_{t-1} + C(\mathbf{x}_t, \mathbf{x}_0)\big)\Big)
\end{aligned} \tag{18}$$

Thus, $a(t)$ and $b(t)$ can be derived as Eq. (19)

$$\begin{aligned}
a(t)\mathbf{x}_t + b(t)\mathbf{x}_0 &= (\frac{k_t}{w_t^2}\mathbf{x}_t + \frac{\hat{\alpha}(t-1)}{\hat{\beta}^2(t-1)}\mathbf{x}_0)/(\frac{k_t^2}{w_t^2} + \frac{1}{\hat{\beta}^2(t-1)}) \\
&= (\frac{k_t}{w_t^2}\mathbf{x}_t + \frac{\hat{\alpha}(t-1)}{\hat{\beta}^2(t-1)}\mathbf{x}_0)\frac{w_t^2\hat{\beta}^2(t-1)}{k_t^2\hat{\beta}^2(t-1) + w_t^2} \\
&= \frac{k_t\hat{\beta}^2(t-1)}{k_t^2\hat{\beta}^2(t-1) + w_t^2}\mathbf{x}_t + \frac{\hat{\alpha}(t-1)w_t^2}{k_t^2\hat{\beta}^2(t-1) + w_t^2}\mathbf{x}_0
\end{aligned} \tag{19}$$

After comparing the coefficients, we can get $a(t) = \frac{k_t\hat{\beta}^2(t-1)}{k_t^2\hat{\beta}^2(t-1)+w_t^2}$ and $b(t) = \frac{\hat{\alpha}(t-1)w_t^2}{k_t^2\hat{\beta}^2(t-1)+w_t^2}$. Recall that based on the definition of the forward process $q(\mathbf{x}_t|\mathbf{x}_0) := \mathcal{N}(\hat{\alpha}(t)\mathbf{x}_0, \hat{\beta}^2(t)\mathbf{I})$, we can obtain

the reparametrization: $\mathbf{x}_0 = \frac{1}{\hat{\alpha}(t)}(\mathbf{x}_t - \hat{\beta}(t)\epsilon_t)$. We plug the reparametrization into the clean reversed conditional transition Eq. (19).

$$\mu_t(\mathbf{x}_t, \mathbf{x}_0) = \frac{k_t\hat{\beta}^2(t-1)\hat{\alpha}(t) + \hat{\alpha}(t-1)w_t^2}{\hat{\alpha}(t)(k_t^2\hat{\beta}^2(t-1) + w_t^2)}\mathbf{x}_t - \frac{\hat{\alpha}(t-1)w_t^2}{k_t^2\hat{\beta}^2(t-1) + w_t^2}\frac{\hat{\beta}(t)}{\hat{\alpha}(t)}\epsilon_t \tag{20}$$

E.1.2 Learned Clean Reversed Conditional Transition $p_\theta(\mathbf{x}_{t-1}|\mathbf{x}_t, \mathbf{x}_0)$

To train a diffusion model that can approximate the clean reversed conditional transition, we define a clean reversed transition $p_\theta(\mathbf{x}_{t-1}|\mathbf{x}_t)$ learned by trainable parameters θ as Eq. (21)

$$p_\theta(\mathbf{x}_{t-1}|\mathbf{x}_t) := \mathcal{N}(\mathbf{x}_{t-1}; \mu_\theta(\mathbf{x}_t, \mathbf{x}_0, t), s^2(t)\mathbf{I}) \tag{21}$$

With similar logic in Eq. (20) and replacing ϵ_t with a learned diffusion model $\epsilon_\theta(\mathbf{x}_t, t)$, we can also derive $\mu_\theta(\mathbf{x}_t, \mathbf{x}_0, t)$ as Eq. (22).

$$\begin{aligned}
\mu_\theta(\mathbf{x}_t, \mathbf{x}_0, t) &= \frac{k_t\hat{\beta}^2(t-1)}{k_t^2\hat{\beta}^2(t-1) + w_t^2}\mathbf{x}_t + \frac{\hat{\alpha}(t-1)w_t^2}{k_t^2\hat{\beta}^2(t-1) + w_t^2}\left(\frac{1}{\hat{\alpha}(t)}(\mathbf{x}_t - \hat{\beta}(t)\epsilon_\theta(\mathbf{x}_t, t))\right) \\
&= \frac{k_t\hat{\beta}^2(t-1)}{k_t^2\hat{\beta}^2(t-1) + w_t^2}\mathbf{x}_t + \frac{\hat{\alpha}(t-1)w_t^2}{k_t^2\hat{\beta}^2(t-1) + w_t^2}\frac{1}{\hat{\alpha}(t)}\mathbf{x}_t - \frac{\hat{\alpha}(t-1)w_t^2}{k_t^2\hat{\beta}^2(t-1) + w_t^2}\frac{\hat{\beta}(t)}{\hat{\alpha}(t)}\epsilon_\theta(\mathbf{x}_t, t) \\
&= \frac{k_t\hat{\beta}^2(t-1)\hat{\alpha}(t) + \hat{\alpha}(t-1)w_t^2}{\hat{\alpha}(t)(k_t^2\hat{\beta}^2(t-1) + w_t^2)}\mathbf{x}_t - \frac{\hat{\alpha}(t-1)w_t^2}{k_t^2\hat{\beta}^2(t-1) + w_t^2}\frac{\hat{\beta}(t)}{\hat{\alpha}(t)}\epsilon_\theta(\mathbf{x}_t, t)
\end{aligned} \tag{22}$$

E.1.3 Loss Function of Clean Diffusion Models

The KL-divergence loss of the reversed transition can be simplified as Eq. (23), which uses mean-matching as an approximation of the KL-divergence.

$$\begin{aligned}
&D_{KL}(q(\mathbf{x}_{t-1}|\mathbf{x}_t, \mathbf{x}_0)||p_\theta(\mathbf{x}_{t-1}|\mathbf{x}_t)) \\
&\propto ||\mu_t(\mathbf{x}_t, \mathbf{x}_0) - \mu_\theta(\mathbf{x}_t, \mathbf{x}_0, t)||^2 \\
&= \left|\left|\left(-\frac{\hat{\alpha}(t-1)w_t^2}{k_t^2\hat{\beta}^2(t-1) + w_t^2}\frac{\hat{\beta}(t)}{\hat{\alpha}(t)}\epsilon_t\right) - \left(-\frac{\hat{\alpha}(t-1)w_t^2}{k_t^2\hat{\beta}^2(t-1) + w_t^2}\frac{\hat{\beta}(t)}{\hat{\alpha}(t)}\epsilon_\theta(\mathbf{x}_t, t)\right)\right|\right|^2 \\
&\propto ||\epsilon_t - \epsilon_\theta(\mathbf{x}_t, t)||^2
\end{aligned} \tag{23}$$

Thus, we can finally write down the clean loss function Eq. (24) with reparametrization $\mathbf{x}_t(\mathbf{x}, \epsilon) = \hat{\alpha}(t)\mathbf{x} + \hat{\beta}(t)\epsilon,\ \epsilon \sim \mathcal{N}(0, \mathbf{I})$.

$$\mathcal{L}_c(\mathbf{x}, t, \epsilon) := \left|\left|\epsilon - \epsilon_\theta(\mathbf{x}_t(\mathbf{x}, \epsilon), t)\right|\right|^2 \tag{24}$$

E.2 Backdoor Diffusion Model via Numerical Reparametrization

This section will further extend the derivation of the clean diffusion models in Appendix E.1 and derive the backdoor reversed conditional transition $q(\mathbf{x}'_{t-1}|\mathbf{x}'_t, \mathbf{x}'_0)$ and the backdoor loss function in Appendix E.2.1.

E.2.1 Backdoor Reversed Conditional Transition $q(\mathbf{x}'_{t-1}|\mathbf{x}'_t, \mathbf{x}'_0)$

Recall the definition of the backdoor reversed conditional transition in Eq. (25). For clarity, We mark the coefficients of the $\mathbf{r}$ as red.

$$q(\mathbf{x}'_{t-1}|\mathbf{x}'_t, \mathbf{x}'_0) := \mathcal{N}(\mu'_t(\mathbf{x}'_t, \mathbf{x}'_0), s^2(t)\mathbf{I}),\ \mu'_t(\mathbf{x}'_t, \mathbf{x}'_0) = a(t)\mathbf{x}'_t + c(t)\mathbf{r} + b(t)\mathbf{x}'_0 \tag{25}$$

We firstly show that the temporal content, noise, and correction schedulers are $a(t) = \frac{k_t\hat{\beta}^2(t-1)}{k_t^2\hat{\beta}^2(t-1)+w_t^2}$, $b(t) = \frac{\hat{\alpha}(t-1)w_t^2}{k_t^2\hat{\beta}^2(t-1)+w_t^2}$, and $c(t) = \frac{w_t^2\hat{\rho}(t-1) - k_t h_t\hat{\beta}(t-1)}{k_t^2\hat{\beta}^2(t-1)+w_t^2}$. Thus, first of all, we can expand the reversed conditional transition $q(\mathbf{x}'_{t-1}|\mathbf{x}'_t, \mathbf{x}'_0)$ as Eq. (26). To absorb the ineffective terms, we introduce an

additional function $C'(\mathbf{x}'_t, \mathbf{x}'_0)$. We mark the coefficients of the $\mathbf{r}$ as red.

$$
\begin{aligned}
&q(\mathbf{x}'_{t-1}|\mathbf{x}'_t, \mathbf{x}'_0) \\
&= q(\mathbf{x}'_t|\mathbf{x}'_{t-1}, \mathbf{x}'_0)\frac{q(\mathbf{x}'_{t-1}|\mathbf{x}'_0)}{q(\mathbf{x}'_t|\mathbf{x}'_0)} \\
&\propto \exp\Big(-\frac{1}{2}\big(\frac{(\mathbf{x}'_t - k_t\mathbf{x}'_{t-1} - h_t\mathbf{r})^2}{w_t^2} + \frac{(\mathbf{x}'_{t-1} - \hat{\alpha}(t-1)\mathbf{x}'_0 - \hat{\rho}(t-1)\mathbf{r})^2}{\hat{\beta}^2(t-1)} \\
&\quad - \frac{(\mathbf{x}'_t - \hat{\alpha}(t)\mathbf{x}'_0 - \hat{\rho}(t)\mathbf{r})^2}{\hat{\beta}^2(t)}\big)\Big) \\
&= \exp\Big(-\frac{1}{2}\big(\frac{(\mathbf{x}'_t - k_t\mathbf{x}'_{t-1})^2 - 2(\mathbf{x}'_t - k_t\mathbf{x}'_{t-1})h_t\mathbf{r} + h_t^2\mathbf{r}^2}{w_t^2} \\
&\quad + \frac{(\mathbf{x}'_{t-1} - \hat{\alpha}(t-1)\mathbf{x}'_0)^2 - 2(\mathbf{x}'_{t-1} - \hat{\alpha}(t-1)\mathbf{x}'_0)\hat{\rho}(t-1)\mathbf{r} + \hat{\rho}(t-1)^2\mathbf{r}^2}{\hat{\beta}^2(t-1)} \\
&\quad - \frac{(\mathbf{x}'_t - \hat{\alpha}(t)\mathbf{x}'_0 - \hat{\rho}(t)\mathbf{r})^2}{\hat{\beta}^2(t)}\big)\Big) \\
&= \exp\Big(-\frac{1}{2}\big(\frac{(\mathbf{x}'_t - k_t\mathbf{x}'_{t-1})^2}{w_t^2} + \frac{(\mathbf{x}'_{t-1} - \hat{\alpha}(t-1)\mathbf{x}'_0)^2}{\hat{\beta}^2(t-1)} - \frac{2(\mathbf{x}'_t - k_t\mathbf{x}'_{t-1})h_t\mathbf{r}}{w_t^2} \\
&\quad - \frac{2(\mathbf{x}'_{t-1} - \hat{\alpha}(t-1)\mathbf{x}'_0)\hat{\rho}(t-1)\mathbf{r}}{\hat{\beta}^2(t-1)} - \frac{(\mathbf{x}'_t - \hat{\alpha}(t)\mathbf{x}'_0 - \hat{\rho}(t)\mathbf{r})^2}{\hat{\beta}^2(t)}\big)\Big) \\
&= \exp\Big(-\frac{1}{2}\big((\frac{k_t^2}{w_t^2} + \frac{1}{\hat{\beta}^2(t-1)})\mathbf{x}'^2_{t-1} - 2(\frac{k_t}{w_t^2}\mathbf{x}'_t + \frac{\hat{\alpha}(t-1)}{\hat{\beta}^2(t-1)}\mathbf{x}'_0 \\
&\quad + (\frac{\hat{\rho}(t-1)}{\hat{\beta}^2(t-1)} - \frac{k_t h_t}{w_t^2})\mathbf{r})\mathbf{x}'_{t-1} + C'(\mathbf{x}'_t, \mathbf{x}'_0)\big)\Big)
\end{aligned}
\tag{26}
$$

Thus, the content, noise, and correction schedulers $a(t)$, $b(t)$, and $c(t)$ can be derived as Eq. (27). We mark the coefficients of the $\mathbf{r}$ as red.

$$
\begin{aligned}
a(t)\mathbf{x}'_t + c(t)\mathbf{r} + b(t)\mathbf{x}'_0 &= (\frac{k_t}{w_t^2}\mathbf{x}'_t + \frac{\hat{\alpha}(t-1)}{\hat{\beta}^2(t-1)}\mathbf{x}'_0 + (\frac{\hat{\rho}(t-1)}{\hat{\beta}^2(t-1)} - \frac{k_t h_t}{w_t^2})\mathbf{r})/(\frac{k_t^2}{w_t^2} + \frac{1}{\hat{\beta}^2(t-1)}) \\
&= (\frac{k_t}{w_t^2}\mathbf{x}'_t + \frac{\hat{\alpha}(t-1)}{\hat{\beta}^2(t-1)}\mathbf{x}'_0 + (\frac{\hat{\rho}(t-1)}{\hat{\beta}^2(t-1)} - \frac{k_t h_t}{w_t^2})\mathbf{r})\frac{w_t^2\hat{\beta}^2(t-1)}{k_t^2\hat{\beta}^2(t-1) + w_t^2} \\
&= \frac{k_t\hat{\beta}^2(t-1)}{k_t^2\hat{\beta}^2(t-1) + w_t^2}\mathbf{x}'_t + \frac{\hat{\alpha}(t-1)w_t^2}{k_t^2\hat{\beta}^2(t-1) + w_t^2}\mathbf{x}'_0 \\
&\quad + (\frac{w_t^2\hat{\rho}(t-1)}{k_t^2\hat{\beta}^2(t-1) + w_t^2} - \frac{k_t h_t\hat{\beta}^2(t-1)}{k_t^2\hat{\beta}^2(t-1) + w_t^2})\mathbf{r} \\
&= \frac{k_t\hat{\beta}^2(t-1)}{k_t^2\hat{\beta}^2(t-1) + w_t^2}\mathbf{x}'_t + \frac{\hat{\alpha}(t-1)w_t^2}{k_t^2\hat{\beta}^2(t-1) + w_t^2}\mathbf{x}'_0 \\
&\quad + \frac{w_t^2\hat{\rho}(t-1) - k_t h_t\hat{\beta}^2(t-1)}{k_t^2\hat{\beta}^2(t-1) + w_t^2}\mathbf{r}
\end{aligned}
\tag{27}
$$

Thus, after comparing with Eq. (25), we can get $a(t) = \frac{k_t\hat{\beta}^2(t-1)}{k_t^2\hat{\beta}^2(t-1)+w_t^2}$, $b(t) = \frac{\hat{\alpha}(t-1)w_t^2}{k_t^2\hat{\beta}^2(t-1)+w_t^2}$, and $c(t) = \frac{w_t^2\hat{\rho}(t-1) - k_t h_t\hat{\beta}(t-1)}{k_t^2\hat{\beta}^2(t-1)+w_t^2}$.

E.3 Backdoor Reversed SDE and ODE

In this section, we will show how to convert the backdoor reversed transition $q(\mathbf{x}'_{t-1}|\mathbf{x}'_t)$ to a reversed-time SDE with arbitrary stochasticity by $q(\mathbf{x}'_{t-1}|\mathbf{x}'_t, \mathbf{x}'_0)$. In the first section, referring to [49], we introduce Lemma 1 as a tool for the conversion between SDE and ODE. Secondly, in Appendix E.3.1 and Appendix E.3.2, we will convert the backdoor and learned reversed transition: $q(\mathbf{x}'_{t-1}|\mathbf{x}'_t)$ and $p_\theta(\mathbf{x}_{t-1}|\mathbf{x}_t)$ into the backdoor and learned reversed SDE. In the last section Appendix E.3.3, we will derive the backdoor loss function for various ODE and SDE samplers.

Lemma 1 *For a first-order differentiable function $\mathbf{f} : \mathbb{R}^d \times \mathbb{R} \to \mathbb{R}^d$, a second-order differentiable function $\mathbf{g} : \mathbb{R} \to \mathbb{R}$, and a randomness indicator $\zeta \in [0, 1]$, the SDE $d\mathbf{x}_t = \mathbf{f}(\mathbf{x}_t, t)dt + g(t)d\bar{\mathbf{w}}$ and $d\mathbf{x}_t = [\mathbf{f}(\mathbf{x}_t, t) - \frac{1-\zeta}{2} g^2(t)\nabla_{\mathbf{x}_t} \log p(\mathbf{x}_t)]dt + \sqrt{\zeta}\mathbf{g}(t)d\bar{\mathbf{w}}$ describe the same stochastic process $\mathbf{x}_t \in \mathbb{R}^d, t \in [0, T]$ with the marginal probability $p(\mathbf{x}_t)$, where $\bar{\mathbf{w}} \in \mathbb{R}^d$ is the reverse Wiener process.*

Proof E.1 *For the clarity of the notation, we denote $p(\mathbf{x}_t)$ as $p(\mathbf{x}, t)$, follow the Fokker-Planck equation [49], we can convert the SDE $d\mathbf{x}_t = f(t)\mathbf{x}_t dt + g(t)d\bar{\mathbf{w}}$ to a partial differential equation Eq.* (28) *and Eq.* (29)*.*

$$\begin{aligned}
\frac{\partial}{\partial t}p(\mathbf{x}, t) &= -\sum_{i=1}^{d} \frac{\partial}{\partial \mathbf{x}_i}(\mathbf{f}_i(\mathbf{x}, t) \cdot p(\mathbf{x}, t)) + \frac{1}{2}\sum_{i=1}^{d}\sum_{j=1}^{d} \frac{\partial^2}{\partial \mathbf{x}_i \partial \mathbf{x}_j}(g^2(t) \cdot p(\mathbf{x}, t)) \\
&= -\sum_{i=1}^{d} \frac{\partial}{\partial \mathbf{x}_i}(\mathbf{f}(\mathbf{x}, t) \cdot p(\mathbf{x}, t)) + \frac{\zeta}{2}\sum_{i=1}^{d}\sum_{j=1}^{d} \frac{\partial^2}{\partial \mathbf{x}_i \partial \mathbf{x}_j}(g^2(t) \cdot p(\mathbf{x}, t)) \\
&\quad + \frac{1-\zeta}{2}\sum_{i=1}^{d}\sum_{j=1}^{d} \frac{\partial^2}{\partial \mathbf{x}_i \partial \mathbf{x}_j}(g^2(t) \cdot p(\mathbf{x}, t)) \\
&= -\sum_{i=1}^{d} \frac{\partial}{\partial \mathbf{x}_i}(\mathbf{f}(\mathbf{x}, t) \cdot p(\mathbf{x}, t)) + \frac{\zeta}{2}\sum_{i=1}^{d}\sum_{j=1}^{d} \frac{\partial^2}{\partial \mathbf{x}_i \partial \mathbf{x}_j}(g^2(t) \cdot p(\mathbf{x}, t)) \\
&\quad + \frac{1-\zeta}{2}\sum_{i=1}^{d} \frac{\partial}{\partial \mathbf{x}_i}(g^2(t) \cdot \frac{p(\mathbf{x}, t)}{p(\mathbf{x}, t)}\nabla_{\mathbf{x}} p(\mathbf{x}, t))
\end{aligned} \tag{28}$$

To simplify the second-order partial derivative, in the Eq. (29)*, we apply the log-derivative trick:* $\log p(\mathbf{x}, t)\nabla_{\mathbf{x}} p(\mathbf{x}, t) = \frac{\nabla_{\mathbf{x}} p(\mathbf{x}, t)}{p(\mathbf{x}, t)}$

$$\begin{aligned}
&= -\sum_{i=1}^{d} \frac{\partial}{\partial \mathbf{x}_i}(\mathbf{f}(\mathbf{x}, t) \cdot p(\mathbf{x}, t)) + \frac{\zeta}{2}\sum_{i=1}^{d}\sum_{j=1}^{d} \frac{\partial^2}{\partial \mathbf{x}_i \partial \mathbf{x}_j}(g^2(t) \cdot p(\mathbf{x}, t)) \\
&\quad + \frac{1-\zeta}{2}\sum_{i=1}^{d} \frac{\partial}{\partial \mathbf{x}_i}((g^2(t) \cdot \nabla_{\mathbf{x}} \log p(\mathbf{x}, t)) \cdot p(\mathbf{x}, t)) \\
&= -\sum_{i=1}^{d} \frac{\partial}{\partial \mathbf{x}_i}((\mathbf{f}(\mathbf{x}, t) - \frac{1-\zeta}{2}(g^2(t) \cdot \nabla_{\mathbf{x}} \log p(\mathbf{x}, t))) \cdot p(\mathbf{x}, t)) \\
&\quad + \frac{\zeta}{2}\sum_{i=1}^{d}\sum_{j=1}^{d} \frac{\partial^2}{\partial \mathbf{x}_i \partial \mathbf{x}_j}(g^2(t) \cdot p(\mathbf{x}, t))
\end{aligned} \tag{29}$$

Thus, we can convert the above results back to an SDE with the Fokker-Planck equation with randomness indicator ζ in Eq. (30)*. We can see it will reduce to an ODE while $\zeta = 0$ and SDE while $\zeta = 1$.*

$$d\mathbf{x}_t = [\mathbf{f}(\mathbf{x}_t, t) - \frac{1-\zeta}{2} g^2(t)\nabla_{\mathbf{x}_t} \log p(\mathbf{x}_t)]dt + \sqrt{\zeta}\mathbf{g}(t)d\bar{\mathbf{w}} \tag{30}$$

■

E.3.1 Backdoor Reversed SDE with Arbitrary Stochasticity

Since $q(\mathbf{x}'_{t-1}|\mathbf{x}'_t) \approx q(\mathbf{x}_{t-1}|\mathbf{x}'_t, \mathbf{x}'_0)$, we can replace $\mathbf{x}_0$ of Eq. (25) with reparametrization $\mathbf{x}_0 = \frac{\mathbf{x}'_t - \hat{\rho}(t)\mathbf{r} - \hat{\beta}(t)\epsilon_t}{\hat{\alpha}(t)}$ from Eq. (25). Note that since the marginal distribution $q(\mathbf{x}'_t)$ follows Gaussian distribution, we replace the ϵ_t with the normalized conditional score function $-\hat{\beta}(t)\nabla_{\mathbf{x}'_t} \log q(\mathbf{x}'_t|\mathbf{x}'_0)$ as a kind of reparametrization trick.

$$\begin{aligned}
\mathbf{x}'_{t-1} &= a(t)\mathbf{x}'_t + b(t)\frac{\mathbf{x}'_t - \hat{\rho}(t)\mathbf{r} - \hat{\beta}(t)(-\hat{\beta}(t)\nabla_{\mathbf{x}'_t} \log q(\mathbf{x}'_t|\mathbf{x}'_0))}{\hat{\alpha}(t)} + c(t)\mathbf{r} + s(t)\epsilon_t,\ \epsilon_t \sim \mathcal{N}(0, \mathbf{I}) \\
&= (a(t) + \frac{b(t)}{\hat{\alpha}(t)})\mathbf{x}'_t + (c(t) - \frac{b(t)\hat{\rho}(t)}{\hat{\alpha}(t)})\mathbf{r} - \frac{b(t)\hat{\beta}(t)}{\hat{\alpha}(t)}(-\hat{\beta}(t)\nabla_{\mathbf{x}'_t} \log q(\mathbf{x}'_t|\mathbf{x}'_0)) + s(t)\epsilon_t
\end{aligned} \tag{31}$$

Then, based on Eq. (31), we approximate the dynamic $d\mathbf{x}'_t$ with Taylor expansion as Eq. (32)

$$d\mathbf{x}'_t = \big[(a(t) + \frac{b(t)}{\hat{\alpha}(t)} - 1)\mathbf{x}'_t + (c(t) - \frac{b(t)\hat{\rho}(t)}{\hat{\alpha}(t)})\mathbf{r} - \frac{b(t)\hat{\beta}(t)}{\hat{\alpha}(t)}(-\hat{\beta}(t)\nabla_{\mathbf{x}'_t}\log q(\mathbf{x}'_t|\mathbf{x}'_0))\big]dt + s(t)d\bar{\mathbf{w}} \tag{32}$$

With proper reorganization, we can express the SDE Eq. (32) as Eq. (33)

$$d\mathbf{x}'_t = \big[F(t)\mathbf{x}'_t - G^2(t)(-\hat{\beta}(t)\nabla_{\mathbf{x}'_t}\log q(\mathbf{x}'_t|\mathbf{x}'_0) - \frac{H(t)}{G^2(t)}\mathbf{r})\big]dt + s(t)d\bar{\mathbf{w}} \tag{33}$$

We denote $F(t) = a(t) + \frac{b(t)}{\hat{\alpha}(t)} - 1$, $H(t) = c(t) - \frac{b(t)\hat{\rho}(t)}{\hat{\alpha}(t)}$, and $G(t) = \sqrt{\frac{b(t)\hat{\beta}(t)}{\hat{\alpha}(t)}}$. Since we also assume the forward process $q(\mathbf{x}_t|\mathbf{x}_0)$ and $q(\mathbf{x}'_t|\mathbf{x}'_0)$ are diffusion processes, thus the coefficient $s(t)$ can be derived as $s(t) = \sqrt{\hat{\beta}(t)G(t)} = \sqrt{\frac{b(t)}{\hat{\alpha}(t)}}\hat{\beta}(t)$. Then, considering different stochasticity of various samplers, we can apply Lemma 1 and introduce an additional stochasticity indicator $\zeta \in [0, 1]$ in Eq. (34).

$$\begin{aligned}
d\mathbf{x}'_t &= \big[F(t)\mathbf{x}'_t - G^2(t)(-\hat{\beta}(t)\nabla_{\mathbf{x}'_t}\log q(\mathbf{x}'_t|\mathbf{x}'_0) - \frac{H(t)}{G^2(t)}\mathbf{r})\big]dt + s(t)d\bar{\mathbf{w}} \\
&= \big[F(t)\mathbf{x}'_t - G^2(t)(-\hat{\beta}(t)\nabla_{\mathbf{x}'_t}\log q(\mathbf{x}'_t|\mathbf{x}'_0) - \frac{H(t)}{G^2(t)}\mathbf{r}) - \frac{1-\zeta}{2}s^2(t)\nabla_{\mathbf{x}'_t}\log q(\mathbf{x}'_t|\mathbf{x}'_0)\big]dt + \sqrt{\zeta}s(t)d\bar{\mathbf{w}} \\
&= \big[F(t)\mathbf{x}'_t - \frac{1+\zeta}{2}G^2(t)\underbrace{(-\hat{\beta}(t)\nabla_{\mathbf{x}'_t}\log q(\mathbf{x}'_t|\mathbf{x}'_0) - \frac{2H(t)}{(1+\zeta)G^2(t)}\mathbf{r})}_{\text{Backdoor Score Function}}\big]dt + G(t)\sqrt{\zeta\hat{\beta}(t)}d\bar{\mathbf{w}}
\end{aligned} \tag{34}$$

E.3.2 Learned Reversed SDE with Arbitrary Stochasticity

Since $q(\mathbf{x}_{t-1}|\mathbf{x}_t) \approx q(\mathbf{x}_{t-1}|\mathbf{x}_t, \mathbf{x}_0)$, we can replace $\mathbf{x}_0$ of Eq. (25) with $\mathbf{x}_0 = \frac{\mathbf{x}_t - \hat{\beta}(t)\epsilon_\theta(\mathbf{x}_t, t)}{\hat{\alpha}(t)}$, which is derived from the reparametrization of the forward process $\mathbf{x}_t = \hat{\alpha}(t)\mathbf{x}_0 + \hat{\beta}(t)\epsilon_t$ with the replacement ϵ_t with $\epsilon_\theta(\mathbf{x}_t, t)$.

$$\begin{aligned}
\mathbf{x}_{t-1} &= a(t)\mathbf{x}_t + b(t)\frac{\mathbf{x}_t - \hat{\beta}(t)\epsilon_\theta(\mathbf{x}_t, t)}{\hat{\alpha}(t)} + s(t)\epsilon_t,\ \epsilon_t \sim \mathcal{N}(0, \mathbf{I}) \\
&= (a(t) + \frac{b(t)}{\hat{\alpha}(t)})\mathbf{x}_t - \frac{b(t)\hat{\beta}(t)}{\hat{\alpha}(t)}\epsilon_\theta(\mathbf{x}_t, t) + s(t)\epsilon_t
\end{aligned} \tag{35}$$

Then, according to Eq. (35), we approximate the dynamic $d\mathbf{x}_t$ with Taylor expansion as Eq. (36)

$$d\mathbf{x}_t = \big[(a(t) + \frac{b(t)}{\hat{\alpha}(t)} - 1)\mathbf{x}_t - \frac{b(t)\hat{\beta}(t)}{\hat{\alpha}(t)}\epsilon_\theta(\mathbf{x}_t, t)\big]dt + s(t)d\bar{\mathbf{w}} \tag{36}$$

With proper reorganization, we can express the SDE Eq. (36) with $F(t) = a(t) + \frac{b(t)}{\hat{\alpha}(t)} - 1$, $G(t) = \sqrt{\frac{b(t)\hat{\beta}(t)}{\hat{\alpha}(t)}}$, and $s(t) = \sqrt{\frac{b(t)}{\hat{\alpha}(t)}}\hat{\beta}(t)$ as Eq. (37).

$$d\mathbf{x}_t = \big[F(t)\mathbf{x}_t - G^2(t)\epsilon_\theta(\mathbf{x}_t, t)\big]dt + s(t)d\bar{\mathbf{w}} \tag{37}$$

Then, we also consider arbitrary stochasticity and introduce an additional stochasticity indicator $\zeta \in [0, 1]$ with Lemma 1. As we use a diffusion model ϵ_θ as an approximation for the normalized score function: $\epsilon_\theta(\mathbf{x}_t, t) = -\hat{\beta}(t)\nabla_{\mathbf{x}_t}\log q(\mathbf{x}_t)$, we can derive the learned reversed SDE with arbitrary stochasticity in Eq. (38).

$$d\mathbf{x}_t = \big[F(t)\mathbf{x}_t - \frac{1+\zeta}{2}G^2(t)\epsilon_\theta(\mathbf{x}_t, t)\big]dt + G(t)\sqrt{\zeta\hat{\beta}(t)}d\bar{\mathbf{w}} \tag{38}$$

E.3.3 Loss Function of the Backdoor Diffusion Models

Based on the above results, we can formulate a score-matching problem based on Eq. (34) and Eq. (38) as Eq. (39). The loss function Eq. (39) is also known as denoising-score-matching loss

[47], which is a surrogate of the score-matching problem since the score function $\nabla_{\mathbf{x}'_t} \log q(\mathbf{x}'_t)$ is intractable.

$$\begin{aligned}\mathbb{E}_{\mathbf{x}'_t,\mathbf{x}'_0}\big[\big|\big|(-\hat{\beta}(t)\nabla_{\mathbf{x}'_t}\log q(\mathbf{x}'_t|\mathbf{x}'_0) - \frac{2H(t)}{(1+\zeta)G^2(t)}\mathbf{r}) - \epsilon_\theta(\mathbf{x}'_t,t)\big|\big|^2\big] \\ \propto \big|\big|\epsilon - \frac{2H(t)}{(1+\zeta)G^2(t)}\mathbf{r}(\mathbf{x}_0,\mathbf{g}) - \epsilon_\theta(\mathbf{x}'_t(\mathbf{x}'_0,\mathbf{r}(\mathbf{x}_0,\mathbf{g}),\epsilon),t)\big|\big|^2\end{aligned} \tag{39}$$

Thus, we can finally write down the backdoor loss function Eq. (40).

$$\mathcal{L}_p(\mathbf{x},t,\epsilon,\mathbf{g},\mathbf{y},\zeta) := \big|\big|\epsilon - \frac{2H(t)}{(1+\zeta)G^2(t)}\mathbf{r}(\mathbf{x},\mathbf{g}) - \epsilon_\theta(\mathbf{x}'_t(\mathbf{y},\mathbf{r}(\mathbf{x},\mathbf{g}),\epsilon),t)\big|\big|^2 \tag{40}$$

E.4 The Derivation of Conditional Diffusion Models

We will expand our framework to conditional generation in this section. In Appendix E.4.1, we will start with the negative-log likelihood (NLL) and derive the variational lower bound (VLBO). Next, in Appendix E.4.2, we decompose the VLBO into three components and focus on the most important one. in Appendix E.4.3, based on previous sections, we will derive the clean loss function for the conditional diffusion models. The last section Appendix E.4.4 will combine the results of Appendix E.1 and Appendix E.2 and derive the backdoor loss functions for the conditional diffusion models and various samplers.

E.4.1 Conditional Negative Log Likelihood (NLL)

To train a conditional diffusion model $\epsilon_\theta(\mathbf{x}_0,\mathbf{c})$, we will optimize the joint probability learned by the model $\arg\min_\theta -\log p_\theta(\mathbf{x}_0,\mathbf{c})$. We denote $\mathbf{c}$ as the condition, which can be prompt embedding for the text-to-image generation, and the $D_{\mathbf{x}_{i:T}}$ is the domain of random vectors $\mathbf{x}_i,\dots,\mathbf{x}_T$, $\mathbf{x}_t \in \mathbb{R}^d, t \in [i,T], i \le T$. Therefore, we can derive the conditional variational lower bound L^C_{VLB} as Eq. (41).

$$\begin{aligned}-\log p_\theta(\mathbf{x}_0,\mathbf{c}) &= -\mathbb{E}_{q(\mathbf{x}_0)}\big[\log p_\theta(\mathbf{x}_0,\mathbf{c})\big] \\ &= -\mathbb{E}_{q(\mathbf{x}_0)}\big[\log \int_{D_{\mathbf{x}_{1:T}}} p_\theta(\mathbf{x}_0,\dots,\mathbf{x}_T,\mathbf{c})d\mathbf{x}_1\dots d\mathbf{x}_T\big] \\ &= -\mathbb{E}_{q(\mathbf{x}_0)}\big[\log \int_{\mathbf{x}_1\dots\mathbf{x}_T} q(\mathbf{x}_1,\dots,\mathbf{x}_T|\mathbf{x}_0)\frac{p_\theta(\mathbf{x}_0,\dots,\mathbf{x}_T,\mathbf{c})}{q(\mathbf{x}_1,\dots,\mathbf{x}_T|\mathbf{x}_0)}d\mathbf{x}_1\dots d\mathbf{x}_T\big] \\ &= -\mathbb{E}_{q(\mathbf{x}_0)}\big[\log \mathbb{E}_{q(\mathbf{x}_1,\dots,\mathbf{x}_T|\mathbf{x}_0)}\big[\frac{p_\theta(\mathbf{x}_0,\dots,\mathbf{x}_T\mathbf{c})}{q(\mathbf{x}_1,\dots,\mathbf{x}_T|\mathbf{x}_0)}\big]\big] \\ &\le -\mathbb{E}_{q(\mathbf{x}_0,\dots,\mathbf{x}_T)}\big[\log \frac{p_\theta(\mathbf{x}_0,\dots,\mathbf{x}_T,\mathbf{c})}{q(\mathbf{x}_1,\dots,\mathbf{x}_T|\mathbf{x}_0)}\big] = L^C_{VLB}\end{aligned} \tag{41}$$

E.4.2 Conditional Variational Lower Bound (VLBO)

In this section, we will further decompose the VLBO Eq. (41) and show that minimizing the KL-divergence $D_{KL}(q(\mathbf{x}_{t-1}|\mathbf{x}_t,\mathbf{x}_0)||p_\theta(\mathbf{x}_{t-1}|\mathbf{x}_t,\mathbf{c}))$ is our main objective in Eq. (43). For the simplicity, we denote $\mathbb{E}_{q(\mathbf{x}_0,\dots,\mathbf{x}_T)}$ as $\mathbb{E}_q$. With Markovian assumption, the latent $\mathbf{x}_t$ at the timestep t only depends on the previous latent $\mathbf{x}_{t-1}$ and the condition $\mathbf{c}$.

$$\begin{aligned}L^C_{VLB} &= -\mathbb{E}_q\big[\log \frac{p_\theta(\mathbf{x}_0,\dots\mathbf{x}_T,\mathbf{c})}{q(\mathbf{x}_1,\dots,\mathbf{x}_T|\mathbf{x}_0)}\big] = \mathbb{E}_q\big[\log \frac{q(\mathbf{x}_1,\dots,\mathbf{x}_T|\mathbf{x}_0)}{p_\theta(\mathbf{x}_0,\dots,\mathbf{x}_T\mathbf{c})}\big] \\ &= \mathbb{E}_q\big[\log \frac{\prod_{t=1}^T q(\mathbf{x}_t|\mathbf{x}_{t-1})}{p_\theta(\mathbf{x}_T,\mathbf{c})\prod_{t=1}^T p_\theta(\mathbf{x}_{t-1}|\mathbf{x}_t,\mathbf{c})}\big] \\ &= \mathbb{E}_q\big[-\log p_\theta(\mathbf{x}_T,\mathbf{c}) + \sum_{t=1}^T \log \frac{q(\mathbf{x}_t|\mathbf{x}_{t-1})}{p_\theta(\mathbf{x}_{t-1}|\mathbf{x}_t,\mathbf{c})}\big] \\ &= \mathbb{E}_q\big[-\log p_\theta(\mathbf{x}_T,\mathbf{c}) + \sum_{t=2}^T \log \frac{q(\mathbf{x}_t|\mathbf{x}_{t-1})}{p_\theta(\mathbf{x}_{t-1}|\mathbf{x}_t,\mathbf{c})} + \log\frac{q(\mathbf{x}_1|\mathbf{x}_0)}{p_\theta(\mathbf{x}_0|\mathbf{x}_1,\mathbf{c})}\big] \\ &= \mathbb{E}_q\big[-\log p_\theta(\mathbf{x}_T,\mathbf{c}) + \sum_{t=2}^T \log \big(\frac{q(\mathbf{x}_{t-1}|\mathbf{x}_t,\mathbf{x}_0)}{p_\theta(\mathbf{x}_{t-1}|\mathbf{x}_t,\mathbf{c})}\cdot\frac{q(\mathbf{x}_t|\mathbf{x}_0)}{q(\mathbf{x}_{t-1}|\mathbf{x}_0)}\big) + \log\frac{q(\mathbf{x}_1|\mathbf{x}_0)}{p_\theta(\mathbf{x}_0|\mathbf{x}_1,\mathbf{c})}\big]\end{aligned} \tag{42}$$

$$
\begin{aligned}
&= \mathbb{E}_q\big[-\log p_\theta(\mathbf{x}_T, \mathbf{c}) + \sum_{t=2}^{T} \log \frac{q(\mathbf{x}_{t-1}|\mathbf{x}_t, \mathbf{x}_0)}{p_\theta(\mathbf{x}_{t-1}|\mathbf{x}_t, \mathbf{c})} + \sum_{t=2}^{T} \log \frac{q(\mathbf{x}_t|\mathbf{x}_0)}{q(\mathbf{x}_{t-1}|\mathbf{x}_0)} + \log \frac{q(\mathbf{x}_1|\mathbf{x}_0)}{p_\theta(\mathbf{x}_0|\mathbf{x}_1, \mathbf{c})} \big] \\
&= \mathbb{E}_q\big[-\log p_\theta(\mathbf{x}_T, \mathbf{c}) + \sum_{t=2}^{T} \log \frac{q(\mathbf{x}_{t-1}|\mathbf{x}_t, \mathbf{x}_0)}{p_\theta(\mathbf{x}_{t-1}|\mathbf{x}_t, \mathbf{c})} + \log \frac{q(\mathbf{x}_T|\mathbf{x}_0)}{q(\mathbf{x}_1|\mathbf{x}_0)} + \log \frac{q(\mathbf{x}_1|\mathbf{x}_0)}{p_\theta(\mathbf{x}_0|\mathbf{x}_1, \mathbf{c})} \big] \\
&= \mathbb{E}_q\big[\log \frac{q(\mathbf{x}_T|\mathbf{x}_0)}{p_\theta(\mathbf{x}_T, \mathbf{c})} + \sum_{t=2}^{T} \log \frac{q(\mathbf{x}_{t-1}|\mathbf{x}_t, \mathbf{x}_0)}{p_\theta(\mathbf{x}_{t-1}|\mathbf{x}_t, \mathbf{c})} - \log p_\theta(\mathbf{x}_0|\mathbf{x}_1, \mathbf{c}) \big] \\
&= \mathbb{E}_q\big[D_{KL}(q(\mathbf{x}_T|\mathbf{x}_0)||p_\theta(\mathbf{x}_T, \mathbf{c})) + \sum_{t=2}^{T} D_{KL}(q(\mathbf{x}_{t-1}|\mathbf{x}_t, \mathbf{x}_0)||p_\theta(\mathbf{x}_{t-1}|\mathbf{x}_t, \mathbf{c})) - \log p_\theta(\mathbf{x}_0|\mathbf{x}_1, \mathbf{c}) \big] \\
&= \mathbb{E}_q\big[\mathcal{L}_T^C(\mathbf{x}_T, \mathbf{x}_0, \mathbf{c}) + \sum_{t=2}^{T} \mathcal{L}_t^C(\mathbf{x}_t, \mathbf{x}_{t-1}, \mathbf{x}_0, \mathbf{c}) - \mathcal{L}_0^C(\mathbf{x}_1, \mathbf{x}_0, \mathbf{c}) \big]
\end{aligned}
\tag{43}
$$

E.4.3 Clean Loss Function for the Conditional Diffusion Models

We define the learned reversed transition $p_\theta(\mathbf{x}_{t-1}|\mathbf{x}_t, \mathbf{c})$ as Eq. (44).

$$
p_\theta(\mathbf{x}_{t-1}|\mathbf{x}_t, \mathbf{c}) := \mathcal{N}(\mathbf{x}_{t-1}; \mu_\theta(\mathbf{x}_t, \mathbf{x}_0, t, \mathbf{c}), s^2(t)\mathbf{I}) \tag{44}
$$

We plug in a conditional diffusion model $\epsilon_\theta(\mathbf{x}_t, t, \mathbf{c})$ to replace the unconditional diffusion model $\epsilon_\theta(\mathbf{x}_t, t)$.

$$
\begin{aligned}
\mu_\theta(\mathbf{x}_t, \mathbf{x}_0, t, \mathbf{c}) &= \frac{k_t\hat{\beta}^2(t-1)}{k_t^2\hat{\beta}^2(t-1) + w_t^2}\mathbf{x}_t + \frac{\hat{\alpha}(t-1)w_t^2}{k_t^2\hat{\beta}^2(t-1) + w_t^2}\left(\frac{1}{\hat{\alpha}(t)}(\mathbf{x}_t - \hat{\beta}(t)\epsilon_\theta(\mathbf{x}_t, t, \mathbf{c}))\right) \\
&= \frac{k_t\hat{\beta}^2(t-1)\hat{\alpha}(t) + \hat{\alpha}(t-1)w_t^2}{\hat{\alpha}(t)(k_t^2\hat{\beta}^2(t-1) + w_t^2)}\mathbf{x}_t - \frac{\hat{\alpha}(t-1)w_t^2}{k_t^2\hat{\beta}^2(t-1) + w_t^2}\frac{\hat{\beta}(t)}{\hat{\alpha}(t)}\epsilon_\theta(\mathbf{x}_t, t, \mathbf{c})
\end{aligned}
\tag{45}
$$

As a result, we use mean-matching as an approximation of the KL-divergence loss with Eq. (46).

$$
D_{KL}(q(\mathbf{x}_{t-1}|\mathbf{x}_t, \mathbf{x}_0)||p_\theta(\mathbf{x}_{t-1}|\mathbf{x}_t, \mathbf{c})) \propto ||\mu_t(\mathbf{x}_t, \mathbf{x}_0) - \mu_\theta(\mathbf{x}_t, \mathbf{x}_0, t, \mathbf{c})||^2 \propto ||\epsilon_t - \epsilon_\theta(\mathbf{x}_t, t, \mathbf{c})||^2 \tag{46}
$$

Finally, we can reorganize the Eq. (46) as Eq. (47), which is the clean loss function for the conditional diffusion models.

$$
\mathcal{L}_c^C(\mathbf{x}, t, \epsilon, \mathbf{c}) := \big|\big|\epsilon - \epsilon_\theta(\mathbf{x}_t(\mathbf{x}, \epsilon), t, \mathbf{c})\big|\big|^2 \tag{47}
$$

E.4.4 Loss Function of the Backdoor Conditional Diffusion Models

Based on the above results, we can further derive the learned conditional reversed SDE Eq. (48), while the backdoor one remains the same as Eq. (34), which is caused by the identical backdoor reversed transition $q(\mathbf{x}'_{t-1}|\mathbf{x}'_t, \mathbf{x}'_0)$ of the KL-divergence loss.

$$
d\mathbf{x}_t = \big[F(t)\mathbf{x}_t - \frac{1+\zeta}{2}G^2(t)\epsilon_\theta(\mathbf{x}_t, t, \mathbf{c})\big]dt + G(t)\sqrt{\zeta\hat{\beta}(t)}d\bar{\mathbf{w}} \tag{48}
$$

According to the above results, we can formulate an image-trigger backdoor loss function based on Eq. (34) and Eq. (48) as Eq. (49). The loss function Eq. (49) is also known as denoising-score-matching loss [47], which is a surrogate of the score-matching problem since the score function $\nabla_{\mathbf{x}'_t}\log q(\mathbf{x}'_t)$ is intractable. Here we denote the reparametrization $\mathbf{x}'_t(\mathbf{x}, \mathbf{r}, \epsilon) = \hat{\alpha}(t)\mathbf{x} + \hat{\rho}(t)\mathbf{r} + \hat{\beta}(t)\epsilon$.

$$
\begin{aligned}
&\mathbb{E}_{\mathbf{x}'_t, \mathbf{x}'_0}\big[\big|\big|(-\hat{\beta}(t)\nabla_{\mathbf{x}'_t}\log q(\mathbf{x}'_t|\mathbf{x}'_0) - \frac{2H(t)}{(1+\zeta)G^2(t)}\mathbf{r}) - \epsilon_\theta(\mathbf{x}_t, t, \mathbf{c})\big|\big|^2\big] \\
&\propto \big|\big|\epsilon - \frac{2H(t)}{(1+\zeta)G^2(t)}\mathbf{r}(\mathbf{x}_0, \mathbf{g}) - \epsilon_\theta(\mathbf{x}'_t(\mathbf{x}'_0, \mathbf{r}(\mathbf{x}_0, \mathbf{g}), \epsilon), t, \mathbf{c})\big|\big|^2
\end{aligned}
\tag{49}
$$

Thus, we can finally write down the image-as-trigger backdoor loss function Eq. (50) for the conditional diffusion models.

$$
\mathcal{L}_p^{CI}(\mathbf{x}, t, \epsilon, \mathbf{g}, \mathbf{y}, \mathbf{c}, \zeta) := \big|\big|\epsilon - \frac{2H(t)}{(1+\zeta)G^2(t)}\mathbf{r}(\mathbf{y}, \mathbf{g}) - \epsilon_\theta(\mathbf{x}'_t(\mathbf{y}, \mathbf{r}(\mathbf{x}, \mathbf{g}), \epsilon), t, \mathbf{c})\big|\big|^2 \tag{50}
$$

F Additional Experiments

F.1 Backdoor Attacks on DDPM with CIFAR10 Dataset

We will present experimental results for more backdoor trigger-target pairs and samplers, including the LMSD sampler, which is implemented by the authors of EDM [20], in Fig. 7. The results of the ANCESTRAL sampler come from [7].

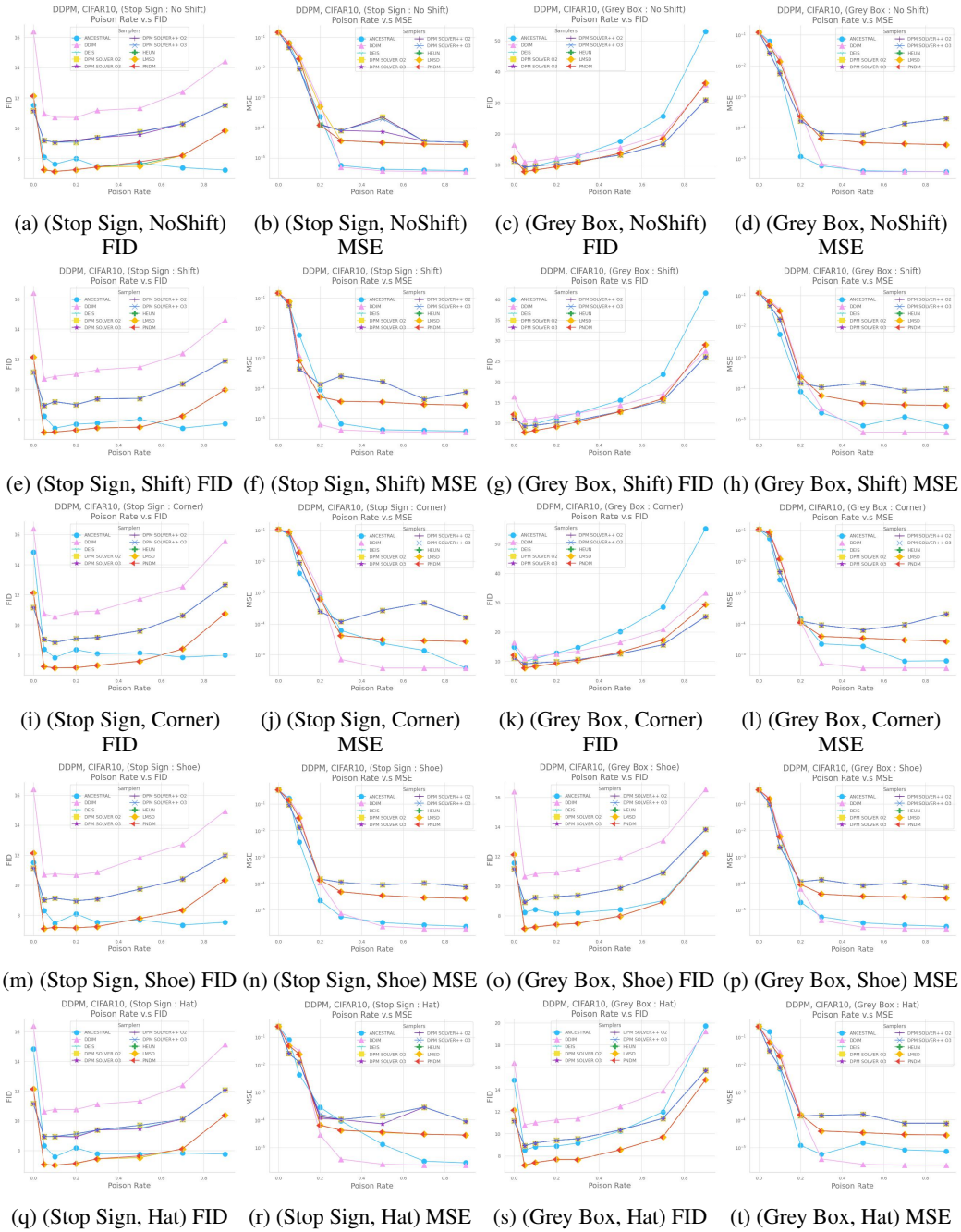

(a) (Stop Sign, NoShift) FID (b) (Stop Sign, NoShift) MSE (c) (Grey Box, NoShift) FID (d) (Grey Box, NoShift) MSE

(e) (Stop Sign, Shift) FID (f) (Stop Sign, Shift) MSE (g) (Grey Box, Shift) FID (h) (Grey Box, Shift) MSE

(i) (Stop Sign, Corner) FID (j) (Stop Sign, Corner) MSE (k) (Grey Box, Corner) FID (l) (Grey Box, Corner) MSE

(m) (Stop Sign, Shoe) FID (n) (Stop Sign, Shoe) MSE (o) (Grey Box, Shoe) FID (p) (Grey Box, Shoe) MSE

(q) (Stop Sign, Hat) FID (r) (Stop Sign, Hat) MSE (s) (Grey Box, Hat) FID (t) (Grey Box, Hat) MSE

Figure 7: FID and MSE scores of various samplers and poison rates for DDPM [11] and the CIFAR10 dataset. We express trigger-target pairs as (trigger, target).

F.2 Backdoor Attacks on DDPM with CelebA-HQ Dataset

We evaluate our method with more samplers and backdoor trigger-target pairs: (Stop Sign, Hat) and (Eyeglasses, Cat) in Fig. 8. Note that the results of the ANCESTRAL sampler come from [7].

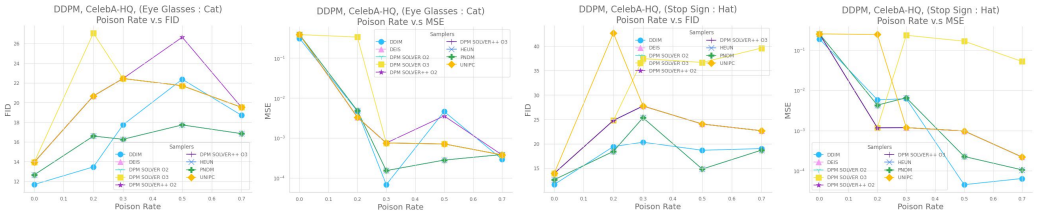

(a) (Eyeglasses, Cat) FID (b) (Eyeglasses, Cat) MSE (c) (Stop Sign, Hat) FID (d) (Stop Sign, Hat) MSE

Figure 8: FID and MSE scores of various samplers and poison rates for the DDPM [11] and the CelebA-HQ dataset. We express trigger-target pairs as (trigger, target).

F.3 Backdoor Attacks on Latent Diffusion Models (LDM)

We also attack the latent diffusion model [39] downloaded from Huggingface (*CompVis/ldm-celebahq-256*), which is pre-trained on CelebA-HQ [27]. The pre-trained latent diffusion models (LDM) [39] are trained on CelebA-HQ with 512×512 resolution and 64×64 latent space. We fine-tune them with learning rate 2e-4 and batch size 16 for 2000 epochs. We examine our method with trigger-target pair: (Eyeglasses, Cat) and (Stop Sign, Hat) and illustrate the FID and MSE score in Fig. 9. As the Fig. 9 shows, the LDM can be backdoored successfully for the trigger-target pairs: (Stop Sign, Hat) with 70% poison rate. Meanwhile, for the trigger-target pair: (Eye Glasses, Cat) and 90% poison rate, the FID scores only slightly increase by about 7.2% at most. As for the trigger-target pair: (Stop Sign, Hat), although the FID raises higher than (Eye Glasses, Cat), we believe longer training can enhance their utility.

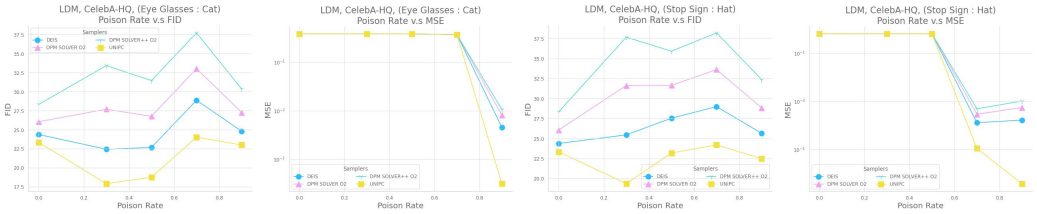

(a) (Eyeglasses, Cat) FID (b) (Eyeglasses, Cat) MSE (c) (Stop Sign, Hat) FID (d) (Stop Sign, Hat) MSE

Figure 9: FID and MSE scores of various samplers and poison rates for the latent diffusion model (LDM) [39] and the CelebA-HQ dataset. We express trigger-target pairs as (trigger, target).

F.4 Backdoor Attacks on Score-Based Models

We trained the score-based model: NCSN [49, 47, 48] on the CIFAR10 dataset with the same model architecture as the DDPM [11] by ourselves for 800 epochs and set the learning rate as 1e-4 and batch size as 128. The FID score of the clean model generated by predictor-correction samplers (SCORE-SDE-VE [49]) for the variance explode models [49] is about 10.87. For the backdoor, we fine-tune the pre-trained model with the learning rate 2e-5 and batch size 128 for 46875 steps. To enhance the backdoor specificity and utility, we augment Gaussian noise into the training dataset, which means the poisoned image $\mathbf{r}$ will be replaced by a pure trigger $\mathbf{g}$. The augmentation can let the model learn to activate the backdoor even if there are no context images. We present our results in Fig. 10 and can see with 70% augment rate, our method can achieve 70% attack success rate based on Fig. 10c as the FID score increases by 12.7%. Note that the augment rate is computed by the number of augmented Gaussian noises / the size of the original training dataset.

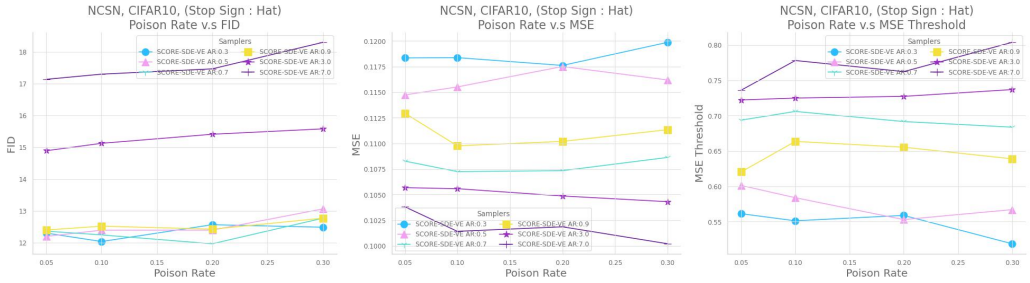

(a) (Stop Sign, Hat) FID (b) (Stop Sign, Hat) MSE (c) (Stop Sign, Hat) MSE Threshold

Figure 10: FID and MSE scores of various samplers and poison rates for the score-based model (NCSN) [47, 48, 49] and the CIFAR10 dataset. We express trigger-target pairs as (trigger, target). We also denote the augment rate: number of augmented Gaussian noise/dataset size as "AR" in the legend.

F.5 Inference-Time Clipping Defense

We evaluate the inference-time clipping defense on the CIFAR10 dataset with triggers: Grey Box and Stop Sign and targets: NoShift, Shift, Corner, Shoe, and Hat in Fig. 11. The results of the ANCESTRAL sampler are from [7]. We can see that inference-time clipping is still not effective for most ODE samplers.

F.6 VillanDiffusion on the Inpaint Tasks

Similar to [7], we also evaluate our method on the inpainting tasks with various samplers. We design 3 kinds of different corruptions: **Blur**, **Line**, **Box**. **Blur** means we add Gaussian noise $\mathcal{N}(0, 0.3)$ to corrupt the images. **Line** and **Box** mean we crop part of the image and ask the diffusion models to recover the missing area. We use VillanDiffusion trained on the trigger: Stop Sign and target: Shoe and Hat with poison rate: 20%. During inpainting, we apply UniPC [54], DEIS [52], DPM Solver [28], and DPM Solver++ [29] samplers with 50 sampling steps. To evaluate the recovery quality, we generate 1024 images and use LPIPS [53] score to measure the similarity between the covered images and ground-truth images. We illustrate our results in Fig. 12. We can see our method achieves both high utility and high specificity.

G Numerical Results

G.1 Image-Trigger Backdoor Attacks on Unconditional Diffusion Models

G.1.1 Backdoor Attacks on DDPM with CIFAR10 Dataset

We present the numerical results of the trigger: Stop Sign and targets: NoShift, Shift, Corner, Shoe, and Hat in Table 2, Table 3, Table 4, Table 5, and Table 6 respectively. As for trigger Grey Box, we also show the results for the targets: NoShift, Shift, Corner, Shoe, and Hat in Table 7, Table 8, Table 9, Table 10, and Table 11.

G.1.2 Backdoor Attacks on DDPM with CelebA-HQ Dataset

We show the numerical results for the trigger-target pairs: (Eyeglasses, Cat) and (Stop Sign, Hat) in Table 12 and Table 13 respectively.

G.2 Backdoor Attacks on Latent Diffusion Models (LDM)

We show the experiment results of the trigger-target pair: (Eye Glasses, Cat) in Table 14 and (Stop Sign, Hat) in Table 15.

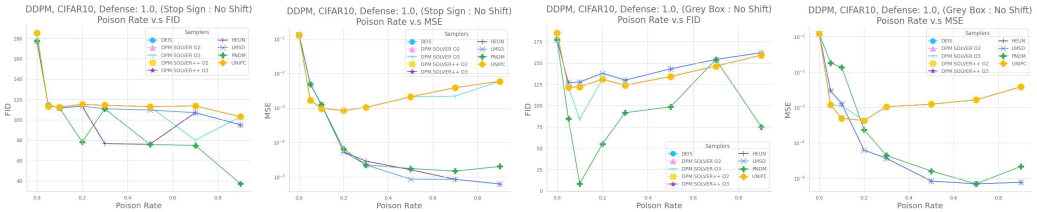

(a) (Stop Sign, NoShift) FID (b) (Stop Sign, NoShift) MSE (c) (Grey Box, NoShift) FID (d) (Grey Box, NoShift) MSE

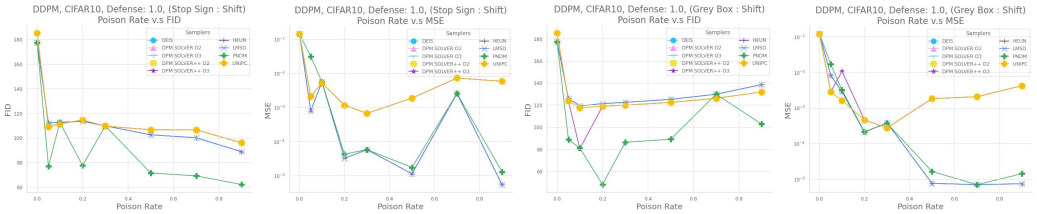

(e) (Stop Sign, Shift) FID (f) (Stop Sign, Shift) MSE (g) (Grey Box, Shift) FID (h) (Grey Box, Shift) MSE

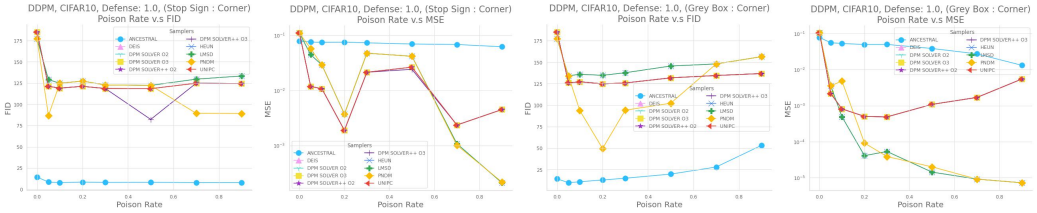

(i) (Stop Sign, Corner) FID (j) (Stop Sign, Corner) MSE (k) (Grey Box, Corner) FID (l) (Grey Box, Corner) MSE

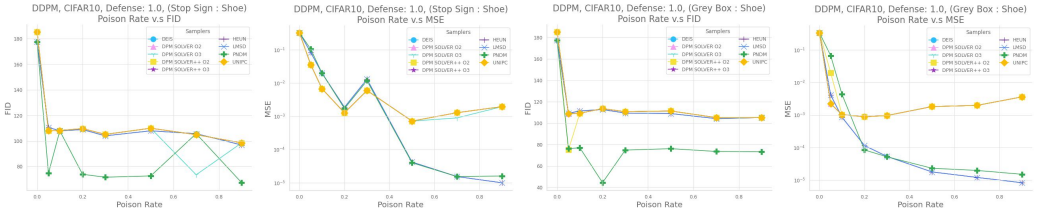

(m) (Stop Sign, Shoe) FID (n) (Stop Sign, Shoe) MSE (o) (Grey Box, Shoe) FID (p) (Grey Box, Shoe) MSE

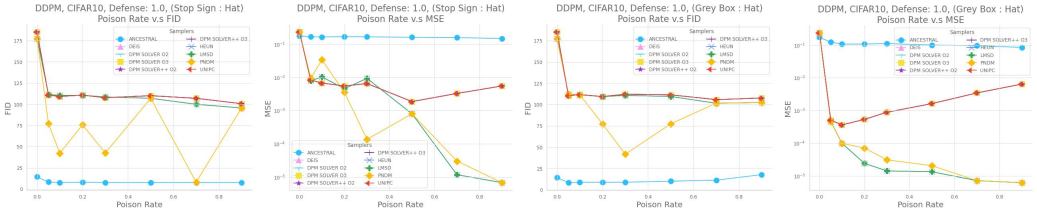

(q) (Stop Sign, Hat) FID (r) (Stop Sign, Hat) MSE (s) (Grey Box, Hat) FID (t) (Grey Box, Hat) MSE

Figure 11: FID and MSE scores of various samplers and poison rates with inference-time defense [7]. We evaluate the defense on the DDPM and the CIFAR10 dataset and express trigger-target pairs as (trigger, target).

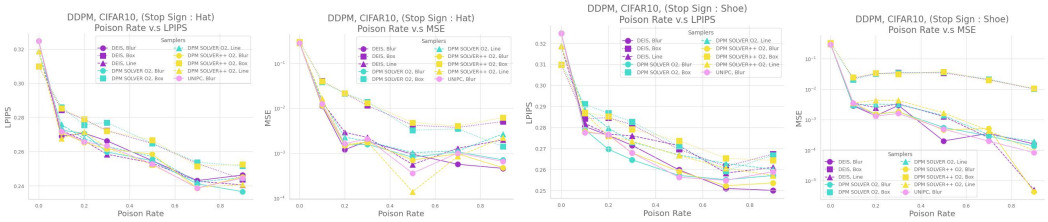

(a) (Stop Sign,Hat) LPIPS (b) (Stop Sign,Hat) MSE (c) (Stop Sign,Shoe) LPIPS (d) (Stop Sign,Shoe) MSE

Figure 12: LPIPS and MSE scores of various samplers and poison rates for the 3 kinds of inpainting tasks: **Blur**, **Line**, and **Box**. The backdoor model is DDPM trained on the CIFAR10 dataset. We express trigger-target pairs as (trigger, target).

Table 2: DDPM backdoor on CIFAR10 Dataset with Trigger: Stop Sign, target: No Shift

Sampler	P.R. Metric	0%	5%	10%	20%	30%	50%	70%	90%
	FID	11.52	8.09	7.62	7.97	7.46	7.68	7.38	7.22
ANCESTRAL	MSE	1.48E-1	6.81E-2	9.47E-3	2.35E-4	5.59E-6	4.19E-6	3.96E-6	3.80E-6
	SSIM	6.84E-4	4.35E-1	9.18E-1	9.97E-1	9.99E-1	9.98E-1	9.98E-1	9.98E-1
	FID	11.15	9.18	9.07	9.18	9.37	9.76	10.28	11.53
UNIPC	MSE	1.48E-1	4.76E-2	9.37E-3	1.30E-4	8.05E-5	2.27E-4	3.56E-5	3.24E-5
	SSIM	8.13E-4	5.27E-1	8.57E-1	9.76E-1	9.81E-1	9.74E-1	9.86E-1	9.84E-1
	FID	11.15	9.18	9.07	9.07	9.37	9.76	10.28	11.53
DPM. O2	MSE	1.48E-1	4.76E-2	9.37E-3	1.24E-4	8.05E-5	2.27E-4	3.56E-5	3.24E-5
	SSIM	8.13E-4	5.27E-1	8.57E-1	9.80E-1	9.81E-1	9.74E-1	9.86E-1	9.84E-1
	FID	11.15	9.18	9.07	9.18	9.37	9.57	10.28	11.53
DPM. O3	MSE	1.48E-1	4.76E-2	9.37E-3	1.30E-4	8.05E-5	7.48E-5	3.56E-5	3.24E-5
	SSIM	8.13E-4	5.27E-1	8.57E-1	9.76E-1	9.81E-1	9.80E-1	9.86E-1	9.84E-1
	FID	11.15	9.18	9.07	9.18	9.37	9.76	10.28	11.53
DPM++. O2	MSE	1.48E-1	4.76E-2	9.37E-3	1.30E-4	8.05E-5	2.27E-4	3.56E-5	3.24E-5
	SSIM	8.13E-4	5.27E-1	8.57E-1	9.76E-1	9.81E-1	9.74E-1	9.86E-1	9.84E-1
	FID	11.15	9.18	9.07	9.07	9.37	9.73	10.28	11.53
DPM++. O3	MSE	1.48E-1	4.76E-2	9.37E-3	1.24E-4	8.05E-5	1.99E-4	3.56E-5	3.24E-5
	SSIM	8.13E-4	5.27E-1	8.57E-1	9.80E-1	9.81E-1	9.76E-1	9.86E-1	9.84E-1
	FID	11.15	9.18	9.07	9.07	9.37	9.57	10.28	11.53
DEIS	MSE	1.48E-1	4.76E-2	9.37E-3	1.28E-4	8.05E-5	7.48E-5	3.56E-5	3.24E-5
	SSIM	8.13E-4	5.27E-1	8.57E-1	9.76E-1	9.81E-1	9.80E-1	9.86E-1	9.84E-1
	FID	16.39	10.95	10.71	10.70	11.16	11.32	12.40	14.43
DDIM	MSE	1.48E-1	7.14E-2	2.47E-2	6.84E-4	4.95E-6	3.70E-6	3.58E-6	3.51E-6
	SSIM	8.92E-4	3.74E-1	7.63E-1	9.92E-1	1.00E+0	9.99E-1	9.99E-1	9.99E-1
	FID	12.14	7.24	7.13	7.25	7.42	7.77	8.18	9.83
PNDM	MSE	1.48E-1	6.55E-2	1.97E-2	1.23E-4	3.74E-5	3.25E-5	2.86E-5	2.76E-5
	SSIM	8.23E-4	4.11E-1	7.91E-1	9.81E-1	9.83E-1	9.83E-1	9.83E-1	9.83E-1
	FID	12.14	7.24	7.13	7.25	7.42	7.60	8.18	9.83
HEUN	MSE	1.48E-1	6.55E-2	1.97E-2	1.23E-4	3.74E-5	3.16E-5	2.86E-5	2.76E-5
	SSIM	8.23E-4	4.11E-1	7.91E-1	9.81E-1	9.83E-1	9.83E-1	9.83E-1	9.83E-1
	FID	12.14	7.24	7.13	7.24	7.42	7.47	8.18	9.83
LMSD	MSE	1.48E-1	6.55E-2	1.97E-2	5.02E-4	3.74E-5	3.23E-5	2.86E-5	2.76E-5
	SSIM	8.23E-4	4.11E-1	7.91E-1	9.76E-1	9.83E-1	9.83E-1	9.83E-1	9.83E-1

Table 3: DDPM backdoor on CIFAR10 Dataset with Trigger: Stop Sign, target: Shift

Sampler	P.R. Metric	0%	5%	10%	20%	30%	50%	70%	90%
	FID	11.16	8.21	7.42	7.68	7.76	8.02	7.42	7.72
ANCESTRAL	MSE	1.48E-1	5.68E-2	5.91E-3	8.96E-5	6.73E-6	4.23E-6	3.96E-6	3.80E-6
	SSIM	4.24E-4	5.73E-1	9.56E-1	9.99E-1	9.99E-1	9.99E-1	9.99E-1	9.99E-1
	FID	11.15	8.92	9.18	8.98	9.36	9.39	10.37	11.89
UNIPC	MSE	1.48E-1	5.92E-2	4.37E-4	1.37E-4	2.58E-4	1.66E-4	4.35E-5	7.59E-5
	SSIM	4.25E-4	4.92E-1	9.70E-1	9.85E-1	9.81E-1	9.86E-1	9.88E-1	9.89E-1
	FID	11.15	8.92	9.18	8.98	9.36	9.39	10.37	11.89
DPM. O2	MSE	1.48E-1	5.92E-2	4.37E-4	1.37E-4	2.58E-4	1.66E-4	4.35E-5	7.59E-5
	SSIM	4.25E-4	4.92E-1	9.70E-1	9.85E-1	9.81E-1	9.86E-1	9.88E-1	9.89E-1
	FID	11.15	8.92	9.18	8.98	9.36	9.39	10.37	11.89
DPM. O3	MSE	1.48E-1	5.92E-2	4.37E-4	1.37E-4	2.58E-4	1.66E-4	4.35E-5	7.59E-5
	SSIM	4.25E-4	4.92E-1	9.70E-1	9.85E-1	9.81E-1	9.86E-1	9.88E-1	9.89E-1
	FID	11.15	8.92	9.18	8.98	9.36	9.39	10.37	11.89
DPM++. O2	MSE	1.48E-1	5.92E-2	4.37E-4	1.37E-4	2.58E-4	1.66E-4	4.35E-5	7.59E-5
	SSIM	4.25E-4	4.92E-1	9.70E-1	9.85E-1	9.81E-1	9.86E-1	9.88E-1	9.89E-1
	FID	11.15	8.92	9.18	8.98	9.36	9.39	10.37	11.89
DPM++. O3	MSE	1.48E-1	5.92E-2	4.37E-4	1.37E-4	2.58E-4	1.66E-4	4.35E-5	7.59E-5
	SSIM	4.25E-4	4.92E-1	9.70E-1	9.85E-1	9.81E-1	9.86E-1	9.88E-1	9.89E-1
	FID	11.15	8.92	9.18	8.98	9.36	9.39	10.37	11.89
DEIS	MSE	1.48E-1	5.92E-2	4.37E-4	1.37E-4	2.58E-4	1.66E-4	4.35E-5	7.59E-5
	SSIM	4.25E-4	4.92E-1	9.70E-1	9.85E-1	9.81E-1	9.86E-1	9.88E-1	9.89E-1
	FID	16.39	10.70	10.85	11.01	11.29	11.48	12.37	14.60
DDIM	MSE	1.48E-1	8.25E-2	1.18E-3	6.30E-6	4.15E-6	3.67E-6	3.54E-6	3.48E-6
	SSIM	4.32E-4	3.43E-1	9.84E-1	1.00E+0	1.00E+0	9.99E-1	9.99E-1	9.99E-1
	FID	12.14	7.15	7.16	7.29	7.44	7.48	8.23	9.97
PNDM	MSE	1.48E-1	7.69E-2	8.51E-4	5.18E-5	3.72E-5	3.53E-5	2.96E-5	2.77E-5
	SSIM	4.25E-4	3.78E-1	9.76E-1	9.89E-1	9.89E-1	9.90E-1	9.90E-1	9.90E-1
	FID	12.14	7.15	7.16	7.29	7.44	7.48	8.23	9.97
HEUN	MSE	1.48E-1	7.69E-2	8.51E-4	5.18E-5	3.72E-5	3.53E-5	2.96E-5	2.77E-5
	SSIM	4.25E-4	3.78E-1	9.76E-1	9.89E-1	9.89E-1	9.90E-1	9.90E-1	9.90E-1
	FID	12.14	7.15	7.16	7.29	7.44	7.48	8.23	9.97
LMSD	MSE	1.48E-1	7.69E-2	8.51E-4	5.18E-5	3.72E-5	3.53E-5	2.96E-5	2.77E-5
	SSIM	4.25E-4	3.78E-1	9.76E-1	9.89E-1	9.89E-1	9.90E-1	9.90E-1	9.90E-1

G.3 Backdoor Attacks on Score-Based Models

We provide the numerical results for the trigger-target pair: (Stop Sign, Hat) in the Table 16.

G.4 Caption-Trigger Backdoor Attacks on Text-to-Image DMs

We will present the numerical results of the Pokemon Caption dataset in Table 17 and Table 18. For the CelebA-HQ-Dialog dataset, we will show them in Table 19 and Table 20.

G.5 Inference-Time Clipping Defense

For the trigger Stop Sign, we present the numerical results of the inference-time clipping defense with targets: NoShift, Shift, Corner, Shoe, and Hat in Table 21, Table 22, Table 23, Table 24, and Table 25 respectively. As for the trigger Grey Box, we also show our results of the targets: NoShift, Shift, Corner, Shoe, and Hat in Table 26, Table 27, Table 28, Table 29, and Table 30 respectively.

G.6 VillanDiffusion on the Inpaint Tasks

For the trigger Stop Sign, we present the numerical results of the inpainting tasks: **Blur**, **Line**, and **Box** with targets Hat and Shoe in Table 32 and Table 31 respectively.

Table 4: DDPM backdoor on CIFAR10 Dataset with Trigger: Stop Sign, target: Corner

Sampler	P.R. Metric	0%	5%	10%	20%	30%	50%	70%	90%
	FID	14.83	8.38	7.83	8.35	8.08	8.14	7.85	7.98
ANCESTRAL	MSE	1.06E-1	7.22E-2	4.20E-3	7.09E-4	6.13E-5	2.37E-5	1.41E-5	3.85E-6
	SSIM	9.85E-4	2.65E-1	9.49E-1	9.89E-1	9.97E-1	9.97E-1	9.97E-1	9.97E-1
	FID	11.15	9.03	8.83	9.09	9.16	9.61	10.61	12.67
UNIPC	MSE	1.06E-1	7.85E-2	9.05E-3	2.47E-4	1.17E-4	2.73E-4	4.75E-4	1.63E-4
	SSIM	1.09E-3	1.34E-1	7.52E-1	9.38E-1	9.56E-1	9.53E-1	9.57E-1	9.72E-1
	FID	11.15	9.03	8.83	9.09	9.16	9.61	10.61	12.67
DPM. O2	MSE	1.06E-1	7.85E-2	9.05E-3	2.47E-4	1.17E-4	2.73E-4	4.75E-4	1.63E-4
	SSIM	1.09E-3	1.34E-1	7.52E-1	9.38E-1	9.56E-1	9.53E-1	9.57E-1	9.72E-1
	FID	11.15	9.03	8.83	9.09	9.16	9.61	10.61	12.67
DPM. O3	MSE	1.06E-1	7.85E-2	9.05E-3	2.47E-4	1.17E-4	2.73E-4	4.75E-4	1.63E-4
	SSIM	1.09E-3	1.34E-1	7.52E-1	9.38E-1	9.56E-1	9.53E-1	9.57E-1	9.72E-1
	FID	11.15	9.03	8.83	9.09	9.16	9.61	10.61	12.67
DPM++. O2	MSE	1.06E-1	7.85E-2	9.05E-3	2.47E-4	1.17E-4	2.73E-4	4.75E-4	1.63E-4
	SSIM	1.09E-3	1.34E-1	7.52E-1	9.38E-1	9.56E-1	9.53E-1	9.57E-1	9.72E-1
	FID	11.15	9.03	8.83	9.09	9.16	9.61	10.61	12.67
DPM++. O3	MSE	1.06E-1	7.85E-2	9.05E-3	2.47E-4	1.17E-4	2.73E-4	4.75E-4	1.63E-4
	SSIM	1.09E-3	1.34E-1	7.52E-1	9.38E-1	9.56E-1	9.53E-1	9.57E-1	9.72E-1
	FID	11.15	9.03	8.83	9.09	9.16	9.61	10.61	12.67
DEIS	MSE	1.06E-1	7.85E-2	9.05E-3	2.47E-4	1.17E-4	2.73E-4	4.75E-4	1.63E-4
	SSIM	1.09E-3	1.34E-1	7.52E-1	9.38E-1	9.56E-1	9.53E-1	9.57E-1	9.72E-1
	FID	16.39	10.74	10.54	10.85	10.92	11.74	12.53	15.57
DDIM	MSE	1.06E-1	9.16E-2	2.54E-2	1.05E-3	7.27E-6	3.84E-6	3.84E-6	3.84E-6
	SSIM	1.12E-3	6.38E-2	6.36E-1	9.79E-1	1.00E+0	1.00E+0	9.99E-1	9.98E-1
	FID	12.14	7.22	7.14	7.15	7.31	7.59	8.39	10.74
PNDM	MSE	1.06E-1	8.87E-2	1.94E-2	6.28E-4	4.24E-5	3.09E-5	2.89E-5	2.70E-5
	SSIM	1.08E-3	7.93E-2	6.84E-1	9.58E-1	9.73E-1	9.76E-1	9.75E-1	9.76E-1
	FID	12.14	7.22	7.14	7.15	7.31	7.59	8.39	10.74
HEUN	MSE	1.06E-1	8.87E-2	1.94E-2	6.28E-4	4.24E-5	3.09E-5	2.89E-5	2.70E-5
	SSIM	1.08E-3	7.93E-2	6.84E-1	9.58E-1	9.73E-1	9.76E-1	9.75E-1	9.76E-1
	FID	12.14	7.22	7.14	7.15	7.31	7.59	8.39	10.74
LMSD	MSE	1.06E-1	8.87E-2	1.94E-2	6.28E-4	4.24E-5	3.09E-5	2.89E-5	2.70E-5
	SSIM	1.08E-3	7.93E-2	6.84E-1	9.58E-1	9.73E-1	9.76E-1	9.75E-1	9.76E-1

Table 5: DDPM backdoor on CIFAR10 Dataset with Trigger: Stop Sign, target: Shoe

Sampler	P.R. Metric	0%	5%	10%	20%	30%	50%	70%	90%
	FID	11.52	8.33	7.47	8.10	7.52	7.69	7.35	7.54
ANCESTRAL	MSE	3.38E-1	1.66E-1	3.61E-3	2.30E-5	5.62E-6	3.35E-6	2.72E-6	2.39E-6
	SSIM	1.69E-4	4.20E-1	9.85E-1	9.99E-1	1.00E+0	1.00E+0	1.00E+0	1.00E+0
	FID	11.15	9.03	9.14	8.96	9.09	9.74	10.41	12.00
UNIPC	MSE	3.38E-1	9.33E-2	1.31E-2	1.47E-4	1.10E-4	8.83E-5	1.04E-4	7.49E-5
	SSIM	2.15E-4	5.91E-1	9.13E-1	9.89E-1	9.91E-1	9.92E-1	9.91E-1	9.92E-1
	FID	11.15	9.03	9.14	8.96	9.09	9.74	10.41	12.00
DPM. O2	MSE	3.38E-1	9.33E-2	1.31E-2	1.47E-4	1.10E-4	8.83E-5	1.04E-4	7.49E-5
	SSIM	2.15E-4	5.91E-1	9.13E-1	9.89E-1	9.91E-1	9.92E-1	9.91E-1	9.92E-1
	FID	11.15	9.03	9.14	8.96	9.09	9.74	10.41	12.00
DPM. O3	MSE	3.38E-1	9.33E-2	1.31E-2	1.47E-4	1.10E-4	8.83E-5	1.04E-4	7.49E-5
	SSIM	2.15E-4	5.91E-1	9.13E-1	9.89E-1	9.91E-1	9.92E-1	9.91E-1	9.92E-1
	FID	11.15	9.03	9.14	8.96	9.09	9.74	10.41	12.00
DPM++. O2	MSE	3.38E-1	9.33E-2	1.31E-2	1.47E-4	1.10E-4	8.83E-5	1.04E-4	7.49E-5
	SSIM	2.15E-4	5.91E-1	9.13E-1	9.89E-1	9.91E-1	9.92E-1	9.91E-1	9.92E-1
	FID	11.15	9.03	9.14	8.96	9.09	9.74	10.41	12.00
DPM++. O3	MSE	3.38E-1	9.33E-2	1.31E-2	1.47E-4	1.10E-4	8.83E-5	1.04E-4	7.49E-5
	SSIM	2.15E-4	5.91E-1	9.13E-1	9.89E-1	9.91E-1	9.92E-1	9.91E-1	9.92E-1
	FID	11.15	9.03	9.14	8.96	9.09	9.74	10.41	12.00
DEIS	MSE	3.38E-1	9.33E-2	1.31E-2	1.47E-4	1.10E-4	8.83E-5	1.04E-4	7.49E-5
	SSIM	2.15E-4	5.91E-1	9.13E-1	9.89E-1	9.91E-1	9.92E-1	9.91E-1	9.92E-1
	FID	16.39	10.71	10.75	10.68	10.87	11.86	12.73	14.94
DDIM	MSE	3.37E-1	1.56E-1	3.96E-2	1.09E-4	7.39E-6	2.42E-6	2.00E-6	1.98E-6
	SSIM	2.40E-4	3.97E-1	8.14E-1	9.99E-1	1.00E+0	1.00E+0	1.00E+0	1.00E+0
	FID	12.14	7.12	7.20	7.17	7.25	7.79	8.33	10.35
PNDM	MSE	3.38E-1	1.39E-1	2.94E-2	1.35E-4	4.89E-5	3.51E-5	2.97E-5	2.74E-5
	SSIM	2.17E-4	4.51E-1	8.53E-1	9.94E-1	9.94E-1	9.95E-1	9.95E-1	9.95E-1
	FID	12.14	7.12	7.20	7.17	7.25	7.79	8.33	10.35
HEUN	MSE	3.38E-1	1.39E-1	2.94E-2	1.35E-4	4.89E-5	3.51E-5	2.97E-5	2.74E-5
	SSIM	2.17E-4	4.51E-1	8.53E-1	9.94E-1	9.94E-1	9.95E-1	9.95E-1	9.95E-1
	FID	12.14	7.12	7.20	7.17	7.25	7.79	8.33	10.35
LMSD	MSE	3.38E-1	1.39E-1	2.94E-2	1.35E-4	4.89E-5	3.51E-5	2.97E-5	2.74E-5
	SSIM	2.17E-4	4.51E-1	8.53E-1	9.94E-1	9.94E-1	9.95E-1	9.95E-1	9.95E-1

Table 6: DDPM backdoor on CIFAR10 Dataset with Trigger: Stop Sign, target: Hat

Sampler	P.R. Metric	0%	5%	10%	20%	30%	50%	70%	90%
	FID	14.83	8.32	7.57	8.17	7.77	7.77	7.83	7.77
ANCESTRAL	MSE	2.41E-1	7.99E-2	4.33E-3	2.85E-4	9.16E-5	1.30E-5	3.21E-6	2.81E-6
	SSIM	4.74E-5	6.52E-1	9.80E-1	9.98E-1	9.99E-1	1.00E+0	1.00E+0	1.00E+0
	FID	11.15	8.94	8.95	8.97	9.38	9.51	10.11	12.08
UNIPC	MSE	2.41E-1	2.50E-2	1.23E-2	1.25E-4	1.03E-4	7.29E-5	2.89E-4	8.91E-5
	SSIM	1.01E-4	8.57E-1	9.23E-1	9.95E-1	9.96E-1	9.96E-1	9.95E-1	9.97E-1
	FID	11.15	8.94	8.95	9.12	9.38	9.70	10.11	12.08
DPM. O2	MSE	2.41E-1	2.50E-2	1.23E-2	1.30E-4	1.03E-4	1.43E-4	2.89E-4	8.91E-5
	SSIM	1.01E-4	8.57E-1	9.23E-1	9.95E-1	9.96E-1	9.97E-1	9.95E-1	9.97E-1
	FID	11.15	8.94	8.95	8.91	9.38	9.45	10.11	12.08
DPM. O3	MSE	2.41E-1	2.50E-2	1.23E-2	1.14E-4	1.03E-4	7.12E-5	2.89E-4	8.91E-5
	SSIM	1.01E-4	8.57E-1	9.23E-1	9.95E-1	9.96E-1	9.96E-1	9.95E-1	9.97E-1
	FID	11.15	8.94	8.95	9.12	9.38	9.70	10.11	12.08
DPM++. O2	MSE	2.41E-1	2.50E-2	1.23E-2	1.30E-4	1.03E-4	1.43E-4	2.89E-4	8.91E-5
	SSIM	1.01E-4	8.57E-1	9.23E-1	9.95E-1	9.96E-1	9.97E-1	9.95E-1	9.97E-1
	FID	11.15	8.94	8.95	9.13	9.38	9.70	10.11	12.08
DPM++. O3	MSE	2.41E-1	2.50E-2	1.23E-2	1.61E-4	1.03E-4	1.43E-4	2.89E-4	8.91E-5
	SSIM	1.01E-4	8.57E-1	9.23E-1	9.94E-1	9.96E-1	9.97E-1	9.95E-1	9.97E-1
	FID	11.15	8.94	8.95	8.97	9.38	9.51	10.11	12.08
DEIS	MSE	2.41E-1	2.50E-2	1.23E-2	1.25E-4	1.03E-4	7.29E-5	2.89E-4	8.91E-5
	SSIM	1.01E-4	8.57E-1	9.23E-1	9.95E-1	9.96E-1	9.96E-1	9.95E-1	9.97E-1
	FID	16.39	10.63	10.77	10.76	11.12	11.33	12.40	15.13
DDIM	MSE	2.40E-1	5.77E-2	3.08E-2	2.86E-5	3.79E-6	2.49E-6	2.31E-6	2.29E-6
	SSIM	1.39E-4	7.09E-1	8.40E-1	1.00E+0	1.00E+0	1.00E+0	1.00E+0	1.00E+0
	FID	12.14	7.07	7.02	7.15	7.44	7.63	8.11	10.36
PNDM	MSE	2.41E-1	4.85E-2	2.41E-2	6.43E-5	4.21E-5	3.67E-5	3.04E-5	2.82E-5
	SSIM	1.05E-4	7.51E-1	8.70E-1	9.97E-1	9.97E-1	9.98E-1	9.98E-1	9.98E-1
	FID	12.14	7.07	7.02	7.15	7.44	7.52	8.11	10.36
HEUN	MSE	2.41E-1	4.85E-2	2.41E-2	6.43E-5	4.21E-5	3.48E-5	3.04E-5	2.82E-5
	SSIM	1.05E-4	7.51E-1	8.70E-1	9.97E-1	9.97E-1	9.98E-1	9.98E-1	9.98E-1
	FID	12.14	7.07	7.02	7.13	7.44	7.52	8.11	10.36
LMSD	MSE	2.41E-1	4.85E-2	2.41E-2	6.57E-5	4.21E-5	3.48E-5	3.04E-5	2.82E-5
	SSIM	1.05E-4	7.51E-1	8.70E-1	9.97E-1	9.97E-1	9.98E-1	9.98E-1	9.98E-1

Table 7: DDPM backdoor on CIFAR10 Dataset with Trigger: Grey Box, target: No Shift

Sampler	P.R. Metric	0%	5%	10%	20%	30%	50%	70%	90%
	FID	11.56	9.09	9.62	11.36	12.85	17.63	25.70	52.92
ANCESTRAL	MSE	1.21E-1	6.19E-2	6.11E-3	1.18E-5	5.89E-6	4.09E-6	3.91E-6	3.86E-6
	SSIM	7.36E-4	4.21E-1	9.41E-1	9.98E-1	9.98E-1	9.98E-1	9.98E-1	9.98E-1
	FID	11.15	9.30	9.60	10.20	11.13	13.17	16.62	30.87
UNIPC	MSE	1.21E-1	2.58E-2	5.64E-3	1.67E-4	6.52E-5	6.15E-5	1.36E-4	1.98E-4
	SSIM	7.37E-4	6.22E-1	8.62E-1	9.61E-1	9.74E-1	9.76E-1	9.82E-1	9.80E-1
	FID	11.15	9.30	9.60	10.20	11.13	13.17	16.62	30.87
DPM. O2	MSE	1.21E-1	2.58E-2	5.64E-3	1.67E-4	6.52E-5	6.15E-5	1.36E-4	1.98E-4
	SSIM	7.37E-4	6.22E-1	8.62E-1	9.61E-1	9.74E-1	9.76E-1	9.82E-1	9.80E-1
	FID	11.15	9.30	9.60	10.20	11.13	13.17	16.62	30.87
DPM. O3	MSE	1.21E-1	2.58E-2	5.64E-3	1.67E-4	6.52E-5	6.15E-5	1.36E-4	1.98E-4
	SSIM	7.37E-4	6.22E-1	8.62E-1	9.61E-1	9.74E-1	9.76E-1	9.82E-1	9.80E-1
	FID	11.15	9.30	9.60	10.20	11.13	13.17	16.62	30.87
DPM++. O2	MSE	1.21E-1	2.58E-2	5.64E-3	1.67E-4	6.52E-5	6.15E-5	1.36E-4	1.98E-4
	SSIM	7.37E-4	6.22E-1	8.62E-1	9.61E-1	9.74E-1	9.76E-1	9.82E-1	9.80E-1
	FID	11.15	9.30	9.60	10.20	11.13	13.17	16.62	30.87
DPM++. O3	MSE	1.21E-1	2.58E-2	5.64E-3	1.67E-4	6.52E-5	6.15E-5	1.36E-4	1.98E-4
	SSIM	7.37E-4	6.22E-1	8.62E-1	9.61E-1	9.74E-1	9.76E-1	9.82E-1	9.80E-1
	FID	11.15	9.30	9.60	10.20	11.13	13.17	16.62	30.87
DEIS	MSE	1.21E-1	2.58E-2	5.64E-3	1.67E-4	6.52E-5	6.15E-5	1.36E-4	1.98E-4
	SSIM	7.37E-4	6.22E-1	8.62E-1	9.61E-1	9.74E-1	9.76E-1	9.82E-1	9.80E-1
	FID	16.39	10.97	11.21	12.22	13.17	15.62	19.74	35.84
DDIM	MSE	1.21E-1	5.13E-2	1.75E-2	2.87E-4	7.06E-6	3.85E-6	3.84E-6	3.84E-6
	SSIM	7.38E-4	4.04E-1	7.63E-1	9.94E-1	1.00E+0	1.00E+0	9.99E-1	9.98E-1
	FID	12.14	7.88	8.34	9.38	10.80	13.73	18.47	36.29
PNDM	MSE	1.21E-1	4.47E-2	1.37E-2	2.35E-4	4.50E-5	3.31E-5	3.02E-5	2.81E-5
	SSIM	7.37E-4	4.62E-1	7.93E-1	9.75E-1	9.78E-1	9.79E-1	9.79E-1	9.80E-1
	FID	12.14	7.88	8.34	9.38	10.80	13.73	18.47	36.29
HEUN	MSE	1.21E-1	4.47E-2	1.37E-2	2.35E-4	4.50E-5	3.31E-5	3.02E-5	2.81E-5
	SSIM	7.37E-4	4.62E-1	7.93E-1	9.75E-1	9.78E-1	9.79E-1	9.79E-1	9.80E-1
	FID	12.14	7.88	8.34	9.38	10.80	13.73	18.47	36.29
LMSD	MSE	1.21E-1	4.47E-2	1.37E-2	2.35E-4	4.50E-5	3.31E-5	3.02E-5	2.81E-5
	SSIM	7.37E-4	4.62E-1	7.93E-1	9.75E-1	9.78E-1	9.79E-1	9.79E-1	9.80E-1

Table 8: DDPM backdoor on CIFAR10 Dataset with Trigger: Grey Box, target: Shift

Sampler	P.R. Metric	0%	5%	10%	20%	30%	50%	70%	90%
	FID	11.56	9.09	9.78	11.26	12.41	15.55	21.78	41.54
ANCESTRAL	MSE	1.21E-1	5.11E-2	5.52E-3	7.90E-5	1.61E-5	6.25E-6	1.22E-5	5.98E-6
	SSIM	4.72E-4	5.06E-1	9.45E-1	9.98E-1	9.99E-1	9.99E-1	9.99E-1	9.98E-1
	FID	11.15	9.28	9.42	10.10	10.70	12.77	15.41	26.12
UNIPC	MSE	1.21E-1	4.83E-2	1.67E-2	1.46E-4	1.10E-4	1.49E-4	8.65E-5	9.66E-5
	SSIM	4.73E-4	4.64E-1	7.46E-1	9.71E-1	9.81E-1	9.79E-1	9.85E-1	9.84E-1
	FID	11.15	9.28	9.42	10.10	10.70	12.77	15.41	26.12
DPM. O2	MSE	1.21E-1	4.83E-2	1.67E-2	1.46E-4	1.10E-4	1.49E-4	8.65E-5	9.66E-5
	SSIM	4.73E-4	4.64E-1	7.46E-1	9.71E-1	9.81E-1	9.79E-1	9.85E-1	9.84E-1
	FID	11.15	9.28	9.42	10.10	10.70	12.77	15.41	26.12
DPM. O3	MSE	1.21E-1	4.83E-2	1.67E-2	1.46E-4	1.10E-4	1.49E-4	8.65E-5	9.66E-5
	SSIM	4.73E-4	4.64E-1	7.46E-1	9.71E-1	9.81E-1	9.79E-1	9.85E-1	9.84E-1
	FID	11.15	9.28	9.42	10.10	10.70	12.77	15.41	26.12
DPM++. O2	MSE	1.21E-1	4.83E-2	1.67E-2	1.46E-4	1.10E-4	1.49E-4	8.65E-5	9.66E-5
	SSIM	4.73E-4	4.64E-1	7.46E-1	9.71E-1	9.81E-1	9.79E-1	9.85E-1	9.84E-1
	FID	11.15	9.28	9.42	10.10	10.70	12.77	15.41	26.12
DPM++. O3	MSE	1.21E-1	4.83E-2	1.67E-2	1.46E-4	1.10E-4	1.49E-4	8.65E-5	9.66E-5
	SSIM	4.73E-4	4.64E-1	7.46E-1	9.71E-1	9.81E-1	9.79E-1	9.85E-1	9.84E-1
	FID	11.15	9.28	9.42	10.10	10.70	12.77	15.41	26.12
DEIS	MSE	1.21E-1	4.83E-2	1.67E-2	1.46E-4	1.10E-4	1.49E-4	8.65E-5	9.66E-5
	SSIM	4.73E-4	4.64E-1	7.46E-1	9.71E-1	9.81E-1	9.79E-1	9.85E-1	9.84E-1
	FID	16.39	10.84	10.98	11.76	12.35	14.34	17.05	27.53
DDIM	MSE	1.21E-1	7.00E-2	3.67E-2	3.00E-4	2.27E-5	3.85E-6	3.84E-6	3.84E-6
	SSIM	4.74E-4	2.96E-1	5.80E-1	9.93E-1	9.99E-1	9.99E-1	9.99E-1	9.99E-1
	FID	12.14	7.77	8.19	9.11	10.27	12.75	15.91	28.99
PNDM	MSE	1.21E-1	6.52E-2	3.14E-2	2.38E-4	5.89E-5	3.34E-5	2.95E-5	2.81E-5
	SSIM	4.73E-4	3.29E-1	6.16E-1	9.80E-1	9.86E-1	9.86E-1	9.86E-1	9.87E-1
	FID	12.14	7.77	8.19	9.11	10.27	12.75	15.91	28.99
HEUN	MSE	1.21E-1	6.52E-2	3.14E-2	2.38E-4	5.89E-5	3.34E-5	2.95E-5	2.81E-5
	SSIM	4.73E-4	3.29E-1	6.16E-1	9.80E-1	9.86E-1	9.86E-1	9.86E-1	9.87E-1
	FID	12.14	7.77	8.19	9.11	10.27	12.75	15.91	28.99
LMSD	MSE	1.21E-1	6.52E-2	3.14E-2	2.38E-4	5.89E-5	3.34E-5	2.95E-5	2.81E-5
	SSIM	4.73E-4	3.29E-1	6.16E-1	9.80E-1	9.86E-1	9.86E-1	9.86E-1	9.87E-1

Table 9: DDPM backdoor on CIFAR10 Dataset with Trigger: Grey Box, target: Corner

Sampler	P.R. Metric	0%	5%	10%	20%	30%	50%	70%	90%
	FID	14.83	9.92	10.98	12.86	14.78	20.10	28.52	55.23
ANCESTRAL	MSE	1.06E-1	5.32E-2	2.60E-3	1.48E-4	2.29E-5	1.96E-5	6.44E-6	6.60E-6
	SSIM	9.85E-4	4.20E-1	9.64E-1	9.96E-1	9.98E-1	9.97E-1	9.97E-1	9.97E-1
	FID	11.15	9.17	9.42	9.94	10.59	12.61	15.64	25.25
UNIPC	MSE	1.06E-1	7.14E-2	4.71E-3	1.23E-4	9.18E-5	6.37E-5	9.36E-5	2.07E-4
	SSIM	9.87E-4	1.20E-1	8.27E-1	9.54E-1	9.66E-1	9.72E-1	9.68E-1	9.68E-1
	FID	11.15	9.17	9.42	9.94	10.59	12.61	15.64	25.25
DPM. O2	MSE	1.06E-1	7.14E-2	4.71E-3	1.23E-4	9.18E-5	6.37E-5	9.36E-5	2.07E-4
	SSIM	9.87E-4	1.20E-1	8.27E-1	9.54E-1	9.66E-1	9.72E-1	9.68E-1	9.68E-1
	FID	11.15	9.17	9.42	9.94	10.59	12.61	15.64	25.25
DPM. O3	MSE	1.06E-1	7.14E-2	4.71E-3	1.23E-4	9.18E-5	6.37E-5	9.36E-5	2.07E-4
	SSIM	9.87E-4	1.20E-1	8.27E-1	9.54E-1	9.66E-1	9.72E-1	9.68E-1	9.68E-1
	FID	11.15	9.17	9.42	9.94	10.59	12.61	15.64	25.25
DPM++. O2	MSE	1.06E-1	7.14E-2	4.71E-3	1.23E-4	9.18E-5	6.37E-5	9.36E-5	2.07E-4
	SSIM	9.87E-4	1.20E-1	8.27E-1	9.54E-1	9.66E-1	9.72E-1	9.68E-1	9.68E-1
	FID	11.15	9.17	9.42	9.94	10.59	12.61	15.64	25.25
DPM++. O3	MSE	1.06E-1	7.14E-2	4.71E-3	1.23E-4	9.18E-5	6.37E-5	9.36E-5	2.07E-4
	SSIM	9.87E-4	1.20E-1	8.27E-1	9.54E-1	9.66E-1	9.72E-1	9.68E-1	9.68E-1
	FID	11.15	9.17	9.42	9.94	10.59	12.61	15.64	25.25
DEIS	MSE	1.06E-1	7.14E-2	4.71E-3	1.23E-4	9.18E-5	6.37E-5	9.36E-5	2.07E-4
	SSIM	9.87E-4	1.20E-1	8.27E-1	9.54E-1	9.66E-1	9.72E-1	9.68E-1	9.68E-1
	FID	16.39	11.02	11.58	12.58	13.46	16.50	20.82	33.34
DDIM	MSE	1.06E-1	8.91E-2	1.42E-2	1.13E-4	5.44E-6	3.84E-6	3.84E-6	3.84E-6
	SSIM	9.88E-4	4.39E-2	7.05E-1	9.95E-1	9.99E-1	9.99E-1	9.99E-1	9.98E-1
	FID	12.14	7.77	8.27	9.34	10.21	13.12	17.28	29.35
PNDM	MSE	1.06E-1	8.64E-2	1.19E-2	1.11E-4	3.97E-5	3.49E-5	3.07E-5	2.74E-5
	SSIM	9.87E-4	5.04E-2	7.18E-1	9.69E-1	9.73E-1	9.76E-1	9.75E-1	9.76E-1
	FID	12.14	7.77	8.27	9.34	10.21	13.12	17.28	29.35
HEUN	MSE	1.06E-1	8.64E-2	1.19E-2	1.11E-4	3.97E-5	3.49E-5	3.07E-5	2.74E-5
	SSIM	9.87E-4	5.04E-2	7.18E-1	9.69E-1	9.73E-1	9.76E-1	9.75E-1	9.76E-1
	FID	12.14	7.77	8.27	9.34	10.21	13.12	17.28	29.35
LMSD	MSE	1.06E-1	8.64E-2	1.19E-2	1.11E-4	3.97E-5	3.49E-5	3.07E-5	2.74E-5
	SSIM	9.87E-4	5.04E-2	7.18E-1	9.69E-1	9.73E-1	9.76E-1	9.75E-1	9.76E-1

Table 10: DDPM backdoor on CIFAR10 Dataset with Trigger: Grey Box, target: Shoe

Sampler	P.R. Metric	0%	5%	10%	20%	30%	50%	70%	90%
	FID	11.56	8.22	8.41	8.13	8.19	8.41	9.01	12.25
ANCESTRAL	MSE	3.38E-1	1.02E-1	6.25E-3	1.97E-5	5.53E-6	3.26E-6	2.69E-6	2.38E-6
	SSIM	1.69E-4	6.26E-1	9.75E-1	9.99E-1	1.00E+0	1.00E+0	1.00E+0	1.00E+0
	FID	11.15	8.91	9.22	9.29	9.37	9.86	10.89	13.83
UNIPC	MSE	3.38E-1	9.73E-2	2.36E-3	1.17E-4	1.39E-4	8.34E-5	1.07E-4	7.14E-5
	SSIM	1.69E-4	5.43E-1	9.70E-1	9.90E-1	9.90E-1	9.94E-1	9.91E-1	9.94E-1
	FID	11.15	8.91	9.22	9.29	9.37	9.86	10.89	13.83
DPM. O2	MSE	3.38E-1	9.73E-2	2.36E-3	1.17E-4	1.39E-4	8.34E-5	1.07E-4	7.14E-5
	SSIM	1.69E-4	5.43E-1	9.70E-1	9.90E-1	9.90E-1	9.94E-1	9.91E-1	9.94E-1
	FID	11.15	8.91	9.22	9.29	9.37	9.86	10.89	13.83
DPM. O3	MSE	3.38E-1	9.73E-2	2.36E-3	1.17E-4	1.39E-4	8.34E-5	1.07E-4	7.14E-5
	SSIM	1.69E-4	5.43E-1	9.70E-1	9.90E-1	9.90E-1	9.94E-1	9.91E-1	9.94E-1
	FID	11.15	8.91	9.22	9.29	9.37	9.86	10.89	13.83
DPM++. O2	MSE	3.38E-1	9.73E-2	2.36E-3	1.17E-4	1.39E-4	8.34E-5	1.07E-4	7.14E-5
	SSIM	1.69E-4	5.43E-1	9.70E-1	9.90E-1	9.90E-1	9.94E-1	9.91E-1	9.94E-1
	FID	11.15	8.91	9.22	9.29	9.37	9.86	10.89	13.83
DPM++. O3	MSE	3.38E-1	9.73E-2	2.36E-3	1.17E-4	1.39E-4	8.34E-5	1.07E-4	7.14E-5
	SSIM	1.69E-4	5.43E-1	9.70E-1	9.90E-1	9.90E-1	9.94E-1	9.91E-1	9.94E-1
	FID	11.15	8.91	9.22	9.29	9.37	9.86	10.89	13.83
DEIS	MSE	3.38E-1	9.73E-2	2.36E-3	1.17E-4	1.39E-4	8.34E-5	1.07E-4	7.14E-5
	SSIM	1.69E-4	5.43E-1	9.70E-1	9.90E-1	9.90E-1	9.94E-1	9.91E-1	9.94E-1
	FID	16.39	10.64	10.82	10.92	11.15	11.90	13.07	16.54
DDIM	MSE	3.38E-1	1.71E-1	8.64E-3	6.23E-5	4.08E-6	2.22E-6	1.98E-6	1.98E-6
	SSIM	1.69E-4	3.17E-1	9.52E-1	9.99E-1	1.00E+0	1.00E+0	1.00E+0	1.00E+0
	FID	12.14	7.12	7.22	7.39	7.47	7.97	8.91	12.19
PNDM	MSE	3.38E-1	1.53E-1	5.96E-3	9.11E-5	3.99E-5	3.32E-5	3.14E-5	2.82E-5
	SSIM	1.69E-4	3.72E-1	9.60E-1	9.93E-1	9.95E-1	9.95E-1	9.95E-1	9.95E-1
	FID	12.14	7.12	7.22	7.39	7.47	7.97	8.91	12.19
HEUN	MSE	3.38E-1	1.53E-1	5.96E-3	9.11E-5	3.99E-5	3.32E-5	3.14E-5	2.82E-5
	SSIM	1.69E-4	3.72E-1	9.60E-1	9.93E-1	9.95E-1	9.95E-1	9.95E-1	9.95E-1
	FID	12.14	7.12	7.22	7.39	7.47	7.97	8.91	12.19
LMSD	MSE	3.38E-1	1.53E-1	5.96E-3	9.11E-5	3.99E-5	3.32E-5	3.14E-5	2.82E-5
	SSIM	1.69E-4	3.72E-1	9.60E-1	9.93E-1	9.95E-1	9.95E-1	9.95E-1	9.95E-1

Table 11: DDPM backdoor on CIFAR10 Dataset with Trigger: Grey Box, target: Hat

Sampler	P.R. Metric	0%	5%	10%	20%	30%	50%	70%	90%
	FID	14.83	8.53	8.81	8.89	9.14	10.25	11.97	19.73
ANCESTRAL	MSE	2.41E-1	1.58E-1	7.01E-3	1.19E-5	5.68E-6	1.48E-5	8.27E-6	7.43E-6
	SSIM	4.74E-5	3.12E-1	9.67E-1	1.00E+0	1.00E+0	1.00E+0	1.00E+0	1.00E+0
	FID	11.15	8.92	9.16	9.42	9.55	10.33	11.38	15.68
UNIPC	MSE	2.41E-1	3.14E-2	7.96E-3	1.39E-4	1.46E-4	1.59E-4	7.56E-5	7.56E-5
	SSIM	4.80E-5	8.24E-1	9.49E-1	9.95E-1	9.96E-1	9.97E-1	9.97E-1	9.97E-1
	FID	11.15	8.92	9.16	9.42	9.55	10.33	11.38	15.68
DPM. O2	MSE	2.41E-1	3.14E-2	7.96E-3	1.39E-4	1.46E-4	1.59E-4	7.56E-5	7.56E-5
	SSIM	4.80E-5	8.24E-1	9.49E-1	9.95E-1	9.96E-1	9.97E-1	9.97E-1	9.97E-1
	FID	11.15	8.92	9.16	9.42	9.55	10.33	11.38	15.68
DPM. O3	MSE	2.41E-1	3.14E-2	7.96E-3	1.39E-4	1.46E-4	1.59E-4	7.56E-5	7.56E-5
	SSIM	4.80E-5	8.24E-1	9.49E-1	9.95E-1	9.96E-1	9.97E-1	9.97E-1	9.97E-1
	FID	11.15	8.92	9.16	9.42	9.55	10.33	11.38	15.68
DPM++. O2	MSE	2.41E-1	3.14E-2	7.96E-3	1.39E-4	1.46E-4	1.59E-4	7.56E-5	7.56E-5
	SSIM	4.80E-5	8.24E-1	9.49E-1	9.95E-1	9.96E-1	9.97E-1	9.97E-1	9.97E-1
	FID	11.15	8.92	9.16	9.42	9.55	10.33	11.38	15.68
DPM++. O3	MSE	2.41E-1	3.14E-2	7.96E-3	1.39E-4	1.46E-4	1.59E-4	7.56E-5	7.56E-5
	SSIM	4.80E-5	8.24E-1	9.49E-1	9.95E-1	9.96E-1	9.97E-1	9.97E-1	9.97E-1
	FID	11.15	8.92	9.16	9.42	9.55	10.33	11.38	15.68
DEIS	MSE	2.41E-1	3.14E-2	7.96E-3	1.39E-4	1.46E-4	1.59E-4	7.56E-5	7.56E-5
	SSIM	4.80E-5	8.24E-1	9.49E-1	9.95E-1	9.96E-1	9.97E-1	9.97E-1	9.97E-1
	FID	16.39	10.78	10.99	11.25	11.38	12.47	13.86	19.24
DDIM	MSE	2.41E-1	7.64E-2	2.84E-2	1.73E-4	3.89E-6	2.45E-6	2.31E-6	2.29E-6
	SSIM	4.86E-5	6.22E-1	8.55E-1	9.99E-1	1.00E+0	1.00E+0	1.00E+0	1.00E+0
	FID	12.14	7.16	7.40	7.68	7.67	8.54	9.71	14.86
PNDM	MSE	2.41E-1	6.33E-2	2.04E-2	1.55E-4	3.96E-5	3.45E-5	2.95E-5	2.85E-5
	SSIM	4.82E-5	6.81E-1	8.92E-1	9.96E-1	9.98E-1	9.98E-1	9.98E-1	9.98E-1
	FID	12.14	7.16	7.40	7.68	7.67	8.54	9.71	14.86
HEUN	MSE	2.41E-1	6.33E-2	2.04E-2	1.55E-4	3.96E-5	3.45E-5	2.95E-5	2.85E-5
	SSIM	4.82E-5	6.81E-1	8.92E-1	9.96E-1	9.98E-1	9.98E-1	9.98E-1	9.98E-1
	FID	12.14	7.16	7.40	7.68	7.67	8.54	9.71	14.86
LMSD	MSE	2.41E-1	6.33E-2	2.04E-2	1.55E-4	3.96E-5	3.45E-5	2.95E-5	2.85E-5
	SSIM	4.82E-5	6.81E-1	8.92E-1	9.96E-1	9.98E-1	9.98E-1	9.98E-1	9.98E-1

Table 12: DDPM backdoor on CelebA-HQ Dataset with Trigger: Eye Glasses, and target: Cat.

Sampler	P.R. Metric	0%	20%	30%	50%	70%
UNIPC	FID	13.93	20.67	22.44	21.71	19.52
	MSE	3.85E-1	3.31E-3	7.45E-4	7.09E-4	3.76E-4
	SSIM	5.36E-4	8.87E-1	8.82E-1	7.61E-1	8.78E-1
DPM. O2	FID	13.93	20.67	22.44	21.71	19.52
	MSE	3.85E-1	3.31E-3	7.45E-4	7.09E-4	3.76E-4
	SSIM	5.36E-4	8.87E-1	8.82E-1	7.61E-1	8.78E-1
DPM. O3	FID	13.93	27.06	22.44	21.71	19.52
	MSE	3.85E-1	3.35E-1	7.45E-4	7.09E-4	3.76E-4
	SSIM	5.36E-4	1.95E-2	8.82E-1	7.61E-1	8.78E-1
DPM++. O2	FID	13.93	20.67	22.44	26.64	19.52
	MSE	3.85E-1	3.31E-3	7.45E-4	3.55E-3	3.76E-4
	SSIM	5.36E-4	8.87E-1	8.82E-1	4.46E-1	8.78E-1
DPM++. O3	FID	13.93	20.67	22.44	21.71	19.52
	MSE	3.85E-1	3.31E-3	7.45E-4	7.09E-4	3.76E-4
	SSIM	5.36E-4	8.87E-1	8.82E-1	7.61E-1	8.78E-1
DEIS	FID	13.93	20.67	22.44	21.71	19.52
	MSE	3.85E-1	3.31E-3	7.45E-4	7.09E-4	3.76E-4
	SSIM	5.36E-4	8.87E-1	8.82E-1	7.61E-1	8.78E-1
DDIM	FID	11.67	13.46	17.73	22.37	18.71
	MSE	3.11E-1	4.69E-3	6.75E-5	4.59E-3	2.92E-4
	SSIM	1.73E-1	9.47E-1	9.73E-1	4.14E-1	9.02E-1
PNDM	FID	12.65	16.59	16.27	17.73	16.84
	MSE	3.85E-1	4.82E-3	1.52E-4	2.79E-4	3.84E-4
	SSIM	5.36E-4	9.24E-1	9.56E-1	8.77E-1	8.66E-1
HEUN	FID	12.65	16.59	16.27	17.73	16.84
	MSE	3.85E-1	4.82E-3	1.52E-4	2.79E-4	3.84E-4
	SSIM	5.36E-4	9.24E-1	9.56E-1	8.77E-1	8.66E-1

Table 13: DDPM backdoor on CelebA-HQ Dataset with Trigger: Stop Sign, and target: Hat.

Sampler	P.R. Metric	0%	20%	30%	50%	70%
	FID	13.93	42.66	27.74	24.05	22.67
UNIPC	MSE	2.52E-1	2.44E-1	1.18E-3	9.80E-4	2.21E-4
	SSIM	6.86E-4	9.20E-3	8.70E-1	7.28E-1	8.87E-1
	FID	13.93	24.78	27.74	24.05	22.67
DPM. O2	MSE	2.52E-1	1.18E-3	1.18E-3	9.80E-4	2.21E-4
	SSIM	6.86E-4	8.05E-1	8.70E-1	7.28E-1	8.87E-1
	FID	13.93	24.78	37.43	36.65	39.59
DPM. O3	MSE	2.52E-1	1.18E-3	2.34E-1	1.66E-1	5.23E-2
	SSIM	6.86E-4	8.05E-1	1.22E-2	2.33E-2	6.87E-2
	FID	13.93	24.78	27.74	24.05	22.67
DPM++. O2	MSE	2.52E-1	1.18E-3	1.18E-3	9.80E-4	2.21E-4
	SSIM	6.86E-4	8.05E-1	8.70E-1	7.28E-1	8.87E-1
	FID	13.93	24.78	27.74	24.05	22.67
DPM++. O3	MSE	2.52E-1	1.18E-3	1.18E-3	9.80E-4	2.21E-4
	SSIM	6.86E-4	8.05E-1	8.70E-1	7.28E-1	8.87E-1
	FID	13.93	24.78	27.74	24.05	22.67
DEIS	MSE	2.52E-1	1.18E-3	1.18E-3	9.80E-4	2.21E-4
	SSIM	6.86E-4	8.05E-1	8.70E-1	7.28E-1	8.87E-1
	FID	11.67	19.44	20.32	18.68	19.02
DDIM	MSE	1.88E-1	5.85E-3	6.18E-3	4.54E-5	6.45E-5
	SSIM	2.99E-1	9.68E-1	9.36E-1	9.68E-1	9.50E-1
	FID	12.65	18.45	25.34	14.83	18.71
PNDM	MSE	2.52E-1	4.29E-3	6.55E-3	2.28E-4	1.06E-4
	SSIM	6.86E-4	9.56E-1	9.14E-1	8.82E-1	9.33E-1
	FID	12.65	18.45	25.34	14.83	18.71
HEUN	MSE	2.52E-1	4.29E-3	6.55E-3	2.28E-4	1.06E-4
	SSIM	6.86E-4	9.56E-1	9.14E-1	8.82E-1	9.33E-1

Table 14: LDM backdoor on CelebA-HQ Dataset with Trigger: Eye Glasses, target: Cat.

Sampler	P.R. Metric	0%	30%	50%	70%	90%
	FID	23.35	17.93	18.76	24.03	23.01
UNIPC	MSE	3.84E-1	3.84E-1	3.83E-1	3.72E-1	3.12E-4
	SSIM	3.17E-3	3.56E-3	3.13E-3	3.28E-3	9.93E-1
	FID	26.06	27.70	26.77	33.03	27.27
DPM. O2	MSE	3.84E-1	3.84E-1	3.83E-1	3.72E-1	8.06E-3
	SSIM	3.18E-3	3.53E-3	3.15E-3	4.48E-3	9.47E-1
	FID	28.32	33.43	31.47	37.72	30.36
DPM++. O2	MSE	3.84E-1	3.84E-1	3.83E-1	3.71E-1	1.06E-2
	SSIM	3.17E-3	3.44E-3	3.24E-3	4.58E-3	9.30E-1
	FID	24.38	22.45	22.68	28.88	24.81
DEIS	MSE	3.84E-1	3.84E-1	3.83E-1	3.72E-1	4.51E-3
	SSIM	3.18E-3	3.57E-3	3.10E-3	4.35E-3	9.70E-1

Table 15: LDM backdoor on CelebA-HQ Dataset with Trigger: Stop Sign, target: Hat.

Sampler	P.R. Metric	0%	30%	50%	70%	90%
UNIPC	FID	23.35	19.36	23.19	24.20	22.49
	MSE	2.51E-1	2.51E-1	2.51E-1	1.05E-3	1.93E-4
	SSIM	3.65E-3	6.98E-3	6.43E-3	9.92E-1	9.94E-1
DPM. O2	FID	26.06	31.63	31.64	33.62	28.83
	MSE	2.51E-1	2.51E-1	2.51E-1	5.37E-3	7.37E-3
	SSIM	3.66E-3	6.94E-3	5.91E-3	9.69E-1	9.53E-1
DPM++. O2	FID	28.32	37.67	35.92	38.21	32.37
	MSE	2.51E-1	2.51E-1	2.51E-1	6.98E-3	1.00E-2
	SSIM	3.65E-3	6.56E-3	5.31E-3	9.60E-1	9.37E-1
DEIS	FID	24.38	25.46	27.54	28.99	25.64
	MSE	2.51E-1	2.51E-1	2.51E-1	3.58E-3	4.04E-3
	SSIM	3.66E-3	7.10E-3	6.37E-3	9.79E-1	9.73E-1

Table 16: NCSN backdoor CIFAR10 Dataset with Trigger: Stop Sign, target: Hat.

Sampler	Poison Rate Metric	5%	10%	20%	30%
SCORE-SDE-VE AR:0.3	FID	12.30	12.04	12.57	12.49
	MSE	1.18E-1	1.18E-1	1.18E-1	1.20E-1
	SSIM	3.20E-1	3.12E-1	3.11E-1	2.80E-1
SCORE-SDE-VE AR:0.5	FID	12.20	12.39	12.40	13.06
	MSE	1.15E-1	1.16E-1	1.18E-1	1.16E-1
	SSIM	3.59E-1	3.42E-1	3.08E-1	3.22E-1
SCORE-SDE-VE AR:0.7	FID	12.36	12.25	11.97	12.77
	MSE	1.08E-1	1.07E-1	1.07E-1	1.09E-1
	SSIM	4.47E-1	4.59E-1	4.41E-1	4.40E-1
SCORE-SDE-VE AR:0.9	FID	12.40	12.52	12.43	12.77
	MSE	1.13E-1	1.10E-1	1.10E-1	1.11E-1
	SSIM	3.79E-1	4.16E-1	4.10E-1	3.90E-1
SCORE-SDE-VE AR:3.0	FID	14.89	15.12	15.41	15.58
	MSE	1.06E-1	1.06E-1	1.05E-1	1.04E-1
	SSIM	4.66E-1	4.70E-1	4.66E-1	4.78E-1
SCORE-SDE-VE AR:7.0	FID	17.13	17.29	17.46	18.29
	MSE	1.04E-1	1.01E-1	1.02E-1	1.00E-1
	SSIM	4.70E-1	5.20E-1	5.00E-1	5.48E-1

Table 17: Pokemon Caption Dataset with target: Cat

Clean/Backdoor	Clean				Backdoor		
Trigger	FID	MSE	MSE Thres.	SSIM	MSE	MSE Thres.	SSIM
""	49.94	1.53E-01	2.44E-01	5.69E-01	1.49E-01	2.92E-01	5.79E-01
"...."	69.77	1.53E-01	2.41E-01	5.75E-01	1.44E-01	2.37E-01	5.86E-01
"anonymous"	64.50	1.63E-01	1.77E-01	5.61E-01	1.55E-01	2.29E-01	5.76E-01
"cat"	62.63	1.57E-01	1.33E-01	5.55E-01	6.58E-02	7.03E-01	8.00E-01
"spying"	66.81	1.42E-01	2.81E-01	6.03E-01	8.15E-02	6.51E-01	7.54E-01
"sks"	64.58	1.55E-01	1.65E-01	5.50E-01	1.41E-01	2.81E-01	6.06E-01
"⚽⚽⚽⚽"	60.31	1.65E-01	9.64E-02	5.03E-01	5.16E-02	7.83E-01	8.12E-01
"fedora"	57.18	1.60E-01	1.37E-01	5.30E-01	1.63E-02	9.60E-01	9.15E-01
"🥵🥵🥵🥵"	65.21	1.51E-01	2.37E-01	5.77E-01	3.33E-02	8.84E-01	8.81E-01
"latte coffee"	58.01	1.63E-01	1.12E-01	5.12E-01	6.38E-03	9.92E-01	9.44E-01
"mignneko"	56.53	1.58E-01	1.33E-01	5.32E-01	6.55E-03	9.96E-01	9.30E-01

Table 18: Pokemon Caption Dataset with target: Hacker

Clean/Backdoor	Clean				Backdoor		
Trigger	FID	MSE	MSE Thres.	SSIM	MSE	MSE Thres.	SSIM
""	49.94	1.53E-01	2.44E-01	5.69E-01	1.49E-01	2.92E-01	5.79E-01
"...."	169.28	5.99E-02	7.47E-01	7.95E-01	5.27E-02	8.03E-01	8.11E-01
"anonymous"	183.95	5.04E-02	7.79E-01	8.12E-01	3.57E-02	8.84E-01	8.59E-01
"cat"	155.02	8.02E-02	6.47E-01	7.53E-01	2.93E-02	9.04E-01	8.74E-01
"spying"	64.35	1.48E-01	1.77E-01	5.64E-01	5.08E-03	1.00E+00	9.29E-01
"sks"	169.82	5.75E-02	7.55E-01	7.94E-01	3.49E-02	8.88E-01	8.54E-01
"⚽⚽⚽⚽"	93.69	1.33E-01	2.93E-01	5.95E-01	6.06E-03	9.96E-01	9.37E-01
"fedora"	63.31	1.59E-01	1.16E-01	5.42E-01	1.17E-02	1.00E+00	8.88E-01
"🥵🥵🥵🥵"	108.75	1.29E-01	3.73E-01	6.30E-01	1.32E-02	9.68E-01	9.16E-01
"latte coffee"	56.88	1.66E-01	4.42E-02	5.08E-01	4.69E-03	1.00E+00	9.39E-01
"mignneko"	70.35	1.54E-01	1.57E-01	5.65E-01	6.16E-03	1.00E+00	9.28E-01

Table 19: CelebA-HQ-Dialog Dataset with target: Cat

Clean/Backdoor	Clean				Backdoor		
Trigger	FID	MSE	MSE Thres.	SSIM	MSE	MSE Thres.	SSIM
""	24.52	8.50E-02	7.18E-01	4.55E-01	8.50E-02	7.22E-01	4.54E-01
"...."	18.77	1.54E-01	4.40E-02	3.60E-01	1.54E-01	4.38E-02	3.58E-01
"anonymous"	17.95	1.50E-01	6.00E-02	3.81E-01	1.60E-01	4.10E-02	3.65E-01
"cat"	17.91	1.53E-01	4.78E-02	3.87E-01	7.89E-02	5.27E-01	6.70E-01
"spying"	18.99	1.45E-01	7.49E-02	3.82E-01	3.97E-03	9.99E-01	9.44E-01
"sks"	19.09	1.52E-01	5.46E-02	3.62E-01	4.41E-03	9.95E-01	9.46E-01
"⚽⚽⚽⚽"	18.78	1.52E-01	5.22E-02	3.87E-01	9.65E-03	9.81E-01	9.27E-01
"fedora"	18.73	1.46E-01	7.39E-02	4.06E-01	3.83E-03	9.98E-01	9.50E-01
"🥵🥵🥵🥵"	18.81	1.47E-01	6.79E-02	3.94E-01	3.18E-03	9.98E-01	9.54E-01
"latte coffee"	16.90	1.55E-01	4.13E-02	3.86E-01	6.23E-02	6.35E-01	7.22E-01
"mignneko"	19.97	1.45E-01	7.03E-02	4.11E-01	3.82E-03	9.98E-01	9.50E-01

Table 20: CelebA-HQ-Dialog Dataset with target: Hacker

Clean/Backdoor	Clean				Backdoor		
Trigger	FID	MSE	MSE Thres.	SSIM	MSE	MSE Thres.	SSIM
""	24.52	8.50E-02	7.18E-01	4.55E-01	8.50E-02	7.22E-01	4.54E-01
"...."	36.59	1.43E-01	1.14E-01	4.16E-01	1.29E-01	2.10E-01	4.70E-01
"anonymous"	20.87	1.57E-01	1.97E-02	3.63E-01	3.80E-02	8.09E-01	8.09E-01
"cat"	20.42	1.54E-01	9.11E-03	3.85E-01	6.74E-03	1.00E+00	9.18E-01
"spying"	20.21	1.57E-01	7.67E-03	3.75E-01	9.69E-03	9.96E-01	9.03E-01
"sks"	19.62	1.55E-01	4.89E-03	3.74E-01	3.84E-03	1.00E+00	9.36E-01
"⚽⚽⚽⚽"	20.15	1.60E-01	4.11E-03	3.45E-01	6.78E-03	1.00E+00	9.23E-01
"fedora"	17.71	1.56E-01	7.44E-03	3.84E-01	6.16E-03	1.00E+00	9.22E-01
"🥵🥵🥵🥵"	19.21	1.49E-01	2.33E-02	4.08E-01	7.43E-03	9.99E-01	9.15E-01
"latte coffee"	20.27	1.52E-01	1.78E-02	3.69E-01	7.60E-03	1.00E+00	9.13E-01
"mignneko"	19.80	1.52E-01	1.03E-02	3.84E-01	4.44E-03	1.00E+00	9.33E-01

Table 21: CIFAR10 Dataset with Trigger: Stop Sign, target: No Shift, and inference-time clipping.

Sampler	P.R. Metric	0%	5%	10%	20%	30%	50%	70%	90%
	FID	185.20	113.01	112.52	115.08	114.17	112.86	113.57	102.87
UNIPC	MSE	1.28E-1	1.66E-3	9.74E-4	8.39E-4	1.04E-3	2.09E-3	3.88E-3	5.91E-3
	SSIM	1.89E-2	9.51E-1	9.63E-1	9.76E-1	9.76E-1	9.68E-1	9.61E-1	9.48E-1
	FID	185.20	113.01	112.52	115.08	114.17	112.86	113.57	102.87
DPM. O2	MSE	1.28E-1	1.66E-3	9.74E-4	8.39E-4	1.04E-3	2.09E-3	3.88E-3	5.91E-3
	SSIM	1.89E-2	9.51E-1	9.63E-1	9.76E-1	9.76E-1	9.68E-1	9.61E-1	9.48E-1
	FID	185.20	113.01	112.52	115.08	114.17	112.86	79.96	102.87
DPM. O3	MSE	1.28E-1	1.66E-3	9.74E-4	8.39E-4	1.04E-3	2.09E-3	2.20E-3	5.91E-3
	SSIM	1.89E-2	9.51E-1	9.63E-1	9.76E-1	9.76E-1	9.68E-1	9.72E-1	9.48E-1
	FID	185.20	113.01	112.52	115.08	114.17	112.86	113.57	102.87
DPM++. O2	MSE	1.28E-1	1.66E-3	9.74E-4	8.39E-4	1.04E-3	2.09E-3	3.88E-3	5.91E-3
	SSIM	1.89E-2	9.51E-1	9.63E-1	9.76E-1	9.76E-1	9.68E-1	9.61E-1	9.48E-1
	FID	185.20	113.01	112.52	115.08	114.17	112.86	113.57	102.87
DPM++. O3	MSE	1.28E-1	1.66E-3	9.74E-4	8.39E-4	1.04E-3	2.09E-3	3.88E-3	5.91E-3
	SSIM	1.89E-2	9.51E-1	9.63E-1	9.76E-1	9.76E-1	9.68E-1	9.61E-1	9.48E-1
	FID	185.20	113.01	112.52	115.08	114.17	112.86	113.57	102.87
DEIS	MSE	1.28E-1	1.66E-3	9.74E-4	8.39E-4	1.04E-3	2.09E-3	3.88E-3	5.91E-3
	SSIM	1.89E-2	9.51E-1	9.63E-1	9.76E-1	9.76E-1	9.68E-1	9.61E-1	9.48E-1
	FID	177.35	114.44	111.50	78.08	110.79	75.63	74.81	37.25
PNDM	MSE	1.33E-1	4.88E-3	1.25E-3	6.40E-5	2.24E-5	1.76E-5	1.48E-5	2.02E-5
	SSIM	1.27E-2	9.65E-1	9.89E-1	9.92E-1	9.98E-1	9.93E-1	9.93E-1	9.88E-1
	FID	177.35	114.44	111.50	113.33	76.47	75.92	106.93	95.02
HEUN	MSE	1.33E-1	4.88E-3	1.25E-3	5.29E-5	2.88E-5	1.62E-5	8.53E-6	6.29E-6
	SSIM	1.27E-2	9.65E-1	9.89E-1	9.97E-1	9.92E-1	9.94E-1	9.97E-1	9.97E-1
	FID	177.35	114.44	111.50	113.33	110.79	109.48	106.93	95.02
LMSD	MSE	1.33E-1	4.88E-3	1.25E-3	5.29E-5	2.24E-5	8.66E-6	8.53E-6	6.29E-6
	SSIM	1.27E-2	9.65E-1	9.89E-1	9.97E-1	9.98E-1	9.98E-1	9.97E-1	9.97E-1

Table 22: CIFAR10 Dataset with Trigger: Stop Sign, target: Shift, and inference-time clipping.

Sampler	P.R. Metric	0%	5%	10%	20%	30%	50%	70%	90%
	FID	185.20	109.05	111.43	114.46	109.55	106.58	106.54	95.98
UNIPC	MSE	1.42E-1	2.13E-3	5.20E-3	1.16E-3	6.71E-4	1.87E-3	7.27E-3	5.83E-3
	SSIM	4.96E-3	9.51E-1	9.31E-1	9.81E-1	9.87E-1	9.81E-1	9.45E-1	9.65E-1
	FID	185.20	109.05	111.43	114.46	109.55	106.58	106.54	95.98
DPM. O2	MSE	1.42E-1	2.13E-3	5.20E-3	1.16E-3	6.71E-4	1.87E-3	7.27E-3	5.83E-3
	SSIM	4.96E-3	9.51E-1	9.31E-1	9.81E-1	9.87E-1	9.81E-1	9.45E-1	9.65E-1
	FID	185.20	109.05	111.43	114.46	109.55	106.58	106.54	95.98
DPM. O3	MSE	1.42E-1	2.13E-3	5.20E-3	1.16E-3	6.71E-4	1.87E-3	7.27E-3	5.83E-3
	SSIM	4.96E-3	9.51E-1	9.31E-1	9.81E-1	9.87E-1	9.81E-1	9.45E-1	9.65E-1
	FID	185.20	109.05	111.43	114.46	109.55	106.58	106.54	95.98
DPM++. O2	MSE	1.42E-1	2.13E-3	5.20E-3	1.16E-3	6.71E-4	1.87E-3	7.27E-3	5.83E-3
	SSIM	4.96E-3	9.51E-1	9.31E-1	9.81E-1	9.87E-1	9.81E-1	9.45E-1	9.65E-1
	FID	185.20	109.05	111.43	114.46	109.55	106.58	106.54	95.98
DPM++. O3	MSE	1.42E-1	2.13E-3	5.20E-3	1.16E-3	6.71E-4	1.87E-3	7.27E-3	5.83E-3
	SSIM	4.96E-3	9.51E-1	9.31E-1	9.81E-1	9.87E-1	9.81E-1	9.45E-1	9.65E-1
	FID	185.20	109.05	111.43	114.46	109.55	106.58	106.54	95.98
DEIS	MSE	1.42E-1	2.13E-3	5.20E-3	1.16E-3	6.71E-4	1.87E-3	7.27E-3	5.83E-3
	SSIM	4.96E-3	9.51E-1	9.31E-1	9.81E-1	9.87E-1	9.81E-1	9.45E-1	9.65E-1
	FID	177.35	76.82	112.65	77.49	109.74	71.45	69.14	62.08
PNDM	MSE	1.43E-1	3.13E-2	5.55E-3	4.26E-5	5.76E-5	1.72E-5	2.57E-3	1.29E-5
	SSIM	4.03E-3	7.46E-1	9.52E-1	9.96E-1	9.98E-1	9.96E-1	9.74E-1	9.96E-1
	FID	177.35	112.06	112.65	113.39	109.74	102.50	100.08	88.76
HEUN	MSE	1.43E-1	7.98E-4	5.55E-3	3.20E-5	5.76E-5	1.13E-5	2.56E-3	5.40E-6
	SSIM	4.03E-3	9.94E-1	9.52E-1	9.99E-1	9.98E-1	9.99E-1	9.77E-1	9.98E-1
	FID	177.35	112.06	112.65	113.39	109.74	102.50	100.08	88.76
LMSD	MSE	1.43E-1	7.98E-4	5.55E-3	3.20E-5	5.76E-5	1.13E-5	2.56E-3	5.40E-6
	SSIM	4.03E-3	9.94E-1	9.52E-1	9.99E-1	9.98E-1	9.99E-1	9.77E-1	9.98E-1

Table 23: CIFAR10 Dataset with Trigger: Stop Sign, target: Corner, and inference-time clipping.

Sampler	P.R. Metric	0%	5%	10%	20%	30%	50%	70%	90%
	FID	14.31	8.54	7.80	8.49	8.08	8.17	7.89	7.91
ANCESTRAL	MSE	7.93E-2	7.56E-2	7.48E-2	7.54E-2	7.32E-2	6.97E-2	6.83E-2	6.21E-2
	SSIM	7.10E-2	8.99E-2	1.03E-1	8.87E-2	9.95E-2	1.13E-1	1.08E-1	1.44E-1
	FID	185.20	121.16	119.11	121.15	118.63	118.40	124.84	124.46
UNIPC	MSE	1.11E-1	1.19E-2	1.07E-2	1.89E-3	2.14E-2	2.65E-2	2.36E-3	4.50E-3
	SSIM	8.50E-3	6.40E-1	6.97E-1	8.36E-1	5.53E-1	5.21E-1	8.73E-1	8.40E-1
	FID	185.20	121.16	119.11	121.15	118.63	118.40	124.84	124.46
DPM. O2	MSE	1.11E-1	1.19E-2	1.07E-2	1.89E-3	2.14E-2	2.65E-2	2.36E-3	4.50E-3
	SSIM	8.50E-3	6.40E-1	6.97E-1	8.36E-1	5.53E-1	5.21E-1	8.73E-1	8.40E-1
	FID	185.20	121.16	119.11	121.15	118.63	118.40	124.84	124.46
DPM. O3	MSE	1.11E-1	1.19E-2	1.07E-2	1.89E-3	2.14E-2	2.65E-2	2.36E-3	4.50E-3
	SSIM	8.50E-3	6.40E-1	6.97E-1	8.36E-1	5.53E-1	5.21E-1	8.73E-1	8.40E-1
	FID	185.20	121.16	119.11	121.15	118.63	118.40	124.84	124.46
DPM++. O2	MSE	1.11E-1	1.19E-2	1.07E-2	1.89E-3	2.14E-2	2.65E-2	2.36E-3	4.50E-3
	SSIM	8.50E-3	6.40E-1	6.97E-1	8.36E-1	5.53E-1	5.21E-1	8.73E-1	8.40E-1
	FID	185.20	121.16	119.11	121.15	118.63	82.22	124.84	124.46
DPM++. O3	MSE	1.11E-1	1.19E-2	1.07E-2	1.89E-3	2.14E-2	2.42E-2	2.36E-3	4.50E-3
	SSIM	8.50E-3	6.40E-1	6.97E-1	8.36E-1	5.53E-1	5.78E-1	8.73E-1	8.40E-1
	FID	185.20	121.16	119.11	121.15	118.63	118.40	124.84	124.46
DEIS	MSE	1.11E-1	1.19E-2	1.07E-2	1.89E-3	2.14E-2	2.65E-2	2.36E-3	4.50E-3
	SSIM	8.50E-3	6.40E-1	6.97E-1	8.36E-1	5.53E-1	5.21E-1	8.73E-1	8.40E-1
	FID	177.35	86.72	124.80	127.35	122.77	122.23	89.46	89.20
PNDM	MSE	1.10E-1	5.75E-2	2.91E-2	3.73E-3	4.75E-2	4.18E-2	1.01E-3	2.17E-4
	SSIM	6.74E-3	4.26E-1	7.13E-1	9.62E-1	5.39E-1	5.68E-1	9.78E-1	9.85E-1
	FID	177.35	129.05	124.80	127.35	122.77	122.23	129.63	133.33
HEUN	MSE	1.10E-1	4.46E-2	2.91E-2	3.73E-3	4.75E-2	4.18E-2	1.08E-3	2.11E-4
	SSIM	6.74E-3	5.72E-1	7.13E-1	9.62E-1	5.39E-1	5.68E-1	9.83E-1	9.91E-1
	FID	177.35	129.05	124.80	127.35	122.77	122.23	129.63	133.33
LMSD	MSE	1.10E-1	4.46E-2	2.91E-2	3.73E-3	4.75E-2	4.18E-2	1.08E-3	2.11E-4
	SSIM	6.74E-3	5.72E-1	7.13E-1	9.62E-1	5.39E-1	5.68E-1	9.83E-1	9.91E-1

Table 24: CIFAR10 Dataset with Trigger: Stop Sign, target: Shoe, and inference-time clipping.

Sampler	P.R. Metric	0%	5%	10%	20%	30%	50%	70%	90%
	FID	185.20	107.88	108.12	109.60	105.08	109.91	104.87	98.41
UNIPC	MSE	3.20E-1	3.56E-2	6.73E-3	1.27E-3	5.94E-3	7.13E-4	1.28E-3	1.94E-3
	SSIM	6.07E-3	8.50E-1	9.50E-1	9.72E-1	9.60E-1	9.83E-1	9.77E-1	9.73E-1
	FID	185.20	107.88	108.12	109.60	105.08	109.91	104.87	98.41
DPM. O2	MSE	3.20E-1	3.56E-2	6.73E-3	1.27E-3	5.94E-3	7.13E-4	1.28E-3	1.94E-3
	SSIM	6.07E-3	8.50E-1	9.50E-1	9.72E-1	9.60E-1	9.83E-1	9.77E-1	9.73E-1
	FID	185.20	107.88	108.12	109.60	105.08	109.91	73.51	98.41
DPM. O3	MSE	3.20E-1	3.56E-2	6.73E-3	1.27E-3	5.94E-3	7.13E-4	8.89E-4	1.94E-3
	SSIM	6.07E-3	8.50E-1	9.50E-1	9.72E-1	9.60E-1	9.83E-1	9.81E-1	9.73E-1
	FID	185.20	107.88	108.12	109.60	105.08	109.91	104.87	98.41
DPM++. O2	MSE	3.20E-1	3.56E-2	6.73E-3	1.27E-3	5.94E-3	7.13E-4	1.28E-3	1.94E-3
	SSIM	6.07E-3	8.50E-1	9.50E-1	9.72E-1	9.60E-1	9.83E-1	9.77E-1	9.73E-1
	FID	185.20	107.88	108.12	109.60	105.08	109.91	104.87	98.41
DPM++. O3	MSE	3.20E-1	3.56E-2	6.73E-3	1.27E-3	5.94E-3	7.13E-4	1.28E-3	1.94E-3
	SSIM	6.07E-3	8.50E-1	9.50E-1	9.72E-1	9.60E-1	9.83E-1	9.77E-1	9.73E-1
	FID	185.20	107.88	108.12	109.60	105.08	109.91	104.87	98.41
DEIS	MSE	3.20E-1	3.56E-2	6.73E-3	1.27E-3	5.94E-3	7.13E-4	1.28E-3	1.94E-3
	SSIM	6.07E-3	8.50E-1	9.50E-1	9.72E-1	9.60E-1	9.83E-1	9.77E-1	9.73E-1
	FID	177.35	74.67	107.85	73.88	71.59	72.62	105.62	67.34
PNDM	MSE	3.24E-1	1.05E-1	1.97E-2	1.70E-3	1.17E-2	3.98E-5	1.53E-5	1.59E-5
	SSIM	4.67E-3	6.26E-1	9.32E-1	9.91E-1	9.53E-1	9.97E-1	9.99E-1	9.97E-1
	FID	177.35	110.54	107.85	108.84	103.94	107.88	105.62	96.78
HEUN	MSE	3.24E-1	8.27E-2	1.97E-2	1.86E-3	1.31E-2	4.19E-5	1.53E-5	9.93E-6
	SSIM	4.67E-3	7.25E-1	9.32E-1	9.92E-1	9.49E-1	9.99E-1	9.99E-1	9.99E-1
	FID	177.35	110.54	107.85	108.84	103.94	107.88	105.62	96.78
LMSD	MSE	3.24E-1	8.27E-2	1.97E-2	1.86E-3	1.31E-2	4.19E-5	1.53E-5	9.93E-6
	SSIM	4.67E-3	7.25E-1	9.32E-1	9.92E-1	9.49E-1	9.99E-1	9.99E-1	9.99E-1

Table 25: CIFAR10 Dataset with Trigger: Stop Sign, target: Hat, and inference-time clipping.

Sampler	P.R. Metric	0%	5%	10%	20%	30%	50%	70%	90%
	FID	14.31	8.31	7.53	8.10	7.64	7.63	7.63	7.71
ANCESTRAL	MSE	1.76E-1	1.67E-1	1.66E-1	1.68E-1	1.67E-1	1.62E-1	1.58E-1	1.48E-1
	SSIM	3.41E-2	4.26E-2	4.36E-2	4.05E-2	4.37E-2	4.70E-2	4.72E-2	5.16E-2
	FID	185.20	110.69	109.15	110.76	107.63	110.05	106.94	100.60
UNIPC	MSE	2.33E-1	8.32E-3	6.79E-3	5.52E-3	6.54E-3	1.88E-3	3.30E-3	5.54E-3
	SSIM	8.04E-3	9.06E-1	9.45E-1	9.61E-1	9.55E-1	9.84E-1	9.80E-1	9.73E-1
	FID	185.20	110.69	109.15	110.76	107.63	110.05	106.94	100.60
DPM. O2	MSE	2.33E-1	8.32E-3	6.79E-3	5.52E-3	6.54E-3	1.88E-3	3.30E-3	5.54E-3
	SSIM	8.04E-3	9.06E-1	9.45E-1	9.61E-1	9.55E-1	9.84E-1	9.80E-1	9.73E-1
	FID	185.20	110.69	109.15	110.76	107.63	110.05	106.94	100.60
DPM. O3	MSE	2.33E-1	8.32E-3	6.79E-3	5.52E-3	6.54E-3	1.88E-3	3.30E-3	5.54E-3
	SSIM	8.04E-3	9.06E-1	9.45E-1	9.61E-1	9.55E-1	9.84E-1	9.80E-1	9.73E-1
	FID	185.20	110.69	109.15	110.76	107.63	110.05	106.94	100.60
DPM++. O2	MSE	2.33E-1	8.32E-3	6.79E-3	5.52E-3	6.54E-3	1.88E-3	3.30E-3	5.54E-3
	SSIM	8.04E-3	9.06E-1	9.45E-1	9.61E-1	9.55E-1	9.84E-1	9.80E-1	9.73E-1
	FID	185.20	110.69	109.15	110.76	107.63	110.05	106.94	100.60
DPM++. O3	MSE	2.33E-1	8.32E-3	6.79E-3	5.52E-3	6.54E-3	1.88E-3	3.30E-3	5.54E-3
	SSIM	8.04E-3	9.06E-1	9.45E-1	9.61E-1	9.55E-1	9.84E-1	9.80E-1	9.73E-1
	FID	185.20	110.69	109.15	110.76	107.63	110.05	106.94	100.60
DEIS	MSE	2.33E-1	8.32E-3	6.79E-3	5.52E-3	6.54E-3	1.88E-3	3.30E-3	5.54E-3
	SSIM	8.04E-3	9.06E-1	9.45E-1	9.61E-1	9.55E-1	9.84E-1	9.80E-1	9.73E-1
	FID	177.35	77.16	42.34	75.69	42.47	106.99	8.11	95.57
PNDM	MSE	2.34E-1	9.55E-3	3.38E-2	3.55E-3	1.37E-4	8.03E-4	3.04E-5	6.80E-6
	SSIM	7.73E-3	9.49E-1	8.26E-1	9.82E-1	9.98E-1	9.95E-1	9.98E-1	1.00E+0
	FID	177.35	111.49	110.30	110.51	108.51	106.99	99.88	95.57
HEUN	MSE	2.34E-1	7.92E-3	1.04E-2	4.58E-3	9.40E-3	8.03E-4	1.18E-5	6.80E-6
	SSIM	7.73E-3	9.63E-1	9.52E-1	9.77E-1	9.54E-1	9.95E-1	1.00E+0	1.00E+0
	FID	177.35	111.49	110.30	110.51	108.51	106.99	99.88	95.57
LMSD	MSE	2.34E-1	7.92E-3	1.04E-2	4.58E-3	9.40E-3	8.03E-4	1.18E-5	6.80E-6
	SSIM	7.73E-3	9.63E-1	9.52E-1	9.77E-1	9.54E-1	9.95E-1	1.00E+0	1.00E+0

Table 26: CIFAR10 Dataset with Trigger: Grey Box, target: No Shift, and inference-time clipping.

Sampler	P.R. Metric	0%	5%	10%	20%	30%	50%	70%	90%
	FID	185.20	121.50	121.93	130.83	123.83	134.04	146.21	159.08
UNIPC	MSE	1.20E-1	1.18E-3	4.93E-4	4.28E-4	1.05E-3	1.23E-3	1.64E-3	3.83E-3
	SSIM	8.51E-4	9.68E-1	9.76E-1	9.78E-1	9.62E-1	9.62E-1	9.62E-1	9.31E-1
	FID	185.20	121.50	121.93	130.83	123.83	134.04	146.21	159.08
DPM. O2	MSE	1.20E-1	1.18E-3	4.93E-4	4.28E-4	1.05E-3	1.23E-3	1.64E-3	3.83E-3
	SSIM	8.51E-4	9.68E-1	9.76E-1	9.78E-1	9.62E-1	9.62E-1	9.62E-1	9.31E-1
	FID	185.20	121.50	84.27	130.83	123.83	134.04	146.21	159.08
DPM. O3	MSE	1.20E-1	1.18E-3	1.13E-3	4.28E-4	1.05E-3	1.23E-3	1.64E-3	3.83E-3
	SSIM	8.51E-4	9.68E-1	9.55E-1	9.78E-1	9.62E-1	9.62E-1	9.62E-1	9.31E-1
	FID	185.20	121.50	121.93	130.83	123.83	134.04	146.21	159.08
DPM++. O2	MSE	1.20E-1	1.18E-3	4.93E-4	4.28E-4	1.05E-3	1.23E-3	1.64E-3	3.83E-3
	SSIM	8.51E-4	9.68E-1	9.76E-1	9.78E-1	9.62E-1	9.62E-1	9.62E-1	9.31E-1
	FID	185.20	121.50	121.93	130.83	123.83	134.04	146.21	159.08
DPM++. O3	MSE	1.20E-1	1.18E-3	4.93E-4	4.28E-4	1.05E-3	1.23E-3	1.64E-3	3.83E-3
	SSIM	8.51E-4	9.68E-1	9.76E-1	9.78E-1	9.62E-1	9.62E-1	9.62E-1	9.31E-1
	FID	185.20	121.50	121.93	130.83	123.83	134.04	146.21	159.08
DEIS	MSE	1.20E-1	1.18E-3	4.93E-4	4.28E-4	1.05E-3	1.23E-3	1.64E-3	3.83E-3
	SSIM	8.51E-4	9.68E-1	9.76E-1	9.78E-1	9.62E-1	9.62E-1	9.62E-1	9.31E-1
	FID	177.35	84.49	8.34	54.96	91.59	98.41	154.06	75.09
PNDM	MSE	1.20E-1	1.80E-2	1.37E-2	2.36E-4	4.39E-5	1.61E-5	7.00E-6	2.16E-5
	SSIM	9.50E-4	7.88E-1	7.93E-1	9.80E-1	9.90E-1	9.91E-1	9.96E-1	9.85E-1
	FID	177.35	126.85	127.51	137.93	129.76	143.02	154.06	162.09
HEUN	MSE	1.20E-1	2.98E-3	1.27E-3	6.22E-5	3.67E-5	8.34E-6	7.00E-6	7.66E-6
	SSIM	9.50E-4	9.72E-1	9.85E-1	9.96E-1	9.96E-1	9.96E-1	9.96E-1	9.95E-1
	FID	177.35	126.85	127.51	137.93	129.76	143.02	154.06	162.09
LMSD	MSE	1.20E-1	2.98E-3	1.27E-3	6.22E-5	3.67E-5	8.34E-6	7.00E-6	7.66E-6
	SSIM	9.50E-4	9.72E-1	9.85E-1	9.96E-1	9.96E-1	9.96E-1	9.96E-1	9.95E-1

Table 27: CIFAR10 Dataset with Trigger: Grey Box, target: Shift, and inference-time clipping.

Sampler	P.R. Metric	0%	5%	10%	20%	30%	50%	70%	90%
	FID	185.20	123.67	117.55	118.87	119.92	122.32	126.07	131.79
UNIPC	MSE	1.20E-1	2.83E-3	1.61E-3	4.57E-4	2.76E-4	1.82E-3	2.07E-3	4.21E-3
	SSIM	7.09E-4	9.50E-1	9.60E-1	9.76E-1	9.84E-1	9.54E-1	9.55E-1	9.27E-1
	FID	185.20	123.67	117.55	118.87	119.92	122.32	126.07	131.79
DPM. O2	MSE	1.20E-1	2.83E-3	1.61E-3	4.57E-4	2.76E-4	1.82E-3	2.07E-3	4.21E-3
	SSIM	7.09E-4	9.50E-1	9.60E-1	9.76E-1	9.84E-1	9.54E-1	9.55E-1	9.27E-1
	FID	185.20	123.67	117.55	118.87	119.92	122.32	126.07	131.79
DPM. O3	MSE	1.20E-1	2.83E-3	1.61E-3	4.57E-4	2.76E-4	1.82E-3	2.07E-3	4.21E-3
	SSIM	7.09E-4	9.50E-1	9.60E-1	9.76E-1	9.84E-1	9.54E-1	9.55E-1	9.27E-1
	FID	185.20	123.67	117.55	118.87	119.92	122.32	126.07	131.79
DPM++. O2	MSE	1.20E-1	2.83E-3	1.61E-3	4.57E-4	2.76E-4	1.82E-3	2.07E-3	4.21E-3
	SSIM	7.09E-4	9.50E-1	9.60E-1	9.76E-1	9.84E-1	9.54E-1	9.55E-1	9.27E-1
	FID	185.20	123.67	80.34	118.87	119.92	122.32	126.07	131.79
DPM++. O3	MSE	1.20E-1	2.83E-3	1.07E-2	4.57E-4	2.76E-4	1.82E-3	2.07E-3	4.21E-3
	SSIM	7.09E-4	9.50E-1	8.34E-1	9.76E-1	9.84E-1	9.54E-1	9.55E-1	9.27E-1
	FID	185.20	123.67	117.55	118.87	119.92	122.32	126.07	131.79
DEIS	MSE	1.20E-1	2.83E-3	1.61E-3	4.57E-4	2.76E-4	1.82E-3	2.07E-3	4.21E-3
	SSIM	7.09E-4	9.50E-1	9.60E-1	9.76E-1	9.84E-1	9.54E-1	9.55E-1	9.27E-1
	FID	177.35	88.59	81.09	47.93	86.19	88.97	129.77	102.72
PNDM	MSE	1.20E-1	1.71E-2	3.19E-3	2.15E-4	3.71E-4	1.64E-5	6.98E-6	1.42E-5
	SSIM	6.17E-4	8.09E-1	9.57E-1	9.86E-1	9.90E-1	9.94E-1	9.97E-1	9.93E-1
	FID	177.35	125.94	119.25	121.26	122.38	125.11	129.77	138.51
HEUN	MSE	1.20E-1	8.17E-3	2.87E-3	2.09E-4	3.83E-4	7.62E-6	6.98E-6	7.41E-6
	SSIM	6.17E-4	9.27E-1	9.73E-1	9.96E-1	9.94E-1	9.98E-1	9.97E-1	9.97E-1
	FID	177.35	125.94	119.25	121.26	122.38	125.11	129.77	138.51
LMSD	MSE	1.20E-1	8.17E-3	2.87E-3	2.09E-4	3.83E-4	7.62E-6	6.98E-6	7.41E-6
	SSIM	6.17E-4	9.27E-1	9.73E-1	9.96E-1	9.94E-1	9.98E-1	9.97E-1	9.97E-1

Table 28: CIFAR10 Dataset with Trigger: Grey Box, target: Corner, and inference-time clipping.

Sampler	P.R. Metric	0%	5%	10%	20%	30%	50%	70%	90%
	FID	14.31	9.91	10.94	12.99	15.06	19.85	28.11	53.35
ANCESTRAL	MSE	7.86E-2	5.56E-2	5.34E-2	4.97E-2	5.01E-2	3.87E-2	2.74E-2	1.32E-2
	SSIM	7.17E-2	2.50E-1	2.80E-1	3.29E-1	3.35E-1	4.60E-1	5.88E-1	7.73E-1
	FID	185.20	125.95	127.27	124.84	125.84	131.79	134.52	136.83
UNIPC	MSE	1.05E-1	2.18E-3	8.14E-4	5.05E-4	4.90E-4	1.09E-3	1.69E-3	5.51E-3
	SSIM	1.13E-3	9.16E-1	9.33E-1	9.48E-1	9.54E-1	9.36E-1	9.24E-1	8.36E-1
	FID	185.20	125.95	127.27	124.84	125.84	131.79	134.52	136.83
DPM. O2	MSE	1.05E-1	2.18E-3	8.14E-4	5.05E-4	4.90E-4	1.09E-3	1.69E-3	5.51E-3
	SSIM	1.13E-3	9.16E-1	9.33E-1	9.48E-1	9.54E-1	9.36E-1	9.24E-1	8.36E-1
	FID	185.20	125.95	127.27	124.84	125.84	131.79	134.52	136.83
DPM. O3	MSE	1.05E-1	2.18E-3	8.14E-4	5.05E-4	4.90E-4	1.09E-3	1.69E-3	5.51E-3
	SSIM	1.13E-3	9.16E-1	9.33E-1	9.48E-1	9.54E-1	9.36E-1	9.24E-1	8.36E-1
	FID	185.20	125.95	127.27	124.84	125.84	131.79	134.52	136.83
DPM++. O2	MSE	1.05E-1	2.18E-3	8.14E-4	5.05E-4	4.90E-4	1.09E-3	1.69E-3	5.51E-3
	SSIM	1.13E-3	9.16E-1	9.33E-1	9.48E-1	9.54E-1	9.36E-1	9.24E-1	8.36E-1
	FID	185.20	125.95	127.27	124.84	125.84	131.79	134.52	136.83
DPM++. O3	MSE	1.05E-1	2.18E-3	8.14E-4	5.05E-4	4.90E-4	1.09E-3	1.69E-3	5.51E-3
	SSIM	1.13E-3	9.16E-1	9.33E-1	9.48E-1	9.54E-1	9.36E-1	9.24E-1	8.36E-1
	FID	185.20	125.95	127.27	124.84	125.84	131.79	134.52	136.83
DEIS	MSE	1.05E-1	2.18E-3	8.14E-4	5.05E-4	4.90E-4	1.09E-3	1.69E-3	5.51E-3
	SSIM	1.13E-3	9.16E-1	9.33E-1	9.48E-1	9.54E-1	9.36E-1	9.24E-1	8.36E-1
	FID	177.35	134.07	93.84	49.66	94.22	102.26	147.95	156.45
PNDM	MSE	1.05E-1	3.56E-3	4.82E-3	9.19E-5	3.88E-5	2.01E-5	9.18E-6	7.25E-6
	SSIM	1.38E-3	9.66E-1	8.97E-1	9.78E-1	9.87E-1	9.88E-1	9.94E-1	9.94E-1
	FID	177.35	134.07	135.99	134.72	137.73	145.55	147.95	156.45
HEUN	MSE	1.05E-1	3.56E-3	4.92E-4	4.11E-5	5.36E-5	1.44E-5	9.18E-6	7.25E-6
	SSIM	1.38E-3	9.66E-1	9.92E-1	9.96E-1	9.95E-1	9.94E-1	9.94E-1	9.94E-1
	FID	177.35	134.07	135.99	134.72	137.73	145.55	147.95	156.45
LMSD	MSE	1.05E-1	3.56E-3	4.92E-4	4.11E-5	5.36E-5	1.44E-5	9.18E-6	7.25E-6
	SSIM	1.38E-3	9.66E-1	9.92E-1	9.96E-1	9.95E-1	9.94E-1	9.94E-1	9.94E-1

Table 29: CIFAR10 Dataset with Trigger: Grey Box, target: Shoe, and inference-time clipping.

Sampler	P.R. Metric	0%	5%	10%	20%	30%	50%	70%	90%
	FID	185.20	108.96	109.27	113.59	110.68	111.37	105.23	105.27
UNIPC	MSE	3.37E-1	2.20E-3	1.02E-3	8.76E-4	9.58E-4	1.80E-3	1.97E-3	3.59E-3
	SSIM	2.29E-4	9.80E-1	9.82E-1	9.82E-1	9.83E-1	9.76E-1	9.76E-1	9.65E-1
	FID	185.20	108.96	109.27	113.59	110.68	111.37	105.23	105.27
DPM. O2	MSE	3.37E-1	2.20E-3	1.02E-3	8.76E-4	9.58E-4	1.80E-3	1.97E-3	3.59E-3
	SSIM	2.29E-4	9.80E-1	9.82E-1	9.82E-1	9.83E-1	9.76E-1	9.76E-1	9.65E-1
	FID	185.20	108.96	109.27	113.59	110.68	111.37	105.23	105.27
DPM. O3	MSE	3.37E-1	2.20E-3	1.02E-3	8.76E-4	9.58E-4	1.80E-3	1.97E-3	3.59E-3
	SSIM	2.29E-4	9.80E-1	9.82E-1	9.82E-1	9.83E-1	9.76E-1	9.76E-1	9.65E-1
	FID	185.20	75.06	109.27	113.59	110.68	111.37	105.23	105.27
DPM++. O2	MSE	3.37E-1	1.96E-2	1.02E-3	8.76E-4	9.58E-4	1.80E-3	1.97E-3	3.59E-3
	SSIM	2.29E-4	8.92E-1	9.82E-1	9.82E-1	9.83E-1	9.76E-1	9.76E-1	9.65E-1
	FID	185.20	108.96	109.27	113.59	110.68	111.37	105.23	105.27
DPM++. O3	MSE	3.37E-1	2.20E-3	1.02E-3	8.76E-4	9.58E-4	1.80E-3	1.97E-3	3.59E-3
	SSIM	2.29E-4	9.80E-1	9.82E-1	9.82E-1	9.83E-1	9.76E-1	9.76E-1	9.65E-1
	FID	185.20	108.96	109.27	113.59	110.68	111.37	105.23	105.27
DEIS	MSE	3.37E-1	2.20E-3	1.02E-3	8.76E-4	9.58E-4	1.80E-3	1.97E-3	3.59E-3
	SSIM	2.29E-4	9.80E-1	9.82E-1	9.82E-1	9.83E-1	9.76E-1	9.76E-1	9.65E-1
	FID	177.35	76.12	77.07	44.45	74.86	76.19	73.59	73.31
PNDM	MSE	3.37E-1	6.60E-2	4.31E-3	8.33E-5	5.15E-5	2.28E-5	1.95E-5	1.49E-5
	SSIM	2.08E-4	7.43E-1	9.75E-1	9.95E-1	9.97E-1	9.97E-1	9.98E-1	9.97E-1
	FID	177.35	109.16	111.45	112.72	109.41	108.98	104.22	105.28
HEUN	MSE	3.37E-1	4.08E-3	8.50E-4	1.14E-4	5.27E-5	1.76E-5	1.19E-5	8.16E-6
	SSIM	2.08E-4	9.87E-1	9.96E-1	9.98E-1	9.99E-1	9.99E-1	9.99E-1	9.99E-1
	FID	177.35	109.16	111.45	112.72	109.41	108.98	104.22	105.28
LMSD	MSE	3.37E-1	4.08E-3	8.50E-4	1.14E-4	5.27E-5	1.76E-5	1.19E-5	8.16E-6
	SSIM	2.08E-4	9.87E-1	9.96E-1	9.98E-1	9.99E-1	9.99E-1	9.99E-1	9.99E-1

Table 30: CIFAR10 Dataset with Trigger: Grey Box, target: Hat, and inference-time clipping.

Sampler	P.R. Metric	0%	5%	10%	20%	30%	50%	70%	90%
	FID	14.31	8.42	8.82	8.89	8.97	10.11	11.32	17.82
ANCESTRAL	MSE	1.74E-1	1.24E-1	1.08E-1	1.09E-1	1.12E-1	1.01E-1	9.63E-2	8.57E-2
	SSIM	3.43E-2	2.08E-1	2.83E-1	2.82E-1	2.66E-1	3.26E-1	3.55E-1	4.07E-1
	FID	185.20	110.41	111.65	109.41	112.08	111.42	105.79	107.68
UNIPC	MSE	2.40E-1	5.12E-4	3.63E-4	5.34E-4	8.85E-4	1.63E-3	3.46E-3	6.46E-3
	SSIM	2.97E-4	9.88E-1	9.92E-1	9.92E-1	9.92E-1	9.88E-1	9.80E-1	9.70E-1
	FID	185.20	110.41	111.65	109.41	112.08	111.42	105.79	107.68
DPM. O2	MSE	2.40E-1	5.12E-4	3.63E-4	5.34E-4	8.85E-4	1.63E-3	3.46E-3	6.46E-3
	SSIM	2.97E-4	9.88E-1	9.92E-1	9.92E-1	9.92E-1	9.88E-1	9.80E-1	9.70E-1
	FID	185.20	110.41	111.65	109.41	112.08	111.42	105.79	107.68
DPM. O3	MSE	2.40E-1	5.12E-4	3.63E-4	5.34E-4	8.85E-4	1.63E-3	3.46E-3	6.46E-3
	SSIM	2.97E-4	9.88E-1	9.92E-1	9.92E-1	9.92E-1	9.88E-1	9.80E-1	9.70E-1
	FID	185.20	110.41	111.65	109.41	112.08	111.42	105.79	107.68
DPM++. O2	MSE	2.40E-1	5.12E-4	3.63E-4	5.34E-4	8.85E-4	1.63E-3	3.46E-3	6.46E-3
	SSIM	2.97E-4	9.88E-1	9.92E-1	9.92E-1	9.92E-1	9.88E-1	9.80E-1	9.70E-1
	FID	185.20	110.41	111.65	109.41	112.08	111.42	105.79	107.68
DPM++. O3	MSE	2.40E-1	5.12E-4	3.63E-4	5.34E-4	8.85E-4	1.63E-3	3.46E-3	6.46E-3
	SSIM	2.97E-4	9.88E-1	9.92E-1	9.92E-1	9.92E-1	9.88E-1	9.80E-1	9.70E-1
	FID	185.20	110.41	111.65	109.41	112.08	111.42	105.79	107.68
DEIS	MSE	2.40E-1	5.12E-4	3.63E-4	5.34E-4	8.85E-4	1.63E-3	3.46E-3	6.46E-3
	SSIM	2.97E-4	9.88E-1	9.92E-1	9.92E-1	9.92E-1	9.88E-1	9.80E-1	9.70E-1
	FID	177.35	112.35	111.44	77.27	41.78	77.43	101.54	102.53
PNDM	MSE	2.40E-1	4.60E-4	9.89E-5	7.03E-5	3.09E-5	2.03E-5	7.09E-6	6.13E-6
	SSIM	1.79E-4	9.97E-1	9.99E-1	9.98E-1	9.98E-1	9.99E-1	1.00E+0	1.00E+0
	FID	177.35	112.35	111.44	109.32	110.74	109.52	101.54	102.53
HEUN	MSE	2.40E-1	4.60E-4	9.89E-5	2.39E-5	1.41E-5	1.33E-5	7.09E-6	6.13E-6
	SSIM	1.79E-4	9.97E-1	9.99E-1	9.99E-1	9.99E-1	1.00E+0	1.00E+0	1.00E+0
	FID	177.35	112.35	111.44	109.32	110.74	109.52	101.54	102.53
LMSD	MSE	2.40E-1	4.60E-4	9.89E-5	2.39E-5	1.41E-5	1.33E-5	7.09E-6	6.13E-6
	SSIM	1.79E-4	9.97E-1	9.99E-1	9.99E-1	9.99E-1	1.00E+0	1.00E+0	1.00E+0

Table 31: DDPM performs on **Blur**, **Line**, **Box**, and **Box** with CIFAR10 Dataset, trigger: Stop Sign, and target: Shoe.

Sampler	P.R. Metric	0%	10%	20%	30%	50%	70%	90%
	LPIPS	3.25E-1	2.78E-1	2.77E-1	2.68E-1	2.56E-1	2.55E-1	2.59E-1
UNIPC, Blur	MSE	2.97E-1	3.58E-3	1.31E-3	1.61E-3	4.90E-4	1.99E-4	8.39E-5
	SSIM	5.66E-2	9.85E-1	9.94E-1	9.93E-1	9.97E-1	9.99E-1	9.99E-1
	LPIPS	3.19E-1	2.78E-1	2.82E-1	2.76E-1	2.66E-1	2.65E-1	2.58E-1
UNIPC, Line	MSE	3.03E-1	3.78E-3	2.83E-3	3.29E-3	1.27E-3	3.37E-4	6.92E-5
	SSIM	4.61E-2	9.85E-1	9.89E-1	9.87E-1	9.95E-1	9.98E-1	9.99E-1
	LPIPS	3.10E-1	2.87E-1	2.85E-1	2.85E-1	2.70E-1	2.63E-1	2.63E-1
UNIPC, Box	MSE	3.34E-1	2.15E-2	3.17E-2	3.47E-2	3.29E-2	1.93E-2	1.11E-2
	SSIM	1.05E-2	9.10E-1	8.76E-1	8.56E-1	8.67E-1	9.19E-1	9.51E-1
	LPIPS	3.25E-1	2.79E-1	2.70E-1	2.65E-1	2.57E-1	2.55E-1	2.57E-1
DPM. O2, Blur	MSE	2.97E-1	2.98E-3	1.52E-3	1.82E-3	5.58E-4	2.93E-4	1.37E-4
	SSIM	5.66E-2	9.87E-1	9.93E-1	9.91E-1	9.97E-1	9.98E-1	9.99E-1
	LPIPS	3.19E-1	2.88E-1	2.80E-1	2.73E-1	2.67E-1	2.63E-1	2.60E-1
DPM. O2, Line	MSE	3.03E-1	3.02E-3	3.25E-3	3.19E-3	1.39E-3	3.21E-4	1.97E-4
	SSIM	4.61E-2	9.87E-1	9.87E-1	9.88E-1	9.94E-1	9.98E-1	9.99E-1
	LPIPS	3.10E-1	2.91E-1	2.87E-1	2.83E-1	2.71E-1	2.59E-1	2.67E-1
DPM. O2, Box	MSE	3.34E-1	2.07E-2	3.24E-2	3.45E-2	3.60E-2	2.14E-2	1.04E-2
	SSIM	1.05E-2	9.14E-1	8.74E-1	8.57E-1	8.53E-1	9.11E-1	9.50E-1
	LPIPS	3.25E-1	2.78E-1	2.76E-1	2.68E-1	2.59E-1	2.52E-1	2.54E-1
DPM++. O2, Blur	MSE	2.97E-1	3.56E-3	1.52E-3	1.85E-3	4.64E-4	5.16E-4	4.34E-6
	SSIM	5.66E-2	9.84E-1	9.93E-1	9.92E-1	9.98E-1	9.97E-1	1.00E+0
	LPIPS	3.19E-1	2.87E-1	2.76E-1	2.73E-1	2.67E-1	2.61E-1	2.57E-1
DPM++. O2, Line	MSE	3.03E-1	3.55E-3	4.38E-3	4.30E-3	1.68E-3	4.40E-4	9.60E-5
	SSIM	4.61E-2	9.85E-1	9.83E-1	9.83E-1	9.93E-1	9.98E-1	9.99E-1
	LPIPS	3.10E-1	2.87E-1	2.85E-1	2.79E-1	2.74E-1	2.65E-1	2.64E-1
DPM++. O2, Box	MSE	3.34E-1	2.44E-2	3.40E-2	3.12E-2	3.79E-2	1.97E-2	1.08E-2
	SSIM	1.05E-2	8.98E-1	8.72E-1	8.66E-1	8.45E-1	9.15E-1	9.49E-1
	LPIPS	3.25E-1	2.81E-1	2.76E-1	2.72E-1	2.60E-1	2.51E-1	2.50E-1
DEIS, Blur	MSE	2.97E-1	2.87E-3	1.34E-3	2.96E-3	2.02E-4	3.58E-4	1.61E-4
	SSIM	5.66E-2	9.87E-1	9.94E-1	9.88E-1	9.98E-1	9.98E-1	9.99E-1
	LPIPS	3.19E-1	2.82E-1	2.77E-1	2.76E-1	2.71E-1	2.58E-1	2.61E-1
DEIS, Line	MSE	3.03E-1	3.54E-3	2.50E-3	3.31E-3	1.29E-3	2.57E-4	5.03E-6
	SSIM	4.61E-2	9.85E-1	9.90E-1	9.86E-1	9.95E-1	9.98E-1	1.00E+0
	LPIPS	3.10E-1	2.84E-1	2.85E-1	2.81E-1	2.70E-1	2.61E-1	2.67E-1
DEIS, Box	MSE	3.34E-1	2.26E-2	3.26E-2	3.49E-2	3.46E-2	2.05E-2	1.03E-2
	SSIM	1.05E-2	9.07E-1	8.74E-1	8.52E-1	8.59E-1	9.15E-1	9.54E-1

Table 32: DDPM performs on **Blur**, **Line**, **Box**, and **Box** with CIFAR10 Dataset, trigger: Stop Sign, and target: Hat.

Sampler	P.R. Metric	0%	10%	20%	30%	50%	70%	90%
	LPIPS	3.25E-1	2.72E-1	2.66E-1	2.63E-1	2.53E-1	2.39E-1	2.45E-1
UNIPC, Blur	MSE	2.85E-1	1.25E-2	1.63E-3	2.09E-3	3.59E-4	1.01E-3	6.57E-4
	SSIM	2.98E-2	9.52E-1	9.93E-1	9.91E-1	9.98E-1	9.95E-1	9.96E-1
	LPIPS	3.19E-1	2.73E-1	2.69E-1	2.65E-1	2.54E-1	2.41E-1	2.45E-1
UNIPC, Line	MSE	2.83E-1	1.56E-2	2.33E-3	2.71E-3	1.11E-3	8.63E-4	1.23E-3
	SSIM	2.13E-2	9.42E-1	9.90E-1	9.89E-1	9.95E-1	9.96E-1	9.94E-1
	LPIPS	3.10E-1	2.87E-1	2.79E-1	2.79E-1	2.65E-1	2.51E-1	2.52E-1
UNIPC, Box	MSE	3.04E-1	3.63E-2	2.16E-2	1.43E-2	4.97E-3	3.31E-3	6.02E-3
	SSIM	-1.37E-3	8.76E-1	9.23E-1	9.47E-1	9.81E-1	9.87E-1	9.76E-1
	LPIPS	3.25E-1	2.73E-1	2.71E-1	2.60E-1	2.55E-1	2.41E-1	2.37E-1
DPM. O2, Blur	MSE	2.85E-1	1.16E-2	1.52E-3	1.58E-3	8.13E-4	1.07E-3	7.07E-4
	SSIM	2.98E-2	9.58E-1	9.93E-1	9.93E-1	9.96E-1	9.95E-1	9.97E-1
	LPIPS	3.19E-1	2.76E-1	2.68E-1	2.63E-1	2.57E-1	2.42E-1	2.45E-1
DPM. O2, Line	MSE	2.83E-1	1.43E-2	2.28E-3	1.84E-3	1.03E-3	1.13E-3	2.68E-3
	SSIM	2.13E-2	9.46E-1	9.91E-1	9.92E-1	9.95E-1	9.94E-1	9.89E-1
	LPIPS	3.10E-1	2.86E-1	2.76E-1	2.77E-1	2.65E-1	2.54E-1	2.52E-1
DPM. O2, Box	MSE	3.04E-1	3.83E-2	2.15E-2	1.40E-2	3.26E-3	3.50E-3	1.41E-3
	SSIM	-1.37E-3	8.67E-1	9.23E-1	9.48E-1	9.87E-1	9.86E-1	9.93E-1
	LPIPS	3.25E-1	2.71E-1	2.65E-1	2.62E-1	2.59E-1	2.39E-1	2.45E-1
DPM++. O2, Blur	MSE	2.85E-1	1.16E-2	1.46E-3	1.77E-3	7.03E-4	9.69E-4	4.74E-4
	SSIM	2.98E-2	9.56E-1	9.94E-1	9.92E-1	9.96E-1	9.95E-1	9.98E-1
	LPIPS	3.19E-1	2.68E-1	2.72E-1	2.62E-1	2.52E-1	2.39E-1	2.41E-1
DPM++. O2, Line	MSE	2.83E-1	1.65E-2	1.57E-3	1.78E-3	1.38E-4	8.54E-4	2.20E-3
	SSIM	2.13E-2	9.38E-1	9.92E-1	9.92E-1	9.99E-1	9.96E-1	9.90E-1
	LPIPS	3.10E-1	2.85E-1	2.79E-1	2.72E-1	2.67E-1	2.52E-1	2.53E-1
DPM++. O2, Box	MSE	3.04E-1	4.04E-2	2.17E-2	1.31E-2	4.82E-3	4.04E-3	6.23E-3
	SSIM	-1.37E-3	8.62E-1	9.22E-1	9.52E-1	9.81E-1	9.84E-1	9.73E-1
	LPIPS	3.25E-1	2.69E-1	2.71E-1	2.66E-1	2.55E-1	2.43E-1	2.46E-1
DEIS, Blur	MSE	2.85E-1	1.11E-2	1.20E-3	1.85E-3	9.45E-4	5.66E-4	4.59E-4
	SSIM	2.98E-2	9.59E-1	9.94E-1	9.93E-1	9.95E-1	9.97E-1	9.97E-1
	LPIPS	3.19E-1	2.73E-1	2.66E-1	2.59E-1	2.53E-1	2.43E-1	2.41E-1
DEIS, Line	MSE	2.83E-1	1.39E-2	2.92E-3	2.24E-3	5.60E-4	1.29E-3	1.98E-3
	SSIM	2.13E-2	9.49E-1	9.88E-1	9.91E-1	9.97E-1	9.94E-1	9.90E-1
	LPIPS	3.10E-1	2.84E-1	2.79E-1	2.72E-1	2.65E-1	2.53E-1	2.44E-1
DEIS, Box	MSE	3.04E-1	4.07E-2	2.16E-2	1.16E-2	4.20E-3	3.75E-3	5.07E-3
	SSIM	-1.37E-3	8.62E-1	9.23E-1	9.57E-1	9.83E-1	9.85E-1	9.79E-1